FISEVIER

Contents lists available at ScienceDirect

### **Quaternary Science Reviews**

journal homepage: www.elsevier.com/locate/quascirev



### Invited review

### Updated cosmogenic chronologies of Pleistocene mountain glaciation in the western United States and associated paleoclimate inferences



Benjamin J.C. Laabs <sup>a, \*</sup>, Joseph M. Licciardi <sup>b</sup>, Eric M. Leonard <sup>c</sup>, Jeffrey S. Munroe <sup>d</sup>, David W. Marchetti <sup>e</sup>

- <sup>a</sup> North Dakota State University, United States
- <sup>b</sup> University of New Hampshire, United States
- <sup>c</sup> Colorado College, United States
- <sup>d</sup> Middlebury College, United States
- <sup>e</sup> Western Colorado University, United States

### ARTICLE INFO

Article history: Received 21 December 2019 Received in revised form 8 June 2020 Accepted 9 June 2020 Available online xxx

Keywords:
Surface-exposure dating
Mountain glaciation
Paleoclimate
Moraines
Terrestrial cosmogenic nuclides
Western United States
Pleistocene

### ABSTRACT

Surface exposure dating with terrestrial cosmogenic nuclides (TCNs) has become the primary method for determining numerical ages of Pleistocene mountain glacial deposits and landforms in the conterminous western United States (U.S.) and in numerous other glaciated settings worldwide. Recent updates to models of TCN production and scaling warrant a reconsideration of published exposure ages of moraines of the last two Pleistocene glaciations and associated paleoclimate inferences. Previously reported TCN exposure ages of moraines are recalculated here using newer production rates and scaling models for nuclides helium-3 (<sup>3</sup>He), beryllium-10 (<sup>10</sup>Be), aluminum-26 (<sup>26</sup>Al), and chlorine-36 (<sup>36</sup>Cl), in most cases yielding significant differences from originally reported ages. Recalculated TCN exposure ages of moraines of the penultimate glaciation display a high degree of variability for individual landforms, particularly toward the younger end of age distributions, suggesting that exposure history is affected by moraine denudation and that older age modes provide the best estimate of the depositional age of these moraines. Oldest exposure ages of penultimate glaciation moraines are well-aligned among mountain ranges across the western U.S. and yield a mean of 138  $\pm$  13 ka, indicating that mountain glaciation occurred in step with global ice volume maxima during marine oxygen isotope stage 6. On average, terminal moraines of the last glaciation date to  $19.5 \pm 2.3$  ka and correspond to the latter part of the global Last Glacial Maximum (LGM). Down-valley recessional moraines representing prolonged glacial stabilizations or readvances to  $\geq$ 75% of maximum lengths have a mean exposure age of 17.0  $\pm$  1.8 ka, suggesting that these moraine positions were last occupied during Heinrich Stadial 1. Evidence for multiple glacial culminations during the last glaciation is found in several mountain ranges and likely reflects at least two phases of Late Pleistocene climate: an earlier phase when glaciers attained their maximum length in response to cooling during the LGM, and a later phase when glaciers persisted at or readvanced to near-maximum lengths in response to sustained cold temperatures and/or increased precipitation.

© 2020 Elsevier Ltd. All rights reserved.

### 1. Introduction

1.1. Emergence of TCN exposure dating of glacial features in the western United States

In the three decades since the first applications of terrestrial

\* Corresponding author. E-mail address: benjamin.laabs@ndsu.edu (B.J.C. Laabs). cosmogenic nuclide (TCN) exposure dating to Pleistocene moraines in the western United States (U.S.) (Phillips et al., 1990; Nishiizumi et al., 1993; Gosse et al., 1995a), these methods have become the most widely applied approach to numerical dating of alpine glacial features in the region (Fig. 1). TCN exposure dating techniques have revolutionized numerical dating of glacial deposits and landforms by overcoming some fundamental limitations of radiocarbon in these settings, such as the typical scarcity of preserved organic matter in glacigenic sediments and the general restriction of

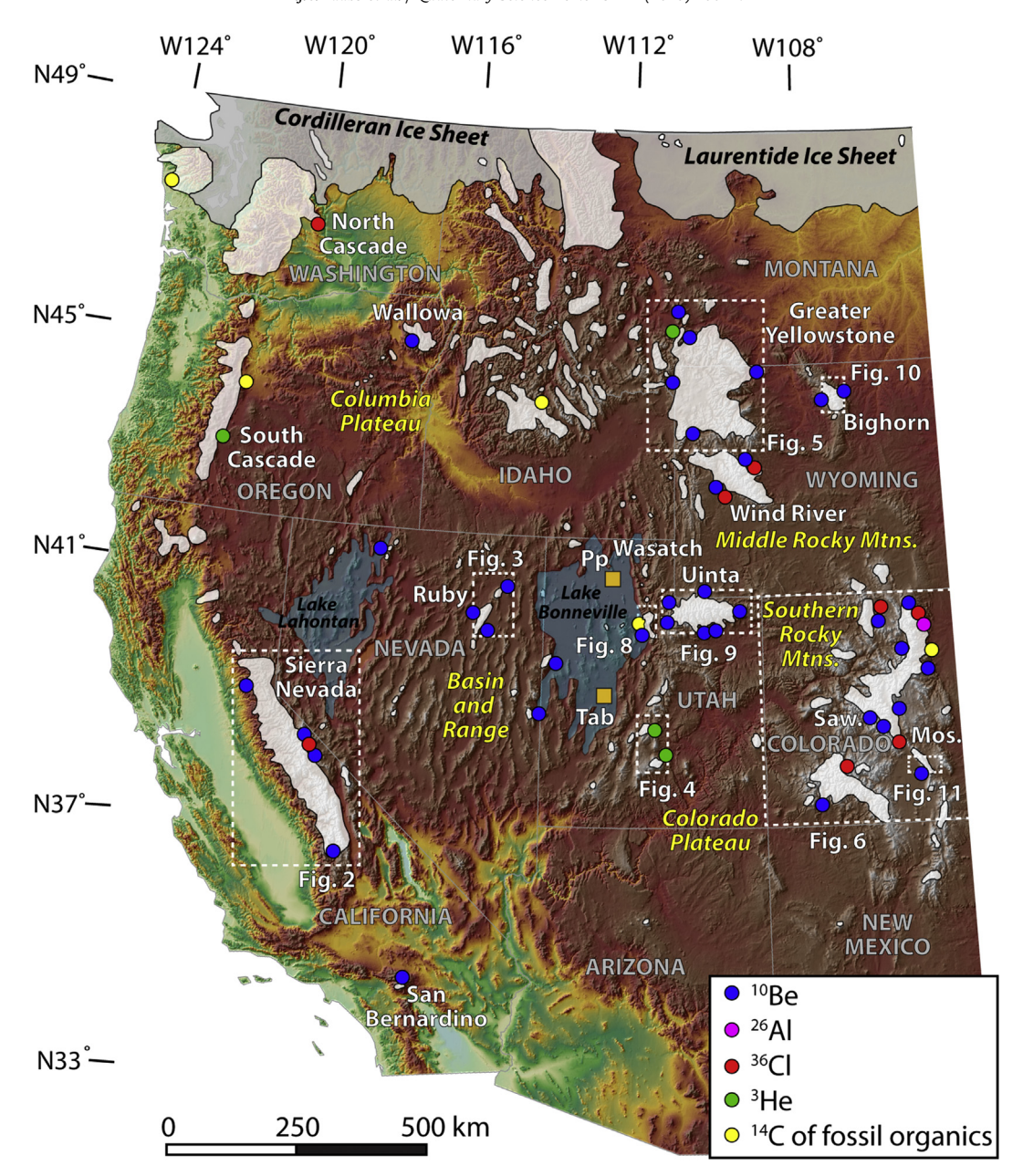


**Fig. 1.** Overview of Pleistocene mountain glaciation in the conterminous western U.S. Color relief map base produced from the National Map (http://www.usgs.gov/core-science-systems/national-geospatial-program/national-map). Physiographic regions described in the text are labeled in yellow. Mountain glacier systems (white) are redrawn from Porter et al. (1983) and Pierce (2003). Circles indicate approximate locations of sites with exposure ages or radiocarbon limits of moraines and/or outwash of the last two Pleistocene glaciations. Squares indicate sites where TCN <sup>10</sup>Be and <sup>3</sup>He spallogenic production rates have been calibrated at Promontory Point (Pp) and Tabernacle Hill (Tab), respectively (Lifton et al., 2015; Goehring et al., 2010). Boxes indicate areas shown in Figs. 2–6 and Figs. 8–11. Areas occupied by (or surrounded by) Great Basin pluvial Lakes Bonneville (Utah) and Lahontan (Nevada) during the last glaciation are shaded blue.

available radiocarbon ages to glaciolacustrine sediments and outwash that provide only minimum or maximum limiting ages of moraines. TCN dating methods have provided a more precise means of determining times of glacial maxima by enabling direct dating of moraine surfaces, which has led to a dramatic expansion of available chronologies of glacial landforms.

TCN exposure chronologies of moraines of the last glaciation now exist for most major glaciated mountain ranges in the conterminous western United States — the Sierra Nevada (e.g., Phillips et al., 1990, 1996; 2009; Nishiizumi et al., 1993; Rood et al., 2011), the Cascade Range and inland Pacific Northwest (e.g., Licciardi et al., 2004; Porter and Swanson, 2008; Speth et al., 2018), portions of the Great Basin/Basin and Range (e.g., Laabs et al., 2013;

Wesnousky et al., 2016), the Colorado Plateau (Marchetti et al., 2005, 2007, 2011) and the Rocky Mountains (e.g., Gosse et al., 1995a, b; Phillips et al., 1997; Licciardi et al., 2001; Benson et al., 2005; Brugger, 2007; Licciardi and Pierce, 2008, 2018; Laabs et al., 2009; Ward et al., 2009; Young et al., 2011; Leonard et al., 2017a; Brugger et al., 2019a, 2019b) (Fig. 1). Many of these studies have focused on dating terminal moraines exclusively as a means of determining the timing of glacial maxima. In studies where multiple moraine crests were dated within single glaciated valleys or within a single mountain range, millennial-scale differences in the timing of glacial maxima and/or the timing of subsequent ice retreat have been found (e.g., Licciardi et al., 2004; Guido et al., 2007; Licciardi and Pierce, 2008; Laabs et al., 2009; Dühnforth

and Anderson, 2011; Young et al., 2011; Leonard et al., 2017a; Marcott et al., 2019). These and similar studies have permitted detailed reconstructions of climate during and following the last glaciation in the western U.S. (e.g., Plummer and Phillips, 2003; Laabs et al., 2006; Refsnider et al., 2008; Leonard et al., 2017a; Quirk et al., 2018).

A smaller number of TCN exposure chronologies have been developed for moraines that predate the last glaciation; these include records in the Sierra Nevada (Rood et al., 2011; Wesnousky et al., 2016; Phillips et al., 2009), the Cascade Range (Porter and Swanson, 2008; Speth et al., 2018), the Great Basin (Laabs et al., 2013), the Colorado Plateau (Marchetti et al., 2011), and the Rocky Mountains (Phillips et al., 1997; Licciardi and Pierce, 2008, 2018; Dahms et al., 2018; Brugger et al., 2019a; Schweinsberg et al., 2020). These studies have correlated moraines of earlier glaciations to known glacial and stadial events of the Middle and Late Pleistocene while acknowledging potential issues regarding exposure history (e.g., burial of moraines by snow or sediment, moraine and boulder surface erosion, or intervals of prior exposure). Most of these studies have focused on the penultimate glaciation in mountains of the conterminous western U.S., finding that this episode corresponds to MIS 6 (191-130 ka; Lisiecki and Raymo, 2005) in numerous mountain ranges (Rood et al., 2011; Licciardi and Pierce, 2008, 2018; Brugger et al., 2019a; Schweinsberg et al., 2020). Other studies have not ruled out the possibility that ice advances occurred during subsequent cold intervals such as MIS 5d or 5b (123-109 ka and 96-87 ka, respectively; Lisiecki and Raymo, 2005) due to the broad range of exposure ages from these surfaces (Phillips et al., 1997: Porter and Swanson, 2008: Wesnousky et al., 2016), A small number of studies have identified signals of mountain glaciation in the conterminous western U.S. during MIS 4 or MIS 3, and these are spatially restricted to coastal settings in the Pacific Northwest and some glacial settings in the Rocky Mountains (e.g., Hall and Shroba, 1995; Thackray, 2001, 2008; Sharp et al., 2003; Pierce et al., 2011).

Most TCN exposure chronologies of glacial deposits are based on isotope production models that have been refined incrementally through numerous efforts to calibrate production rates for TCNs such as <sup>3</sup>He, <sup>10</sup>Be, <sup>26</sup>Al, and <sup>36</sup>Cl. Such efforts have involved measurements of the TCN inventory in independently dated surfaces suitable for exposure dating at a wide range of latitudes, altitudes, and ages, along with studies designed to improve models for scaling production over space and time (see Borchers et al. (2016) and Marrero et al. (2016a) and references therein for summaries of recent production calibrations). A key product of these efforts is a refined set of TCN production models that can be used to compute more accurate and precise TCN exposure ages of glacial deposits, thereby enabling more reliable comparisons of glacial chronologies to other independently dated geologic and paleoclimatic records. Recently developed production models have been incorporated into the most widely used online cosmogenic exposure age calculators (e.g., Balco et al., 2008; Marrero et al., 2016a; Martin et al., 2017). To date, however, few glacial chronologies for the western U.S. have been recalculated using the newer, more accurate production models implemented in these online calculators (e.g., Leonard et al., 2017a, 2017b; Quirk et al., 2018; Licciardi and Pierce, 2018; Marcott et al., 2019), and the variety of production models used in reports of TCN exposure ages of glacial deposits complicates comparisons of these chronologies. Some recent studies have determined that, at most sites, new production models yield <sup>10</sup>Be exposure ages of a few percent to as much as ~15% older than ages computed with earlier production models (e.g., Leonard et al., 2017b). The larger shifts in recalculated exposure ages are greater than isotope-measurement errors and suggest that previous correlations between moraine chronologies and independently dated climate changes should be reconsidered.

#### 1.2. Modern climate in the conterminous western U.S.

Mountain glaciers in the conterminous western U.S. are currently limited almost exclusively to cirques in the highest portions of coastal ranges and the Rocky Mountains. The distribution of glaciers across the region shown in Fig. 1 is governed by a modern climate characterized by strong precipitation gradients and contrasting atmospheric circulation patterns between summer and winter. North of ~40°N latitude, winter (November-March) climate is characterized by westerly flow delivering moisture-laden air derived from the Pacific Ocean (Mitchell, 1976). The mountains of northern California, Oregon, and Washington intercept large amounts of winter precipitation while the ranges further east in northern Utah, northern Colorado, Idaho, Wyoming, and Montana receive less snowfall. South of 40°N latitude, winter airflow is predominantly from the southwest and moisture delivery to the mountains is generally less, due to persistent high atmospheric pressure in the southern Great Basin. Snowfall in the mountains of southern California, the Great Basin, Colorado Plateau, and portions of the Southern Rocky Mountains is more variable and dependent in large part on the El Niño Southern Oscillation (Sheppard et al., 2002; Steenburgh et al., 2013). During the summer (April-October) northwesterly flow is reduced, and much of the region receives less precipitation than during the winter. This is particularly true along the Pacific coast and in the Cascade Range, Sierra Nevada, the Middle and Northern Rocky Mountains, the Basin and Range (in Nevada) and the Columbia Plateau which receive summer moisture only from infrequent intrusions of southwesterly or northwesterly airflow. The southeastern part of the area shown in Fig. 1, including the Colorado Plateau and Southern Rocky Mountains, receives greater amounts of summer precipitation due to the influence of the North American monsoon (Sheppard et al., 2002), and many areas of the U.S. Southwest and Southern Rocky Mountains currently receive more precipitation during the summer than during the winter. Mountain temperatures throughout the region display a strong seasonal contrast as expected for middle latitudes, with the contrast increasing from coastal to inland ranges.

### 1.3. Inferred glacial climate in the conterminous western U.S.

Inferences of paleoclimate in the western U.S. during the last glaciation and early deglaciation are numerous due to the widespread availability of climate proxy records from beyond mountain glacial limits and from numerical simulations of regional climate during the Last Glacial Maximum (LGM) (e.g., COHMAP Members, 1988; Thompson et al., 1993; Hostetler and Clark, 1997; Braconnot et al., 2012). Based on reconstructions of former mountain glacier extents, ice dynamics, and equilibrium-line altitudes (ELAs), the pattern of past glaciation suggests that regional airflow and moisture delivery to mountains was similar to the present, especially in areas far south of the Laurentide and Cordilleran Ice Sheet margins (Fig. 1). Westerly airflow delivered Pacific-derived moisture to the region, nourishing glaciers during the accumulation season and resulting in a pattern of low mountain glacier ELAs in the west and higher ELAs eastward (Porter et al., 1983; Zielinski and McCoy, 1987; Leonard, 1989). Northern mountains closer to ice sheet margins likely experienced larger temperature depressions compared to mountains farther south and were likely drier than modern due to anticyclonic, easterly airflow immediately south of the ice margins (Hostetler and Clark, 1997). Some northern mountains display evidence of muted glacier lengths during the LGM when moisture supply was limited and comparatively greater post-LGM glacier lengths when westerly airflow strengthened as the Laurentide Ice Sheet retreated (Thackray, 2001; Licciardi et al.,

2001). Regionwide data-model comparisons support the idea of a drier LGM climate in the northwestern U.S. and a relatively wet southwestern U.S. (Oster et al., 2015a, b; Hudson et al., 2019). The comparatively wetter glacial climate in the southwestern U.S. has been attributed to a southward displacement of the polar jet stream and associated storm tracks (Antevs, 1955), which is a recurring feature in numerical simulations of LGM climate (Kutzbach and Wright, 1985; Thompson et al., 1993; Bartlein et al., 1998). After the LGM, when glaciers in some mountains were at or near their maximum lengths until as late as 15 ka (Licciardi et al., 2001; Thackray et al., 2004; Munroe et al., 2006; Young et al., 2011), Pacific-derived moisture likely increased throughout the region (Lyle et al., 2012; Munroe and Laabs, 2013; Ibarra et al., 2014) and the position of storm tracks varied across a broad range of latitudes (Lora and Ibarra, 2019; Hudson et al., 2019).

### 1.4. Objectives of this review

In this review, we present a large set of previously reported TCN exposure ages (herein referred to as "exposure ages") augmented with some new <sup>10</sup>Be exposure ages of Middle to Late Pleistocene (MIS 6 to MIS 2) moraines, all of which are recalculated using updated production rates and a selection of scaling models. The goals of this review are to: (1) synthesize TCN chronologies of the last two major Pleistocene glaciations for mountainous regions in the conterminous western U.S. using up-to-date, consistent, and substantiated production rates and scaling methods; and (2) reconsider existing interpretations of Pleistocene climate change in the region and discuss new scenarios based on recalculated cosmogenic ages of glacial deposits. We note that, although direct and indirect evidence of mountain glaciation between MIS 6 and MIS 2 exists in some locations in the conterminous western U.S. (e.g., Hall and Shroba, 1995; Thackray, 2001; Sharp et al., 2003), most pre-LGM moraines in the conterminous western U.S. have exposure ages corresponding to MIS 5 or 6. Therefore, the term "penultimate glaciation" refers to regional-wide glaciation during early MIS 5 or MIS 6 and not to later stadials that were generally less extensive than the MIS 2 glaciation. This review differs from other previous compilations of exposure-dated moraine ages (e.g., Shakun et al., 2015; Heyman et al., 2016; Palacios et al., 2020) by: (1) focusing only on the contiguous western U.S. and examining more TCN glacial chronologies in this region than any previous review, including new chronologies from penultimate-glaciation moraines in the Ruby Mountains (Basin and Range, Nevada) and from last-glaciation moraines in the northern Colorado Plateau (Utah) and the Bighorn Range (Middle Rocky Mountains, Wyoming); (2) considering exposure ages for the last two Pleistocene glaciations; (3) distinguishing TCN exposure ages of terminal and downvalley recessional moraines (representing near-maximum glacier lengths) of the last glaciation; and (4) examining differences between originally reported and recalculated exposure ages. Although this review includes recalculations of all exposure ages of terminal moraines in the western U.S. published as of this writing, the vast majority of these exposure ages are based on <sup>10</sup>Be (Fig. 1). The following section summarizes refinements to the <sup>10</sup>Be production rate and scaling models as an example of how production models have evolved through the history of TCN exposure dating of glacial deposits and landforms. These improvements have been accompanied by a more accurate determination of the  $^{10}\mathrm{Be}$  half-life (Chmeleff et al., 2010), improved AMS standardizations for <sup>10</sup>Be (Nishiizumi et al., 2007), and reduced <sup>10</sup>Be detection limits with AMS, all of which have helped to improve the precision and accuracy of <sup>10</sup>Be exposure dating. Other commonly used cosmogenic isotope dating methods including <sup>3</sup>He and <sup>36</sup>Cl have also benefited from similar improvements and advances over the past three decades, but these isotope-specific developments are not reviewed here for brevity and can be found elsewhere (e.g., Goehring et al., 2010; Marrero et al., 2016b).

### 2. Beryllium-10 production rates and scaling models

### 2.1. Production rates and scaling models used in previous studies

Exposure dating of sediments and landforms with cosmogenic <sup>10</sup>Be has relied chiefly on models of *in situ* production in quartz, which occurs via numerous pathways involving reactions of cosmic radiation with silicon and oxygen, and theoretically with metal impurities in quartz (as summarized by Gosse and Phillips, 2001). Total production is dominated, however, by spallation from fast neutrons and muonic reactions with oxygen and to a lesser degree with silicon. Cosmogenic <sup>10</sup>Be production rates are greatest at material surfaces, but spallogenic production attenuates with depth to a greater degree than muogenic production (Balco, 2017). Production rates at high altitudes in the western U.S. and elsewhere were first estimated in the late 1980s and 1990s at sites with assumed or independently known exposure ages (e.g., Nishiizumi et al., 1989; Brown et al., 1991; Clark et al., 1995). Mathematical models of Lal and Peters (1967) and Yokoyama et al. (1977), as reformulated by Lal (1991), were used to scale production rates at these sites to sea level and high latitude (SLHL), leading to early estimates of in situ SLHL production rates (from spallation and muons) in quartz that ranged from 4.74 to 6.4 atoms  $g^{-1}$   $yr^{-1}$ .

The first applications of cosmogenic <sup>10</sup>Be exposure dating to western U.S. moraines in the Sierra Nevada (Nishiizumi et al., 1993) and in the Wind River Mountains (Gosse et al., 1995a) used a combined spallogenic and muogenic production rate of 6.0 atoms  $g^{-1}$  yr<sup>-1</sup> scaled for altitude and geomagnetic latitude using models compiled by Lal (1991). After a refined production rate and scaling model of Stone (2000) became available, <sup>10</sup>Be exposure dating efforts in the 2000s generally used lower SLHL production rates of 5.0-5.4 atoms  $g^{-1}$  yr<sup>-1</sup> to compute exposure ages (e.g., Schildgen et al., 2002; Licciardi et al., 2001, 2004; Benson et al., 2005; Munroe et al., 2006; Brugger, 2007; Licciardi and Pierce, 2008). Once the first online exposure age calculator developed by the Cosmic-Ray Produced Nuclide Systematics on Earth (CRONUS-Earth) project became available in 2008 (Balco et al., 2008), many subsequent studies began using its implementations of production models for computing <sup>10</sup>Be (and a much smaller number of <sup>26</sup>Al) exposure ages. These <sup>10</sup>Be production models included a constant production rate model, designated "St" (Stone, 2000) and timedependent production models designated "Du" (Dunai, 2001), "Li" (Lifton et al., 2005), "De" (Desilets et al., 2006), and "Lm" (Nishiizumi et al., 1989; Lal, 1991; Stone, 2000). The availability of the original CRONUS calculator led to more consistent approaches for computing <sup>10</sup>Be exposure ages of glacial deposits in the western U.S. and elsewhere and permitted more accurate comparisons of exposure-age differences across mountain ranges (e.g., Licciardi and Pierce, 2008; Laabs et al., 2009; Rood et al., 2011; Young

A newer time-dependent scaling method of Lifton et al. (2014) has been recently implemented in online exposure age calculators. As noted by Phillips et al. (2016a), this scaling model is more physically based and fits global TCN calibration data as well as other time-dependent and time-constant scaling methods (Borchers et al., 2016). The model was used in a global assessment of deglaciation chronologies based on exposure dating and other chronometers (Shakun et al., 2015), in a reanalysis of <sup>36</sup>Cl moraine chronologies in the Sierra Nevada (Phillips et al., 2016b), and in a growing number of recent reports of exposure ages in the western U.S. (e.g., Leonard et al., 2017a, 2017b; Quirk et al., 2018; Licciardi

and Pierce, 2018; Brugger et al., 2019a, 2019b; Marcott et al., 2019; Schweinsberg et al., 2020).

2.2. Production rates and scaling used to recalculate moraine exposure ages in the western U.S.

The compilation of recalculated cosmogenic <sup>10</sup>Be exposure ages presented here takes advantage of newer and more precise production calibration studies (as summarized by Borchers et al., 2016) and updates to online exposure age calculators (e.g., Marrero et al., 2016a). All exposure ages in this review are recalculated using two substantiated and frequently used exposure-age calculators available online, including (1) version 2.0 of CRONUScalc (Marrero et al., 2016a; http://cronus.cosmogenicnuclides.rocks/2.0/) and (2) version 3.0 of the original online calculator described by Balco et al. (2008) and subsequently updated (http://hess.ess.washington.edu; hereafter referred to as the "Version 3 Calculator"). CRONUScalc permits calculation of <sup>3</sup>He, <sup>10</sup>Be, <sup>26</sup>Al, and <sup>36</sup>Cl exposure ages, and the Version 3 Calculator permits calculation of exposure ages from these same TCNs except for <sup>36</sup>Cl. Because it is beyond the scope of this review to compare outputs of all substantiated online exposure age calculators, we do not include recalculated ages generated by the CREp calculator of Martin et al. (2017). The accompanying supplemental material for this review provides all the necessary sample information for users to recalculate exposure ages with

All recalculated <sup>10</sup>Be and <sup>26</sup>Al exposure ages reported in the text of this paper rely on the time-dependent scaling model of Lifton et al. (2014) as implemented in the Version 3 Calculator (in which it is designated "LSDn") and the SLHL <sup>10</sup>Be and <sup>26</sup>Al production rates as determined at Promontory Point in Utah (Lifton et al., 2015). Recalculated <sup>3</sup>He exposure ages discussed in the text also use the LSDn scaling model implemented in the Version 3 Calculator but apply SLHL <sup>3</sup>He production rates determined at Tabernacle Hill in Utah (Cerling and Craig, 1994; Goehring et al., 2010; Lifton et al., 2015). These calibration sites are centrally located among the moraines considered in this review (Fig. 1), have independently dated exposure ages corresponding to latter part of the last glaciation, and have more precise independent age control compared to some earlier TCN production calibration sites in the western U.S (Nishiizumi et al., 1989; Cerling and Craig, 1994). Recalculated <sup>36</sup>Cl exposure ages reported in the text are computed using the same Lifton et al. (2014) scaling scheme as for the other isotopes, but apply the globally averaged <sup>36</sup>Cl production scheme of Marrero et al. (2016b) as implemented in version 2.0 of CRONUScalc (here, the scaling scheme is termed "SA"). For <sup>36</sup>Cl exposure-age recalculations, a fast-neutron attenuation length of 160 g cm<sup>-2</sup> is assumed for all sites and the major element and trace element sample data from original reports of exposure ages are used to compute the total production of <sup>36</sup>Cl. To enable a comparison of exposure ages computed using different options for production rates and scaling schemes, the supplemental tables accompanying this review also include <sup>3</sup>He, <sup>10</sup>Be, and <sup>26</sup>Al exposure ages computed with globally averaged SLHL production rates (mineral- and element-specific where appropriate) derived from Borchers et al. (2016) (available at http://calibration.ice-d.org) and the timeconstant and time-dependent models that combine scaling equations of Lal (1991) and Stone (2000) (abbreviated "St" and "Lm" respectively in the Version 3 Calculator). The tables also include <sup>3</sup>He, <sup>10</sup>Be, and <sup>26</sup>Al exposure ages computed using the globally averaged SLHL production rates and the SA scaling scheme in CRONUScalc to enable comparisons of ages computed by different calculators, as well as the exposure ages reported in the original studies.

For all exposure-age recalculations, the standard atmosphere

model (designated "std" in the Version 3 Calculator) is used. Additionally, the geographic coordinates, topographic shielding factors, and boulder-surface erosion rates provided in the original reports are used in all exposure age recalculations. In most original reports, geographic coordinates and elevations of sample surfaces are measured by handheld GPS and boulder-surface erosion rates are assumed in most studies to be negligible for moraines deposited during the last glaciation. The effects of snow cover on TCN production in sampled surfaces of moraines has been assumed negligible in most original reports of exposure ages in the western U.S. Although it may be significant in some settings (e.g., Benson et al., 2004; Marchetti et al., 2011), it is assumed to be negligible in the age recalculations reported here.

### 3. Interpreting TCN exposure ages of moraines

Among the numerous studies involving exposure dating of moraines compiled for this review, the field methods used for sampling moraine boulders have been generally consistent (following that of Gosse and Phillips, 2001), whereas approaches to interpreting exposure ages have been more variable. In lieu of a complete evaluation of sampling and interpretive strategies, some considerations and sources of error involved in exposure dating of Pleistocene moraines in the western U.S. are briefly described. Similar considerations have been made in process-modeling and comprehensive studies of exposure dating of moraine boulders (e.g., Putkonen and Swanson, 2003; Applegate et al., 2012; Heyman et al., 2016); in this review, we consider only issues that may cause the exposure ages compiled here to deviate from the true age of their respective moraines.

Most sampling strategies used for exposure dating of moraines have targeted the largest and tallest erratic boulders at the moraine crest, with the idea that such boulders have stood as stable, continuously exposed, monumental features since deposition. Although boulders from a single moraine crest or segment are generally assumed to have the same exposure history, samples of multiple boulders are needed to test this assumption and to establish a statistically representative exposure age for the moraine. All studies in the western U.S. have reported some degree of TCN exposure age variability for boulders on a single moraine, suggesting that even the tallest boulders atop moraines may not have the same exposure histories (as noted by Heyman et al., 2016). Although some age inconsistency can be related to AMS measurement uncertainty or lithological differences among boulders from a single moraine, typically the range of exposure ages for a single moraine exceeds that predicted solely by measurement uncertainty or differential boulder-erosion rates (related to compositional differences among erratic boulders) alone and is interpreted to represent pre-depositional exposure or post-depositional processes affecting the exposure history of boulders (Balco, 2011). Model simulations of cosmogenic nuclide production and moraine degradation suggest that inheritance of TCNs from pre-depositional exposure of moraine boulders is less probable (Putkonen and Swanson, 2003; Applegate et al., 2010), but evidence of inheritance has been identified in a small number of published TCN chronologies compiled here (see ages identified as older outliers in Table S1). In some of these cases moraine boulders were deposited by small glaciers (potentially less able to quarry bedrock to the depth necessary to remove the inherited TCN inventory) a few kilometers or less from bedrock outcrops that may have been a source of rockfall becoming supraglacial debris, which may explain why they retain pre-deposition TCN inventories. Altogether, evidence of inherited TCNs is apparent in fewer than 5% of exposure ages compiled here, further supporting the idea that inherited <sup>10</sup>Be is uncommon among boulders of Pleistocene moraines.

Post-depositional processes affecting the exposure of moraine boulders have been posited to explain young outliers in almost half of the data sets compiled for this review. This is especially true for moraines deposited during pre-MIS 2 glaciations, which have been subject to surficial processes for much longer than moraines deposited during MIS 2. The effects of such processes can be identified based on the distribution of exposure ages from a single moraine (e.g., Douglass et al., 2006; Schaefer et al., 2009; Applegate et al., 2012). Non-continuous exposure of moraine boulders in the western U.S. has been linked to seasonal snow cover (e.g., Benson et al., 2004) and boulder exhumation resulting from moraine crest degradation (e.g., Putkonen and Swanson, 2003; Putkonen and O'Neal, 2006). Most studies have assumed that snow cover on terminal moraine crests (which are generally hundreds of meters or more below modern summer snowline and possibly windswept of snow cover) has a minimal impact on exposure history, although Benson et al. (2004) estimated that snow cover since deposition can reduce production rates by as much as 12% for moraines of the last glaciation and possibly more for older Pleistocene moraines

Many studies have adopted sampling and interpretive approaches to help identify evidence of moraine degradation. Where sampling a greater number of boulders to obtain a more statistically meaningful distribution of exposure ages may not be possible, other strategies have been used to more clearly identify exposure ages that overestimate (due to inheritance) or underestimate (due to incomplete exposure) the age of moraine. For example, Schaefer et al. (2009) and Balco (2011) recommend using the reduced chisquared statistic ( $\chi^2$ r) to evaluate the distribution of exposure ages of moraines. The  $\gamma^2$ r statistic represents the distribution of exposure ages about the mean exposure age and can be considered an indication of whether the variance of ages is greater than, less than, or equal to that expected based on the measurement errors of individual exposure ages. If greater, the variability likely reflects some pre- or post-depositional process(es) affecting exposure history. Chauvenet's Criterion has also been used in some studies to identify outliers among a set of exposure ages of a moraine (e.g., Leydet et al., 2018; Marcott et al., 2019). If post-depositional processes have affected exposure history, then the youngest exposure ages can be excluded from consideration and either a mean of the remaining ages or the oldest exposure age can be a more reliable estimate of the true age of the moraine (Applegate et al., 2012). Other studies have used a stratigraphic approach to identify exposure ages reflecting either isotope inheritance from prior exposure or post-depositional disturbance. For example, Young et al. (2011) sampled moraines in the Arkansas River valley in southern Colorado and used an exposure age of glacially scoured bedrock upvalley to identify exposure ages of moraine boulders that underestimated the true age of the moraine. Other studies have obtained exposure ages of multiple moraine crests from the same valley (e.g., Phillips et al., 1996; Gosse et al., 1995a, b; Licciardi and Pierce, 2008) and used known relative-age relationships of moraines to identify exposure ages of boulders that represent young or old outliers. Laabs et al. (2013) applied Bayesian statistics to exposure ages of multiple moraine crests in a valley in the Great Basin to improve the precision of moraine exposure ages.

Most moraines deposited during glaciations prior to MIS 2 display surface morphology reflecting weathering and erosion of the moraine crest to a greater degree than younger moraines. Several studies have interpreted the greater observed variability among exposure ages of pre-MIS 2 moraines as evidence of moraine-crest degradation and favored the oldest exposure age or the oldest grouping of exposure ages as the best estimate of the depositional age of a moraine (e.g., Phillips et al., 1997; Licciardi and Pierce, 2008; Wesnousky et al., 2016). Additionally, evidence of

boulder-surface erosion has been observed on many pre-MIS 2 moraines; erosion has a greater impact on the apparent exposure ages of these moraines compared to impacts on younger moraines. Boulder surface erosion rates are generally unknown and difficult to estimate, however, posing a challenge for accurately determining exposure ages of older moraines. Phillips et al. (1997) used combined <sup>36</sup>Cl and <sup>10</sup>Be data from individual boulders to infer that boulder-surface erosion ranged from near zero to as much as 2.4 mm/kyr. Other studies have inferred boulder-surface erosion rates based on rock surface properties such as weathering features (e.g., pitting, spall; Porter and Swanson, 2008; protrusion of weathering-resistant inclusions; Laabs et al., 2011) or have used regional estimates for granitic bedrock surface erosion rates (e.g., from Benedict, 1993) to estimate impacts on exposure age (Licciardi and Pierce, 2008; Schweinsberg et al., 2020). These issues are discussed in the context of recalculated exposure ages of MIS 6 moraines (see section 4.1 below).

Most studies included in this review consider the exposure age of a moraine, as represented by the mean boulder exposure age or some subset of boulder exposure ages  $\pm 1\sigma$  or  $2\sigma$  uncertainty, to represent the time when the moraine was last occupied by a glacier margin. Many studies have also computed the maximum probable age using cumulative probability or normal kernel density estimates (informally known as "camel plots") and interpret this to represent the time when the moraine was last occupied by ice. Such interpretations are based on the logic that erratic boulders on the moraine crest were the last material deposited before the glacier abandoned the moraine due to terminus retreat or surface lowering. Some studies, however, have interpreted exposure ages in other ways. For example, Munroe et al. (2006) reported the inverse error-weighted mean as the time when moraines in the Uinta Mountains were last occupied by glacier termini. This approach tends to weight younger exposure ages (which have lower age uncertainties at  $1\sigma$  or  $2\sigma$ ) to a greater degree than older exposure ages, which can be problematic for moraines that have experienced degradation. Additionally, some studies, including the seminal study by Gosse et al. (1995a) involving <sup>10</sup>Be exposure dating of terminal moraines in the western Wind River Range, interpreted the range of exposure ages to represent the duration of moraine occupation by ice instead of the using the mean or error-weighted mean. This approach would be appropriate in cases where all boulder exposure ages reflect the time of deposition and do not reflect any prior exposure or post-depositional processes. Later studies, however, have emphasized the high probability that postdepositional processes affect at least some exposure ages (as described above), suggesting that either the mean or the oldest exposure age best represents the true depositional age of the moraine crest.

Other considerations for interpreting cosmogenic chronologies include the possible differences of exposure ages of lateral moraines verses end moraines, both of which have been reported to represent the ages of Pleistocene glaciations. If the start of ice retreat from an end moraine is accompanied by thinning, then every point along the crest of a latero-frontal moraine loop would be abandoned at the same time. Alternatively, if ice terminus retreat and thinning do not occur at the same time, then terminal and lateral moraines could yield different exposure ages. Potential age differences between lateral and end moraines in the same valley are discussed in studies of Late Pleistocene moraine morphology in the Teton Range (Thackray and Staley, 2017; Pierce et al., 2018) and are evident in some sets of exposure ages of lateral and end moraines from the same valley included in this review. Most of the TCN studies compiled in our review report exposure ages of boulders atop segments of lateral or frontal moraines, but not both, and hence we do not consider age differences between

these positions.

### 4. Exposure chronologies of moraines in space and time

The following sections describe the recalculated exposure ages of glacial deposits (chiefly moraines) in the western U.S. The review focuses on terminal moraines (the ice-distal ridge delimiting the maximum glacier length) of the last two glaciations and downvalley recessional moraines of the last glaciation (where available) that delimit glacier lengths within >75% of the maximum. The recessional moraines represent near-maximum positions that were occupied by the glacier front within a few millennia after the terminal moraine was abandoned and likely reflect a stabilization or readvance in response to a significant shift in glacier mass balance. We do not include exposure ages of glacially scoured bedrock or recessional moraines further upvalley that represent much retracted glacier lengths; the latter are abundant in the western U.S. and were recently reviewed by Marcott et al. (2019). Exposure ages of all moraines and outwash discussed here are available in Tables S1-S3 along with all the necessary sample information and data for recalculating exposure ages with other production models. Sample information for most TCN chronologies reviewed here is also available in the Informal Cosmogenic Exposure-age Database (ICE-D Alpine; http://alpine.ice-d.org/allsites/North\_America). For most sets of recalculated exposure ages of moraines considered for this review, we follow the interpretative approach of the authors of the original ages to estimate the age of each moraine and consider the differences between the mean and oldest exposure ages of moraines and outwash of the penultimate glaciation. For all moraines and outwash surfaces shown in Tables S1-S3, the mean exposure age with 1<sub>o</sub> uncertainty of each moraine with and without outliers identified in original reports is computed along with the  $\chi^2$ r statistic of all or a subset of the exposure ages of each

### 4.1. The penultimate glaciation (MIS 6)

Compared to the number of exposure ages of glacial deposits and landforms of the last Pleistocene glaciation, available exposure ages of moraines from earlier glaciations are much scarcer but have expanded in recent years (e.g., Wesnousky et al., 2016; Brugger et al., 2019a; Schweinsberg et al., 2020). Exposure ages are available for moraines and other glacial features representing the Tahoe Glaciation in the Sierra Nevada (as termed by Blackwelder, 1931), the Lamoille Glaciation in the Great Basin/Basin and Range (as termed by Sharp, 1938), and the Bull Lake Glaciation in the Rocky Mountains (as termed by Blackwelder, 1915), all of which have been assumed to represent the penultimate glaciation. For all applications of exposure dating to deposits older than the last Pleistocene glaciation, the potential effects of boulder-surface erosion on in situ nuclide inventory have been considered along with other processes that may have resulted in incomplete exposure of erratic boulders at the moraine crest. In this section, all published exposure ages for pre-LGM moraines representing the penultimate glaciation have been recalculated, with the exception of ages in studies that used the same production models used here, such as Licciardi and Pierce (2018), Brugger et al. (2019a), and Schweinsberg et al. (2020). Sites with exposure-dated pre-LGM moraines include the Sierra Nevada (Phillips et al., 2009; Rood et al., 2011; Wesnousky et al., 2016), the Cascade Range (Porter and Swanson, 2008; Speth et al., 2018), the Greater Yellowstone region (Licciardi and Pierce, 2008, 2018), the Wind River Range (Phillips et al., 1997; Dahms et al., 2018), the Colorado Plateau (Marchetti et al., 2011), the Southern Rocky Mountains in Colorado (Briner, 2009; Brugger et al., 2019a; Schweinsberg et al., 2020), and the Ruby Mountains (Wesnousky et al., 2016) (Fig. 1). Exposure ages of pre-LGM moraines in the northern Cascade Range are based entirely on whole-rock <sup>36</sup>Cl measurements, as are ages of some moraines in the Sierra Nevada and Wind River ranges. Pre-LGM moraines at the Fish Lake Plateau (Utah) and the southern Cascade Range (Oregon) are dated using cosmogenic <sup>3</sup>He (Marchetti et al., 2011; Speth et al., 2018). Elsewhere, chronologies of moraines of the penultimate glaciation are based on <sup>10</sup>Be exposure dating. Many applications of TCN exposure dating to moraines of the penultimate glaciation have assumed boulder-surface erosion rates, whereas a few (e.g., Phillips et al., 1997) have attempted to measure it. The potential for differing boulder-surface erosion rates among glacial valleys in the western U.S. and elsewhere is difficult to assess, which may complicate age comparisons. Here, we report exposure ages using the boulder-surface erosion rate inferred (or measured) in the original reports.

### 4.1.1. The Sierra Nevada (California)

The Sierra Nevada (Fig. 2) features the largest number of exposure ages of moraines and outwash of the penultimate glaciation (termed the Tahoe Glaciation; Blackwelder, 1931). Multiple recent studies have generated <sup>10</sup>Be and <sup>36</sup>Cl exposure ages, chiefly along the eastern front of the range (Phillips et al., 2009; Rood et al., 2011; Wesnousky et al., 2016). The greatest concentration of exposure ages of moraines mapped as Tahoe age are from the Bishop Creek valley, where Phillips et al. (2009) report <sup>36</sup>Cl exposure ages of a suite of glacial deposits mapped as Tahoe 1 (oldest) to Tahoe 6 (youngest) and rely chiefly on the oldest <sup>36</sup>Cl exposure ages from each map unit to limit the time of the penultimate glaciation. Recalculated <sup>36</sup>Cl exposure ages that assume 1.1 mm/kyr erosion (inferred by Phillips et al., 2009) are generally younger than the originally reported ages and are highly variable, the latter being attributed to moraine-crest degradation by Phillips et al. (2009; Table S2). The oldest recalculated <sup>36</sup>Cl exposure ages from the morpho-stratigraphically oldest (Tahoe 1) and youngest (Tahoe 6) deposits there have respective  $^{36}$ Cl exposure ages of ca. 154  $\pm$  4 ka (based on samples BCPR90-28, 29, 30, 32; Table S2) and  $125 \pm 9$  ka (Table 1). The Tahoe-equivalent terminal moraines at Woodfords in the northeastern Sierra Nevada studied by Wesnousky et al. (2016) have an oldest exposure age of  $66.1 \pm 3.1$  ka (assuming zero erosion following Wesnousky et al., 2016; Table S1). The oldest recalculated exposure ages of outwash immediately downstream of the moraines are 146  $\pm$  2 ka and 133  $\pm$  3 ka, and these outwash surface ages are deemed to place more reliable limits on the time of Tahoe glaciation. Rood et al. (2011) assume a boulder surface erosion rate of 0.6 mm/kyr; given this rate, the oldest recalculated <sup>10</sup>Be exposure ages of Tahoe-age moraines at Robinson Creek, Virginia Creek, and Sonora Junction are 133  $\pm$  4 ka, 143  $\pm$  3 ka, and 114  $\pm$  3 ka, respectively. Rood et al. (2011) also report an exposure age of the Tahoe moraine at Green Creek, but with "low confidence" due to the variability of exposure ages. The oldest recalculated exposure age of this surface is 183  $\pm$  4 ka. The oldest recalculated  $^{10}$ Be exposure age of a Tahoe outwash surface at Buckeye Creek is  $148 \pm 2 \text{ ka (Table 1)}.$ 

Overall, the recalculated exposure ages of penultimateglaciation moraines in the Sierra Nevada have oldest individual or oldest groupings of exposure ages of corresponding to the latter part of MIS 6, with the exception of the Tahoe moraine at Woodfords. As noted by Wesnousky et al. (2016), exposure ages of Tahoe outwash surfaces are older than some, but not all, moraines deposited during the same glaciation.

### 4.1.2. The Cascade Range (Oregon and Washington)

On the eastern side of the northern Cascade Range (Fig. 1), Porter and Swanson (2008) report <sup>36</sup>Cl exposure ages for a suite of moraines in Icicle Creek, including ages of three sets of moraines

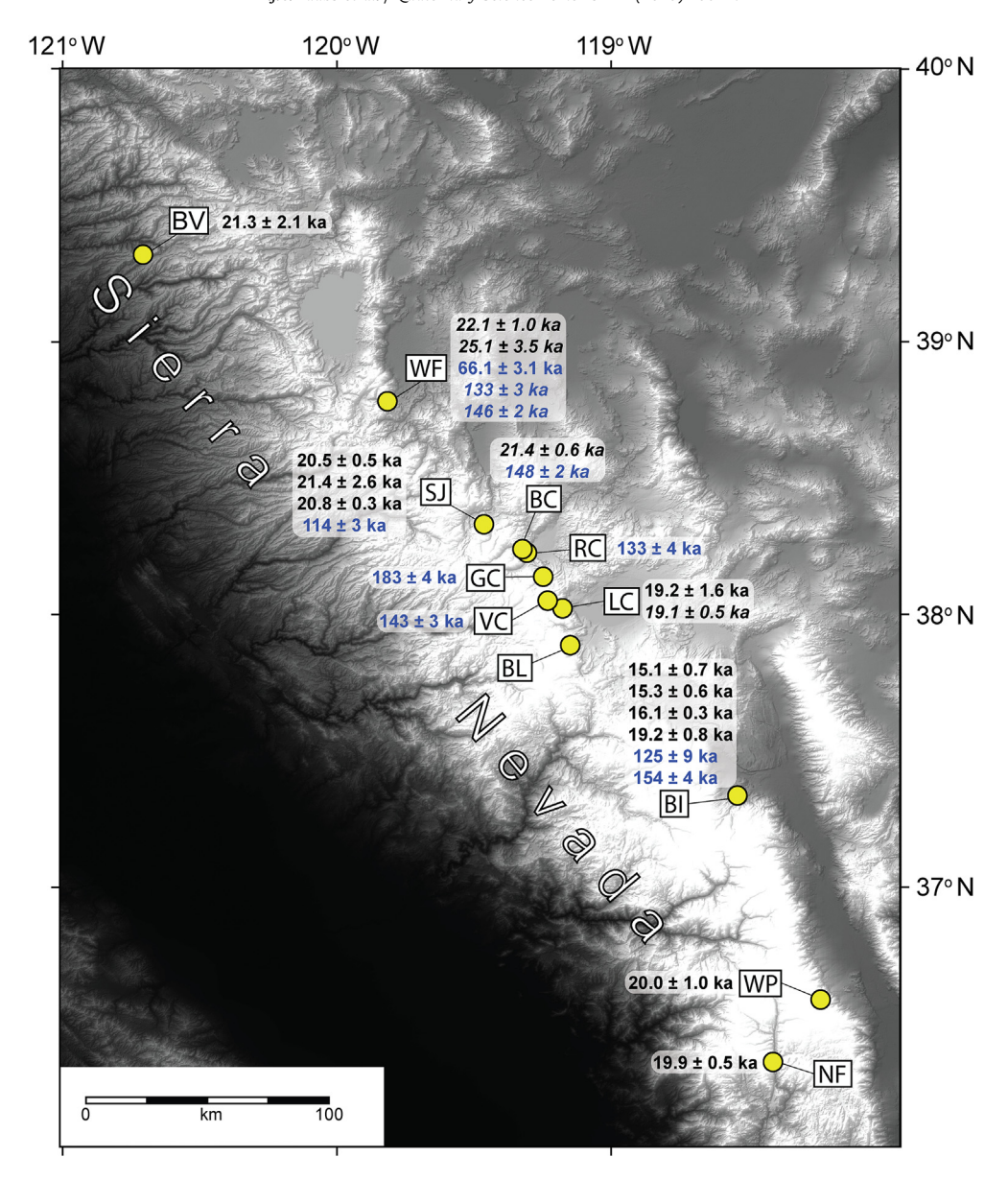


Fig. 2. Digital elevation map of the glaciated portion of the Sierra Nevada. Yellow circles indicate sites with exposure ages of moraines and outwash of the last glaciation (shown in black) and penultimate glaciations (shown in blue). Exposure ages of moraines (unitalicized) and outwash (in italics) of the last glaciation (black) are the mean  $\pm$  1 $\sigma$ , and exposure ages of penultimate glaciation moraines and outwash are the oldest or oldest grouping of exposure ages (blue,  $\pm$  1 $\sigma$  internal uncertainty). BV = Bear Valley (James et al., 2002), WF = Woodfords (Rood et al., 2011; Wesnousky et al., 2016), SJ = Sonora Junction, BC = Buckeye Creek, RC = Robinson Creek, GC = Green Creek, LC = Lundy Canyon, VC = Virginia Creek (Rood et al., 2011), BL = Baboon Lakes (see Marcott et al., 2019 for <sup>10</sup>Be exposure ages of cirque floor moraines), BI = Bishop Creek (ages recalculated from Phillips et al., 2009), WP = Whitney Portal (ages recalculated from Benn et al., 2006), and NF = Soda Springs (ages recalculated from Amos et al., 2010). See Tables S1 and S2 for mean and individual exposure ages from each site.

that predate the last Pleistocene glaciation. Porter and Swanson (2008) assume a boulder-surface erosion rate of 2 mm/kyr and favor a mean  $^{36}\text{Cl}$  exposure age as the depositional age of these moraines (after removing outliers from consideration), although the high coefficient of variation for these age populations (Table 1) suggests that the oldest exposure age may be more accurate. Recalculated ages reported here are significantly older than originally reported due to differences between the locally calibrated production rate used by Porter and Swanson (2008) and the globally calibrated production model used here (as implemented in CRONUScalc; differences shown in Table 1). The recalculated oldest exposure age of the outer (Peshashtin) moraine is 131  $\pm$  2 ka; the oldest exposure ages of the inner moraines (pre-Mountain Home and Mountain Home, respectively) are 135  $\pm$  6 ka and 117  $\pm$  3 ka (Table 1).

In the southern Cascade Range, Speth et al. (2018) report  $^3$ He exposure ages of two pre-LGM moraines near Klamath Lake computed with the Version 3 Calculator and an assumed boulder-surface erosion rate of 1 mm/kyr. These ages are recalculated here with the Tabernacle Hill calibration for consistency with other  $^3$ He exposure age calculations. Individual exposure ages atop the older of the two moraines are variable (*Table S3*) and Speth et al. (2018) interpret the oldest individual age as the best estimate of the depositional age of the moraine. The oldest recalculated exposure age is  $165 \pm 6$  ka (Table 1). The younger of the two moraines also displays variable  $^3$ He exposure ages, with an older grouping of four exposure ages that Speth et al. (2018) interpret to represent the depositional age of the moraine. The mean recalculated exposure age of the older grouping is  $95.1 \pm 5.7$  ka (Tables 1 and S3).

 Table 1

 Cosmogenic exposure ages of moraines and outwash of the penultimate glaciation.

Sample name/ locality	Originally reported mean age ± 1s (ka)	n	_	% diff. from originally reported age	C.V. (%) <sup>b</sup>	Skewness	Recalc. oldest age(s) ± 1s (ka)	External or total uncertainty (kyr) <sup>c</sup>	Erosion rate used in age calculations (cm kyr-1)	oldest	External or total uncertainty (kyr) <sup>c</sup>	Source
SIERRA NEVADA												
Robinson Creek, Tahoe moraine	121 ± 8 <sup>a</sup>	5	122 ± 7	0.3	32	-0.49	133 ± 4	7	6.0E-04	125 ± 3	6	Rood et al. (2011)
Buckeye Creek, Tahoe outwash	$148\pm2^{a}$	4	148 ± 2	-0.1	13	-0.13	148 ± 2	7	6.0E-04	137 ± 2	6	Rood et al. (2011)
Sonora Junction, Tahoe	$77.6 \pm 25.1$	10	79.4 ± 24.9	2.3	31	-0.04	114 ± 3	6	6.0E-04	108 ± 3	5	Rood et al. (2011)
moraine Virginia Creek, Tahoe	$53.4 \pm 43.0$	8	52.3 ± 40.5	-2.1	77	1.88	143 ± 3	7	6.0E-04	132 ± 2	6	Rood et al. (2011)
moraine Woodfords, Tahoe	37.2 ± 13.8	5	41.6 ± 15.9	11.8	38	1.09	66.1 ± 3.1	4	0	66.1 ± 3.1	4	Wesnousky et al. (2016)
moraine Woodfords, Tahoe	101 ± 25	3	116 ± 28	14.9	24	0.89	146 ± 2	6	0	146 ± 2	6	Wesnousky et al. (2016)
outwash A Woodfords, Tahoe	108 ± 33	3	112 ± 33	-3.0	29	-1.66	133 ± 3	5	6.0E-04	125 ± 2	5	Rood et al. (2011)
outwash B Bishop Creek, Tahoe 1 ( <sup>36</sup> Cl)	124 ± 36	12	131 ± 45	5.6	35	0.45	154 ± 4	15	1.1E-03	160 ± 12	21	Phillips et al. (2009)
Bishop Creek, Tahoe 6 ( <sup>36</sup> Cl)	$114 \pm 16^a$	4	109 ± 13	-4.4	41	-1.76	125 ± 9	14	1.1E-03	$122 \pm 6$	12	Phillips et al. (2009)
CASCADE RANGE North Cascade - Mountain Home ( <sup>36</sup> Cl)	$70.9 \pm 1.5^{a}$	6	94.7 ± 13.2	33.6	14	-0.74	117 ± 3	24	2.7E-03	171 ± 6	37	Porter and Swanson (2008)
North Cascade - Pre-Mountain Home ( <sup>36</sup> Cl)	$93.1 \pm 2.6^{a}$	3	123 ± 10	32.1	8	1.29	135 ± 6	27	2.7E-03	178 ± 7	32	Porter and Swanson (2008)
North Cascade - Peshashtin 1 (36Cl)	105 ± 2	8	122 ± 7	15.7	6	-0.11	131 ± 2	30	2.7E-03	182 ± 7	41	Porter and Swanson (2008)
South Cascade - Threemile older ( <sup>3</sup> He)	mean not reported	-	-	_	75	0.85	165 ± 6	10	1.0E-03	143 ± 4	8	Speth et al. (2018)
South Cascade - Sevenmile intermediate ( <sup>3</sup> He)	mean not reported	-	95.1 ± 5.7 <sup>a</sup>	_	49	-0.13	95.1 ± 5.7	7	1.0E-03	87.9 ± 5	6	Speth et al. (2018)
BASIN AND RANG Ruby Mountains - Lamoille		10	128 ± 15	0.0	12	-0.40	150 ± 6	7	6.0E-04	139 ± 6	8	this study
- Lamonie Ruby Mountains - Seitz	$93.9 \pm 27.5$	5	93.9 ± 27.5	0.0	28	-0.73	122 ± 17	17	6.0E-04	115 ± 15	16	this study
Ruby Mountains - Hennen	34.9 ± 14.6	15	37.9 ± 15.9	8.6	42	2.32	87.3 ± 1.5	4	0	87.3 ± 1.5	4	Wesnousky et al. (2016)
COLORADO PLATE Fish Lake Plateau - Jorgensen ( <sup>3</sup> He)		4	118 ± 32	-4.8	27	-1.25	141 ± 5	7	0	141 ± 5	7	Marchetti et al. (2011)
ROCKY MOUNTAL Southern Jackson Hole	NS - <i>GREATER YI</i> 136 ± 13ª		OWSTONE RE 133 ± 13		21	-1.67	150 ± 4	7	1.0E-03	132 ± 2	5	Licciardi and Pierce (2008, 2018)
MIDDLE AND SOL Wind River - Bull			UNTAINS 86 ± 36	-8.7	42	1.90	140 ± 6	26	0	140 ± 6	26	Phillips et al.
Lake II ( <sup>36</sup> Cl) Wind River - Bull Lake XIII ( <sup>36</sup> Cl)		4	97 ± 11	-5.8	11	-0.99	$106 \pm 4$	13	0	106 ± 4	13	(1997) Phillips et al. (1997)
24.10 mi ( Ci)	108 ± 14	7	95 ± 13	-12.0	14	-0.06	110 ± 5	13	0	110 ± 5	13	Phillips et al. (1997)

 $(continued\ on\ next\ page)$ 

Table 1 (continued)

Sample name/ locality	Originally reported mean age ± 1s (ka)		Recalc. mean age ± 1s (ka)	% diff. from originally reported age	C.V. (%) <sup>b</sup>	Skewness	Recalc. oldest age(s) ± 1s (ka)	External or total uncertainty (kyr) <sup>c</sup>	Erosion rate used in age calculations (cm kyr-1)	Zero-erosion oldest exposure age(s) (ka)	External or total uncertainty (kyr) <sup>c</sup>	Source
Wind River - Fremont Lake ( <sup>36</sup> Cl)										_		
Wind River - Nicholas	$127 \pm 35$	3	$120 \pm 32$	-5.5	27	0.09	$152 \pm 6$	10	2.0E-03	119 ± 1	10	Dahms et al. (2018)
Mosquito Range - Iowa Gulch	130 ± 5	2	130 ± 5	0.0	4	N/A	133 ± 3	7	1.0E-03	118 ± 3	7	Brugger et al. (2019a)
Elk Range - Ziegler Reservoir ( <sup>10</sup> Be only)	138 ± 12	1	145 ± 4	5.1	N/A	N/A	145 ± 4	7	0	145 ± 4	7	Mahan et al. (2014)
Sawatch - Dry Gulch	$43.8 \pm 15.8$	9	43.3 ± 15.9	-1.1	37	1.30	$71.7 \pm 1.6$	3.2	0	$71.7 \pm 1.6$	3.2	Briner (2009)
Sawatch - Clear Creek	$164 \pm 28^{a}$	3	$164 \pm 28$	0.0	17	-1.37	$133.4 \pm 0.1^{a}$	6.0	1.0E-03	$120 \pm 0.1$	4.6	Schweinsberg et al. (2020)
Sawatch - Lake Creek	125 ± 7	4	125 ± 7	0.0	6	0.08	132.3 ± 1.1 <sup>d</sup>	8.0	1.0E-03	$119.2 \pm 0.8$	4.7	Schweinsberg et al. (2020)

<sup>&</sup>lt;sup>a</sup> Excludes outliers identified in original report.

# 4.1.3. The Basin and Range and Colorado Plateau (Nevada and Utah)

Three sites in the Nevada sector of the Basin and Range (Fig. 3) have produced exposure ages of moraines mapped as representing the penultimate glaciation in the Ruby Mountains. Wesnousky et al. (2016) report  $^{10}$ Be exposure ages (n = 15) of a lateral moraine in Hennen Canyon in the western Ruby Mountains, assuming zero erosion of boulder surfaces.  $^{10}$ Be exposure ages (n = 10) of a broad, hummocky terminal moraine at the mouth of Lamoille Canyon, the type locality for the penultimate glaciation in the Great Basin (Sharp, 1938) are reported here for the first time, along with <sup>10</sup>Be exposure ages (n = 5) from a right lateral moraine in Seitz Canyon, neighboring to the north of Hennen Canyon. Many of these boulders display evidence of surface erosion; their exposure ages are computed using an assumed boulder-surface erosion rate of 0.6 mm/yr, following that of Rood et al. (2011) in the Sierra Nevada. The exposure ages from Hennen Canyon span a considerably broad range of 24.3  $\pm$  0.6 ka to 87.3  $\pm$  1.5 ka, with most ages concentrated at the younger end of this range. <sup>10</sup>Be exposure ages for moraines in Seitz Canyon, with a similar morphology to those in Hennen Canyon, span  $51.7 \pm 1.8$  ka to  $122 \pm 17$  ka. The new exposure ages from Lamoille Canyon show a bimodal distribution, with the older group of six ages averaging  $150 \pm 6$  ka and younger ages ranging from 123 to 110 ka (Table S1). The disparity of exposure ages among the pre-LGM moraines in Lamoille, Seitz, and Hennen Canyon suggests they formed at different times, as discussed below.

Another setting with exposure ages of a moraine from the penultimate glaciation is at Fish Lake Plateau (Fig. 4), situated in central Utah in the northwestern sector of the Colorado Plateau (Marchetti et al., 2011). Here, Marchetti et al. (2011) sampled a moraine representing the penultimate glaciation north of Fish Lake for  $^3$ He dating, inferring negligible erosion of trachyandesite boulder surfaces. Recalculated zero-erosion exposure ages of boulders atop this moraine span 75 to 147 ka (n = 4, Table S3). The mean of the two oldest ages is  $141 \pm 5$  ka, which Marchetti et al. (2011) interpret as the depositional age of the moraine.

## 4.1.4. The Greater Yellowstone region (Wyoming, Montana, and Idaho)

In the Greater Yellowstone region (Fig. 5), boulders distributed

along a pre-LGM ice limit in southern Jackson Hole were sampled by Licciardi and Pierce (2008) for <sup>10</sup>Be exposure dating. The ice limit is demarcated by low-relief, bouldery ridges that retain recognizable moraine morphology and define the southernmost extent of the Yellowstone ice complex during the penultimate (Bull Lake) glaciation (Pierce and Good, 1992; Pierce et al., 2018). Licciardi and Pierce (2018) recalculate the <sup>10</sup>Be exposure ages from these moraine ridges (n = 8; originally reported in Licciardi and Pierce (2008)) using the same production rate and scaling model combination used here and an estimated boulder-surface erosion rate of 1 mm/kyr. They infer that post-depositional processes are the most likely cause of the broad range of exposure ages (Table S1), which is consistent with the negative skew of the age distribution of -1.66(cf., Applegate et al., 2012, Table 1). They further suggest that the two oldest  $^{10}$ Be exposure ages of 147  $\pm$  2 and 153  $\pm$  2 ka, with a mean of 150  $\pm$  4 ka (1 $\sigma$ ), are most representative of the true age of the moraine (Licciardi and Pierce, 2018).

# 4.1.5. Middle and Southern Rocky Mountains (Wind River, Sawatch, and Mosquito Ranges)

Glacial features of the penultimate glaciation are especially well-preserved in the Wind River Range in Wyoming (Fig. 1), the type locality for the penultimate glaciation in the Rocky Mountains. Phillips et al. (1997) sampled erratic boulders across a well-mapped suite of moraine crests (described in Chadwick et al., 1997) to limit times of moraine deposition. They measured <sup>10</sup>Be and <sup>36</sup>Cl nuclide concentrations from the same boulders to infer that surface erosion rates were negligible; therefore, only zero-erosion exposure ages are recalculated here. The recalculated <sup>36</sup>Cl exposure ages are more variable, and generally younger than the originally reported ages (Table 1), reflecting the updated production rates for the various production pathways for <sup>36</sup>Cl (see Marrero et al., 2016b). The oldest exposure ages from this valley are  $140 \pm 6$  ka for the outermost moraine crest and  $106 \pm 4$  ka for the innermost crest. Additionally, Phillips et al. (1997) obtained <sup>36</sup>Cl exposure ages for a wellpreserved moraine representing the penultimate glaciation at Fremont Lake. The oldest exposure age of this moraine is  $110 \pm 5$  ka. Recently published <sup>10</sup>Be exposure ages of a Bull-Lake equivalent moraine in the southeastern Wind River Range vary greatly, with an oldest age of  $152 \pm 6$  ka based on an assumed erosion rate of 2 mm/

<sup>&</sup>lt;sup>b</sup> Coefficient of variation calculated for all TCN exposure ages of moraine/outwash reported in the source.

<sup>&</sup>lt;sup>c</sup> The uncertainty of the AMS measurement, attenuation rate of cosmic radiation, sample thickness, and production rate. Termed "external" uncertainty by the Version 3 Calculator and "total" uncertainty by CRONUSCalc.

<sup>&</sup>lt;sup>d</sup> The mean exposure age (n = 4) of this surface is shown in Fig. 7 instead of the oldest individual exposure age.

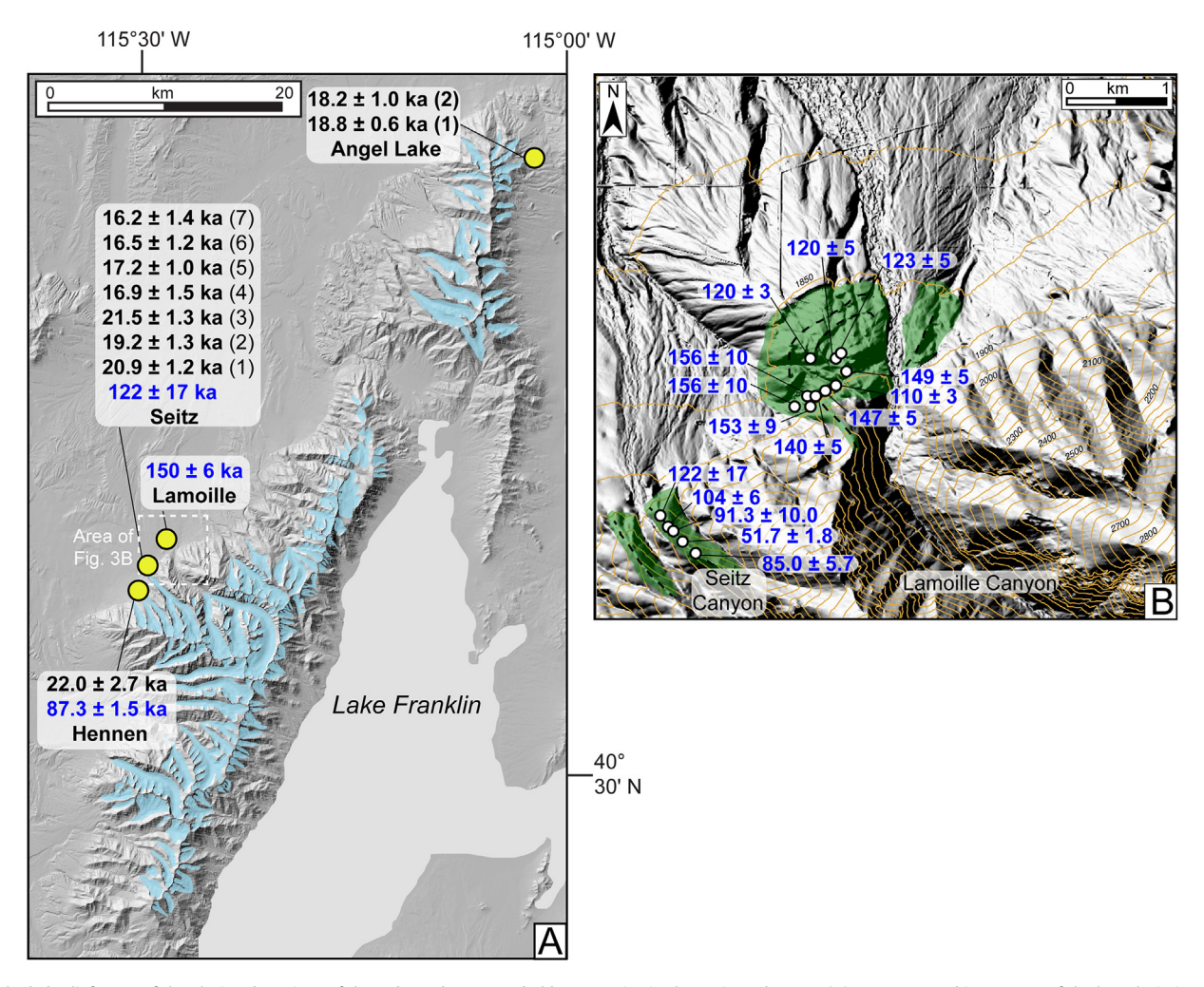


Fig. 3. Shaded relief maps of the glaciated portions of the Ruby and East Humboldt Mountains in the Basin and Range. (A) Reconstructed ice extents of the last glaciation (shaded blue) west of pluvial Lake Franklin. (B) Individual <sup>10</sup>Be exposure ages (ka,  $\pm$  1 $\sigma$ ) of the type Lamoille moraine and the penultimate glaciation moraine at Seitz Canyon (B). Yellow circles in panel A indicate sites with TCN exposure ages of terminal and recessional moraines of the last glaciation and moraines of the penultimate glaciation. Mean  $\pm$  1 $\sigma$  <sup>10</sup>Be exposure ages of last glaciation moraines (black) and oldest <sup>10</sup>Be exposure ages of penultimate glaciation moraines (blue,  $\pm$  1 $\sigma$  internal uncertainty) are from Laabs et al. (2013), Munroe et al. (2015), and Wesnousky et al. (2016). The sequence of moraines of the last glaciation at Seitz Canyon is numbered 1–7 (1 = oldest) as shown in Tables 2 and 3. On panel B, white circles represent locations of erratic boulders atop the broad hummocky moraine at Lamoille Canyon and the narrow lateral moraines at Seitz Canyon (new ages in ka  $\pm$  1 $\sigma$  internal uncertainty are given), both of the penultimate glaciation. Mapped extents of the moraines are shaded green with black dashed lines tracing ridge crests. See Table S1 for mean and individual exposure ages of all moraines shown here.

kyr (see Dahms et al. (2018) for discussion). While the differing boulder-surface erosion rates assumed among glacial valleys in the Wind River Range are justified in the original reports, it complicates the comparison of the <sup>36</sup>Cl and <sup>10</sup>Be exposure ages of moraines of the penultimate glaciation in this study area.

Briner (2009) reported  $^{10}$ Be exposure ages of cobbles and boulders on moraines in the central Sawatch Range in Colorado (Figs. 1 and 6). This study focused on differences between  $^{10}$ Be exposure ages of boulders and cobbles atop moraines, including one moraine believed to represent the penultimate glaciation in Dry Gulch valley. Recalculated exposure ages of this moraine postdate the interval of MIS 6, ranging from  $29.5 \pm 0.5$  to  $71.7 \pm 1.6$  ka (Table S1) and were considered by Briner (2009) to be anomalously young and not representative of the time of the penultimate glaciation. Just north of the drainage studied by Briner (2009), Schweinsberg et al. (2020) developed  $^{10}$ Be exposure ages from boulders on terminal moraines mapped as Bull Lake deposits in the Lake Creek and Clear Creek valleys. The exposure ages reported by Schweinsberg et al. (2020) were computed using the same  $^{10}$ Be Promontory Point-LSDn scheme used here and an inferred boulder-

surface erosion rate of 1 mm/kyr. Four boulders on the Bull Lake moraine at Lake Creek yield exposure ages ranging from  $118\pm1$  ka to  $132\pm1$  ka with an average of  $125\pm7$  ka. Exposure ages from boulders on the Bull Lake moraine at Clear Creek are more scattered and include ages of  $187\pm2$  ka,  $172\pm2$  ka, and  $133\pm1$  ka, excluding one young outlier. The two oldest boulder ages at Clear Creek are ascribed to 10Be inheritance, while the distribution of the remaining exposure ages from Bull Lake moraines reported by Schweinsberg et al. (2020) is comparable to the variability observed in 10Be exposure ages of other moraines of the penultimate glaciation reviewed here.

Finally, two recent studies report exposure ages in ranges neighboring the Sawatch in southern Colorado (Fig. 1). In the Elk Range (west of the Sawatch Range), Mahan et al. (2014) report  $^{10}$ Be and  $^{26}$ Al ages of a single boulder atop a moraine near Snowmass Village. Although an exposure age of a single boulder is by itself insufficient to limit the age of a moraine, the recalculated  $^{10}$ Be and  $^{26}$ Al exposure ages of  $145 \pm 4$  ka and  $137 \pm 5$  ka agree with independent minimum-age limits on the moraine crest reported by Mahan et al. (2014). In the Mosquito Range (east of the Sawatch

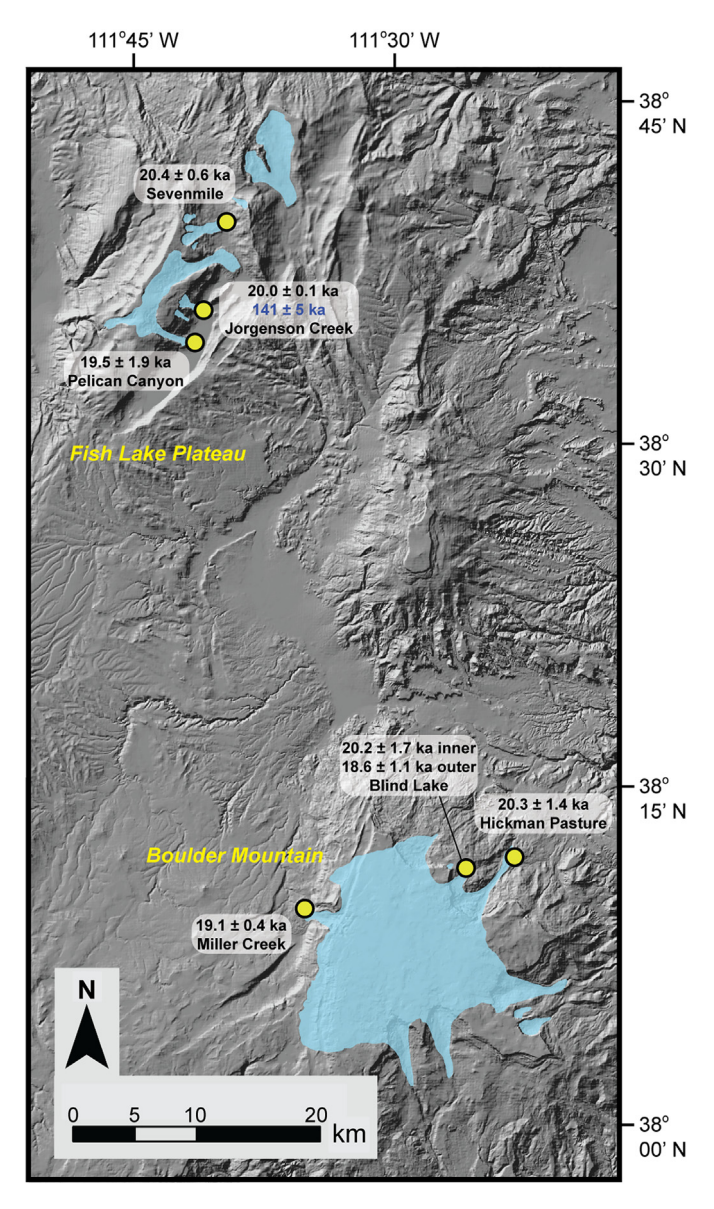


**Fig. 4.** Shaded relief map and reconstructed Pleistocene ice extents of the last glaciation at Fish Lake Plateau and Boulder Mountain, Utah. Glaciated areas are shaded blue. Mean  $^3$ He exposure ages ( $\pm 1\sigma$ ) of terminal moraines of the last glaciation (black) and oldest exposure ages of penultimate glaciation moraines (blue) are recalculated from Marchetti et al. (2005, 2007, 2011). See Table S3 for mean and individual exposure ages.

Range), a recent study by Brugger et al. (2019a) reports two  $^{10}$ Be exposure ages of 127  $\pm$  4 ka and 133  $\pm$  3 ka (Table 1) from a penultimate glaciation moraine in lowa Gulch based on the same production and scaling models used here and assuming a 1 mm/kyr erosion rate of boulder surfaces.

### 4.1.6. Discussion of recalculated exposure ages of Pre-LGM moraines

Recalculated exposure ages of moraines of the penultimate glaciation differ from original reports to varying degrees. Generally, the recalculated <sup>3</sup>He exposure ages are nearly equivalent to previously reported ages because the SLHL production rate estimates for <sup>3</sup>He have changed only slightly through recalibration efforts. For the other TCNs, the recalculated <sup>10</sup>Be exposure ages tend to differ less from previous reports than recalculated <sup>36</sup>Cl exposure ages

(Table 1). The largest adjustments are found for recalculated <sup>36</sup>Cl exposure ages of moraines in the northern Cascade Range, which are 16%–34% older than those originally reported. This result reflects the disparity between the anomalously high production rates used in Porter and Swanson (2008) and the newer <sup>36</sup>Cl production models implemented in CRONUScalc (Marrero et al., 2016b). The recalculated <sup>36</sup>Cl exposure ages of moraines in the Wind River Range (Phillips et al., 1997) are younger than originally reported by 6%–9%. Among the <sup>10</sup>Be exposure ages of moraines and outwash of the penultimate glaciation, recalculated ages are 12%–15% older than originally reported from the Sierra Nevada and 9% older than those reported from the Ruby Mountains (Wesnousky et al., 2016) (Table 1). All other recalculated exposure ages differ from original reports by about 5% or less, which is within the uncertainty of TCN production rates over the past 10<sup>5</sup> yr.

Assessing the accuracy of TCN exposure ages of moraines deposited during pre-MIS 2 glaciations is challenging in part because of uncertainties regarding boulder-surface exposure history, as discussed by Wesnousky et al. (2016). Denudation of moraine crests and attendant boulder exhumation, variable rates of boulder surface erosion, and intermittent sediment or snow cover could result in inconsistent exposure of boulder surfaces. Many studies of pre-MIS 2 moraines, along with numerical modeling of moraine slope processes, have concluded that moraine-crest denudation is the most likely process contributing to the variability of exposure ages on older features (e.g., Putkonen and Swanson, 2003; Applegate et al., 2012). Pre-MIS-2 moraines have endured longer intervals of erosion along with one or more stadials during which hillslope processes on moraines were presumably accelerated. These realities are likely responsible for the high coefficient of variation of exposure ages atop pre-MIS 2 moraines (averaging 28%; Table 1). Furthermore, modeling studies predict that exposure ages of a moraine that has undergone continuous degradation will be skewed toward younger ages (Applegate et al., 2012). This pattern is observed as skew <0 for 11 of 21 pre-MIS 2 moraines compiled here (Table 1). In contrast, 9 of 21 pre-MIS 2 moraines compiled here exhibit positively skewed exposure-age distributions (skew > 0; Table 1). These positively skewed age distributions could reflect boulders with inherited nuclide inventory (Applegate et al., 2012), although all of these moraines were interpreted in their original reports as having experienced crest denudation based on the distribution of the exposure ages. Positive skew may also be expected if denudation rates vary through time.

Comparisons of exposure ages of moraines and outwash surfaces by Hein et al. (2009) and Wesnousky et al. (2016) suggest that outwash surfaces are not subject to the same degree of degradation as moraine crests and might therefore be more suitable for exposure dating, particularly for pre-MIS-2 landforms. Wesnousky et al. (2016) emphasizes this point based on the observation that outwash surfaces of the penultimate (Tahoe) glaciation in the Sierra Nevada have older and less variable <sup>10</sup>Be exposure ages compared to Tahoe moraines. This observation applies to the mean, but not the oldest, exposure ages of moraines when compared to outwash surfaces in the Sierra Nevada, however. Typically, the oldest individual or oldest grouping of exposure ages of moraines overlaps with exposure ages of outwash surfaces. For example, the Woodfords outwash surface yields oldest  $^{10}$ Be exposure ages of  $146 \pm 2$  ka and  $125 \pm 2$  ka ( $1\sigma$ , recalculated from Wesnousky et al., 2016, and Rood et al., 2011, respectively; Table 1). While these exposure ages are ~60-80 kyr older than the oldest exposure age of the corresponding Tahoe moraine at Woodfords, they overlap with the oldest <sup>10</sup>Be exposure ages of Tahoe moraines in other glacial valleys of the Sierra Nevada. The older exposure age of  $146 \pm 2$  ka for Woodfords outwash overlaps with oldest 10Be exposure ages of

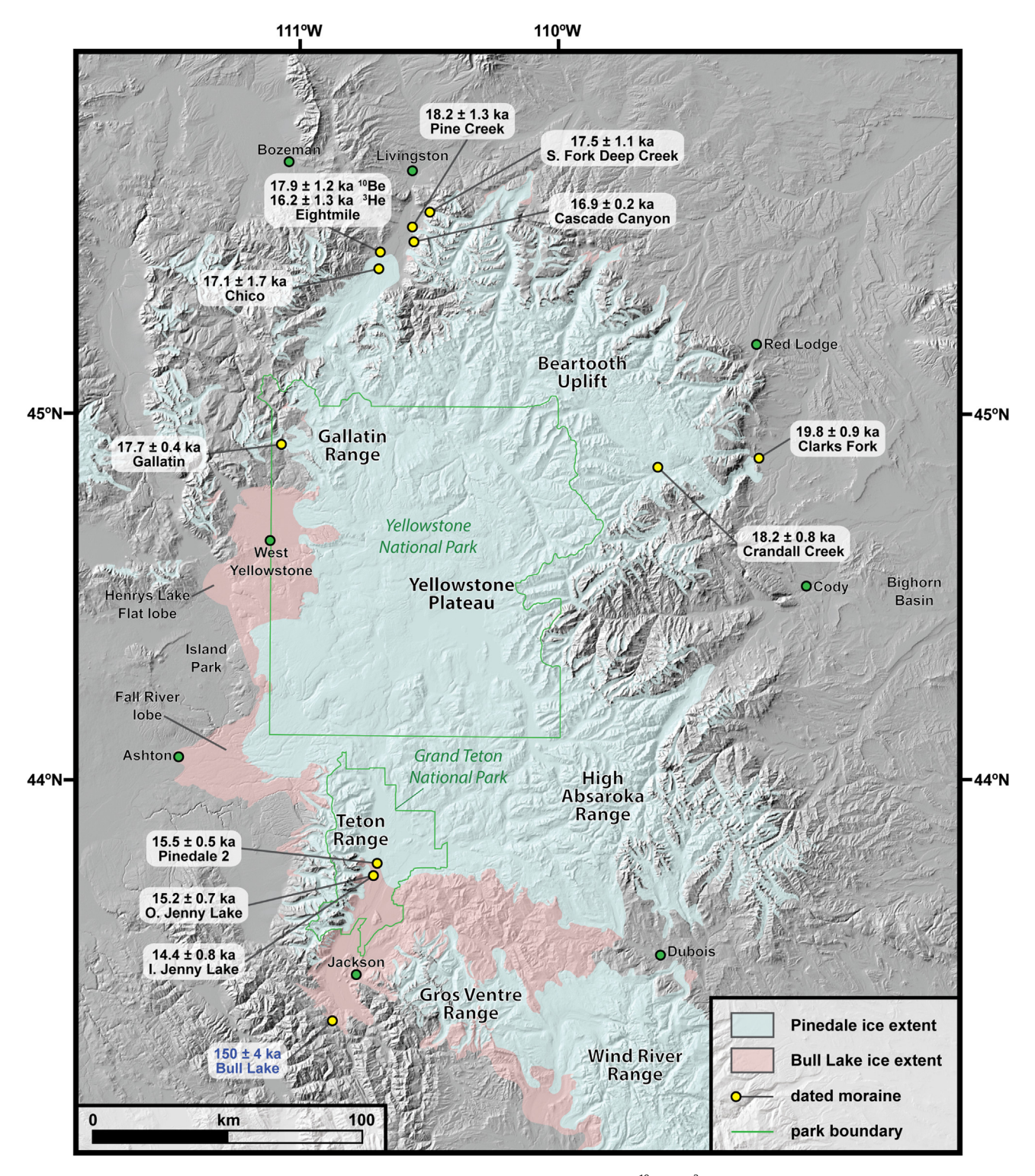


Fig. 5. Shaded relief map of the Greater Yellowstone region with reconstructed Pleistocene ice extents. Mean  $^{10}$ Be and  $^{3}$ He exposure ages ( $\pm 1\sigma$ ) of moraines are from Licciardi and Pierce (2018); previously unpublished mean  $\pm 1\sigma$   $^{10}$ Be exposure ages from Cascade Canyon and South Fork Deep Creek Canyon are newly reported here. Yellow circles indicate sites with exposure ages of moraines. See Tables S1 and S3 for mean and individual exposure ages.

moraines at Robinson Creek and Virginia Creek valleys (Rood et al., 2011) and with  $^{36}$ Cl exposure ages of the Tahoe 1 moraine at Bishop Creek valley (Phillips et al., 2009). Meanwhile, the exposure age of  $125 \pm 2$  ka of the Woodfords outwash surface overlaps with the oldest  $^{36}$ Cl exposure age of the Tahoe 6 moraine at Bishop Creek valley (Phillips et al., 2009) and is only ~11 kyr (10%) older than the

Tahoe moraine at Sonora Junction (Rood et al., 2011). Together, these observations suggest that exposure ages of outwash are not always older than those from moraines.

In our compilation, we find that the oldest exposure ages of penultimate-glaciation moraines throughout the conterminous western U.S. display notably stronger coherency than the mean

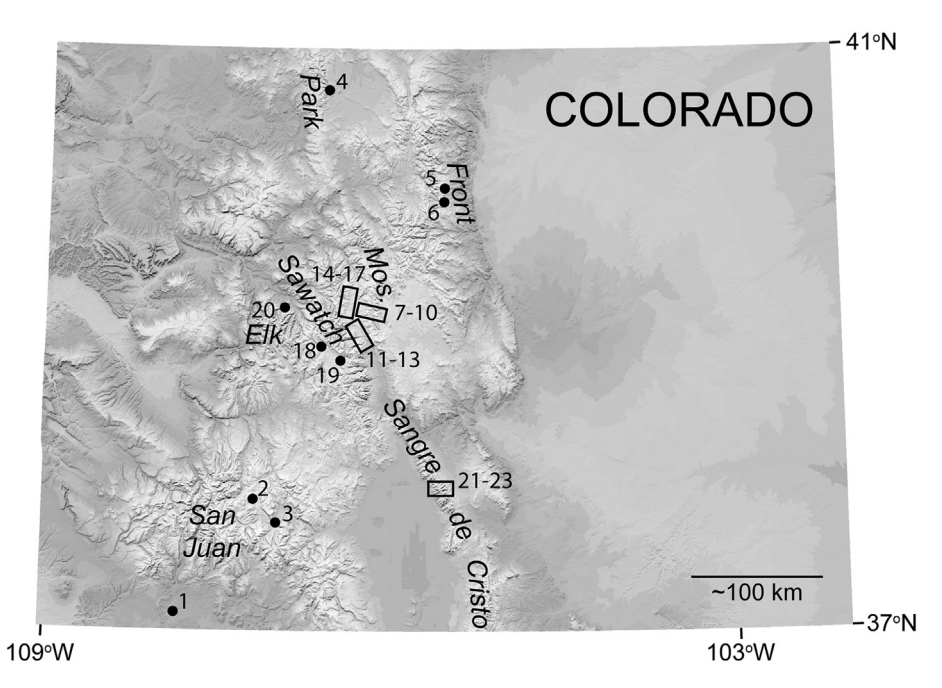
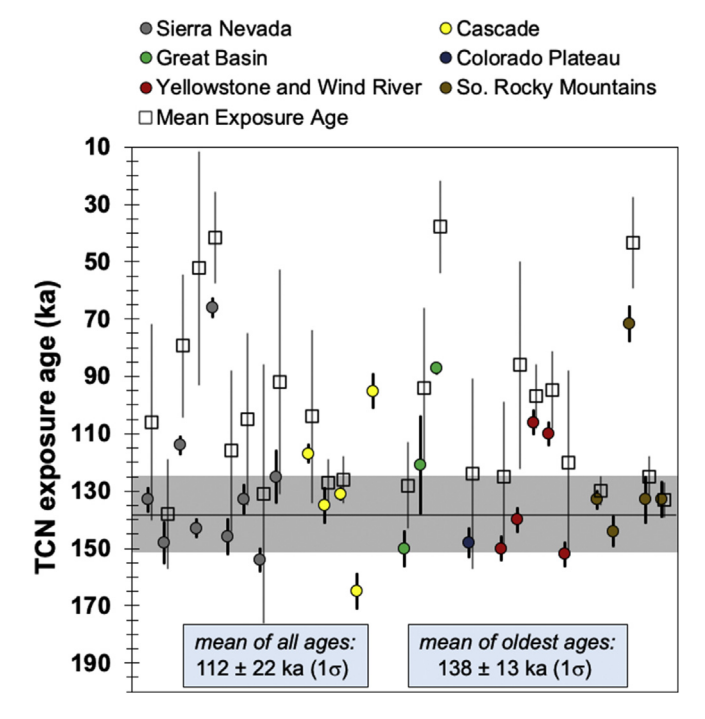


Fig. 6. Shaded relief map of Colorado with numbered locations of exposure-dated Pleistocene glacial features. 1 = Animas River valley, San Juan Mountains (Guido et al., 2007); 2 and 3 = Hogback Mountain and Continental Reservoir, San Juan Mountains (Benson et al., 2005); 4 = Roaring Fork, Park Range (Benson et al., 2005); 5 and 6 = North Creek and Middle Boulder Creek, Front Range (Dühnforth and Anderson, 2011; Ward et al., 2009, respectively); 7–10 = Union Creek, Iowa Gulch, Sacramento Creek, and Fourmile Creek, Mosquito (Mos.) Range (Brugger et al., 2019a); 11–13 = Clear Creek, Lake Creek, and Pine Creek, central Sawatch Range (Briner, 2009; Young et al., 2011; Schweinsberg et al., 2020); 14–17 = Halfmoon Creek, Rock Creek, Lake Fork Creek, and Longs Gulch, northern Sawatch Range (Brugger et al., 2019b); 18 and 19 = Taylor Creek and Texas Creek, southern Sawatch Range/Taylor Basin (Brugger, 2007); 20 = Snowmass Creek valley, Elk Range (Mahan et al., 2014); 21–23 = South Crestone Creek, Willow Creek, and South Colony Creek, Sangre de Cristo Mountains (Leonard et al., 2017a; see also Fig. 11). See Tables S1 and S2 for individual exposure ages.

exposure ages of those same moraines (Fig. 7). In the northern Cascade Range, the oldest <sup>36</sup>Cl exposure ages across the Mountain Home, pre-Mountain Home, and Peshashtin moraines vary by only ~14–18 kyr (Table 1) and are consistent with moraine



**Fig. 7.** Plot of mean and oldest exposure ages of moraines and outwash of the penultimate glaciation. Error bars are  $\pm$  1 $\sigma$  for mean ages (light lines) and internal uncertainty for oldest exposure ages or  $\pm$  1 $\sigma$  for averaged groupings of oldest exposure ages (heavy lines). Gray band shows the region-wide mean  $\pm$  1 $\sigma$  of oldest exposure ages as described in the text and displayed in Table 1.

morphostratigraphy (Porter and Swanson, 2008). These ages also align with the oldest exposure ages of numerous moraines in the Rocky Mountains and the Great Basin (Ruby Mountains - Seitz Canyon), which range from ~140 to 125 ka (Table 1). Oldest exposure ages exceeding 140 ka but still corresponding to MIS 6 for penultimate-glaciation moraines are found in the Great Basin (Ruby Mountains - Lamoille Canyon), the Greater Yellowstone region, the Wind River Range, the Sawatch Range, and the Fish Lake Plateau. Penultimate glaciation moraines with oldest ages of <120 ka are found in only four valleys, one in the Great Basin (Ruby Mountains - Hennen Canyon), the Bull Lake VI moraine in the Wind River Range (Phillips et al., 1997), the moraine in the central Sawatch Range where Briner (2009) compared cobble and boulder exposure ages, and the aforementioned Tahoe moraine at Woodfords (Wesnousky et al., 2016, Table 1). The relatively young moraine in Hennen Canyon with an oldest <sup>10</sup>Be exposure age of  $87.5 \pm 1.5$  ka  $(1\sigma)$  and a coefficient of variation of 42% is immediately adjacent to Seitz Canyon, where a moraine deposited by an outlet of the same icefield has a similar morphology, a much older  $^{10}$ Be exposure age of 122  $\pm$  17 ka, and a coefficient of variation of 28%. Given the similarities in moraine morphologies, lengths, thickness, and hypsometry of the glaciers that deposited the moraines, and the fact that outlet glaciers in both Seitz and Hennen Canyon were sourced from the same icefield, the ~35 kyr difference in the oldest exposure ages of the two moraines does not accurately portray a difference in landform age. We suggest, as did Wesnousky et al. (2016), that the moraine in Hennen Canyon has experienced significant denudation and propose that the true age of the moraine is closer to the <sup>10</sup>Be exposure age of the moraine at Seitz Canyon  $(122 \pm 17 \text{ ka}, \text{Table 1})$ , although we cannot rule out the possibility that both moraines were deposited during later glacial episodes (e.g., MIS 5d or later). The young exposure ages of the Bull Lake VI moraine in the Wind River Range (Phillips et al., 1997) and of the boulders and cobbles atop the Dry Gulch moraine in the central

Sawatch (Briner, 2009) are not consistent with chronologies in other mountain ranges and may represent moraine occupation during later time intervals.

### 4.2. The last glaciation (MIS 2)

Exposure ages of moraines of the last glaciation are more numerous and generally less variable compared to exposure ages of pre-LGM moraines in the western U.S. The widespread application of exposure dating to moraines of the last glaciation affords comparison of the timing of the Tenaya (earlier) and Tioga (later) Glaciations in the Sierra Nevada (termed by Blackwelder, 1931), the Angel Lake Glaciation in the Great Basin sector of the Basin and Range (as termed by Sharp, 1938), and the Pinedale Glaciation in the Rocky Mountains (as termed by Blackwelder, 1915), as well as moraines representing the last glaciation in the Transverse Ranges in California, the Columbia Plateau in eastern Oregon, and the Colorado Plateau in southern Utah.

### 4.2.1. The Sierra Nevada and Transverse Ranges (California)

The southwestern-most mountains in the conterminous U.S. with exposure-dated glacial deposits are both in California: the Sierra Nevada, one of the most heavily glaciated mountains in the western U.S. (Gillespie and Clark, 2011; Fig. 2); and the San Bernardino Range (one of the Transverse Ranges) (Fig. 1). Numerous glaciated valleys in the Sierra Nevada featuring Tioga and Tenaya (both presumed to represent the last glaciation, with Tenaya being older) have been targeted for <sup>10</sup>Be exposure dating (Rood et al., 2011; Wesnousky et al., 2016), chiefly in the eastern sector of the mountains, complementing the extensive set of <sup>36</sup>Cl exposure ages of Phillips et al. (2009, 2016a, b). The San Bernardino Range was sparsely glaciated, but a sequence of well-preserved moraines near San Gorgonio Mountain was exposure dated with <sup>10</sup>Be by Owen et al. (2003).

In the Sierra Nevada, Rood et al. (2011) report <sup>10</sup>Be exposure ages of moraines and outwash with an assumed erosion rate of 0.6 mm/kyr. For Tioga-age moraines and outwash (corresponding to MIS 2), this erosion rate increases apparent exposure ages by less than 1% (far less than measurement uncertainty) and is used here in our age recalculations for consistency with the original report. Three terminal moraines at Sonora Junction (Fig. 2, site SJ), two identified as Tioga-age and another identified as Tenaya-age, yield mean  $^{10}$ Be exposure ages of 20.5  $\pm$  0.5 ka (southern lobe, n = 6), 20.8  $\pm$  0.3 ka (northern lobe, n = 6), and 21.4  $\pm$  2.6 ka (n = 8), respectively (Table 2). The terminal moraine at Lundy Canyon (Fig. 2, site LC) identified as Tioga-age has a mean exposure age of  $19.2 \pm 1.6$  ka (n = 5). A terminal moraine in Bear Valley of the northwestern Sierra Nevada (Fig. 2, site BV) studied by James et al. (2002) has a mean exposure age of 21.3 + 2.1 ka. These mean exposure ages are consistent with or slightly older than those of Tioga-age outwash, which are  $19.1 \pm 0.5$  ka (n = 5) at Lundy Canyon and  $21.4 \pm 0.6$  (n = 4) at Buckeye Creek (Fig. 2, site BC; Table 2). Wesnousky et al. (2016) report <sup>10</sup>Be exposure ages of Tioga-age outwash at Woodfords, the northeastern-most valley (Fig. 2, site WF) with exposure ages of glacial features. There, recalculated exposure ages of outwash have a mean of 25.1  $\pm$  3.5 ka (n = 4), which is older than the mean recalculated  $^{10}$ Be age of 22.1  $\pm$  1.0 ka determined for the same surface by Rood et al. (2011). In the southeastern part of the Sierra Nevada, Benn et al. (2006) report  $^{10}\mbox{Be}$  exposure ages of a terminal moraine at Whitney Portal, which has a recalculated mean of  $20.1 \pm 1.0$  ka (n = 6). In a neighboring glacial valley near Soda Springs, Amos et al. (2010) report <sup>10</sup>Be exposure ages of a terminal moraine with a recalculated mean of  $19.9 \pm 0.5 \text{ ka} (n = 6).$ 

Phillips et al. (1996, 2009, 2016a, b) and Phillips (2017) report

numerous <sup>36</sup>Cl exposure ages from the Bishop Creek valley in the eastern Sierra Nevada (Fig. 2, site BI), where a suite of moraines deposited during the last glaciation have been subdivided into Tioga 1 (oldest), 2, 3, and 4 (youngest) based on their morphostratigraphic ages. Ages from Phillips et al. (2016b) and Phillips (2017) were originally calculated with the same production models used here: therefore, these exposure ages are summarized (but not recalculated) here for comparison with other recalculated <sup>10</sup>Be exposure ages. Although the oldest Tioga 1 and 2 moraines at Bishop Creek were likely deposited during the early part of MIS 2 or prior to it, Phillips (2017) concludes that the Tioga 3 moraines represent the maximum advance of the last glaciation. <sup>36</sup>Cl exposure ages of this moraine have mean of 19.2  $\pm$  0.8 ka (Table 2), consistent with 10Be exposure ages of terminal moraines and outwash elsewhere in the Sierra Nevada. A readvance represented by the Tioga 4 moraine at Bishop Creek has a mean exposure age of  $16.1 \pm 0.3$  ka (Table 3). Tioga 4 moraines were also dated with  $^{36}$ Cl at Humphrey's Basin (Phillips et al., 2016b) and with <sup>10</sup>Be at a nearby site originally dated by Nishiizumi et al. (1989). These moraines, interpreted to represent the end of the Tioga 4 glacial episode, have exposure ages of 15.1  $\pm$  0.7 and 15.3  $\pm$  0.6 ka, respectively, as reported by Phillips (2017) (Table 3). Equivalent Tioga 4 moraines have been identified elsewhere in the Sierra Nevada, but have not been dated (Gillespie and Clark, 2011).

In the San Bernardino Range (Fig. 1), Owen et al. (2003) report  $^{10}$ Be exposure ages of terminal and recessional moraines of the last glaciation on the floor of north-facing cirques near San Gorgonio Mountain, where previous mapping by Sharp et al. (1959) identified multiple stages of moraine deposition during the last glaciation. The "Stage I" moraines are the oldest in the sequence and have mean  $^{10}$ Be exposure ages of  $21.5 \pm 0.4$  ka (n = 4) at Dollar Lake and  $18.8 \pm 2.1$  ka (n = 5) at the adjacent North Fork cirque (Table 2). The "Stage II" moraines are the next-oldest, with mean exposure ages of  $15.7 \pm 1.0$  ka (n = 4) at Dollar Lake,  $17.1 \pm 0.3$  ka (n = 3) at North Fork, and  $17.2 \pm 0.5$  ka (n = 5; end moraine) and  $17.3 \pm 1.0$  ka (n = 5; right lateral moraine) at Dry Lake (Table 3). All recalculated ages are about 8-11% older than originally reported by Owen et al. (2003).

Overall, the mean recalculated exposure ages of terminal moraines in the Sierra Nevada and San Bernardino ranges fall within 21-18 ka and the downvalley recessional moraines date to 17-15 ka.

### 4.2.2. The Cascade Range (Oregon and Washington)

Porter and Swanson (2008) report numerous <sup>36</sup>Cl exposure ages of deposits and landforms of the last glaciation in the Icicle Creek valley of the northern Cascade Range (Fig. 1). Among these are terminal moraine loops and nested recessional moraines of the Leavenworth I and II glacial stages (Porter and Swanson, 2008). The Leavenworth I stage is represented by a terminal moraine and a lateral moraine with overlapping exposure ages reported by Porter and Swanson (2008). Recalculated <sup>36</sup>Cl exposure ages of these moraines (using their inferred boulder-surface erosion rate of 2 mm/kyr) have means of 19.7  $\pm$  2.9 ka (n = 8) and 22.7  $\pm$  3.3 ka (n = 5), respectively (Table 2). The Leavenworth II stage is represented by a recessional moraine loop, which has a recalculated mean exposure age of 18.3  $\pm$  1.1 ka (n = 3) (Table 3). Recalculated mean exposure ages are about 17-20% older than originally reported, largely due to the difference between the production models used here and in the original study.

In the southern Cascade Range, Speth et al. (2018) report  $^3$ He exposure ages of boulders atop a single terminal moraine of the last glaciation in the Sevenmile Creek valley near Klamath Lake. The boulder exposure ages of this moraine are less variable than those atop the older moraine at the same site (see section 4.1.2. above), but the authors identify four outliers among a set of ten exposure ages. Recalculated exposure ages have a mean of  $16.8 \pm 2.1$  ka

 Table 2

 Cosmogenic exposure ages of terminal moraines and outwash of the last glaciation.

Sample name/locality	Originally reported mean age $\pm$ 1s (ka)	n	Recalc. mean age ± 1s (ka) <sup>b</sup>		% diff. from original report	Source
CIEDDA MENADA LIJ. C.I. d	~6c ± 15 (Ka)		-		-	=
SIERRA NEVADA - high confidence <sup>a</sup>	101 00		205 05		7.0	B 1 (1 (2011)
Sonora Junction Tioga South	$19.1 \pm 0.6$		$20.5 \pm 0.5$	7.3	7.3	Rood et al. (2011)
Sonora Junction Tioga North	19.3 ± 0.3		$20.8 \pm 0.3$	1.4	7.4	Rood et al. (2011)
Lundy Canyon Tioga outwash	$17.7 \pm 0.5$		19.1 ± 0.5	9.5	7.9	Rood et al. (2011)
Woodfords Tioga outwash (site b)	23.0 ± 3.5		25.1 ± 3.5	13.9	9.1	Wesnousky et al. (2016)
Soda Springs Tioga	$18.1 \pm 0.5$		$19.9 \pm 0.5$	2.5	9.9	Amos et al. (2010)
Bear Valley Tioga	18.9 ± 1.9		$21.3 \pm 2.1$	9.9	12.7	James et al. (2002)
Bishop Creek Tioga 3 ( <sup>36</sup> Cl)	$19.2 \pm 0.8$	/	$19.2 \pm 0.8$	4.2	0.0	Phillips (2017)
SIERRA NEVADA - medium confidence <sup>a</sup>		_				
Sonora Junction Tenaya	$20.3 \pm 2.8$		$21.4 \pm 2.6$	29.0	5.4	Rood et al. (2011)
Lundy Canyon Tioga	$17.7 \pm 0.5$		$19.2 \pm 1.6$	10.4	8.5	Rood et al. (2011)
Buckeye Creek Tioga outwash	$20.0 \pm 0.7$		$21.4 \pm 0.6$	24.8	7.0	Rood et al. (2011)
Woodfords Tioga outwash (site a)	$20.7 \pm 1.1$		$22.1 \pm 1.1$	5.0	6.8	Rood et al. (2011)
Whitney Portal	$17.8 \pm 1.0$	6	$20.1 \pm 1.0$	5.0	12.9	Benn et al. (2006)
TRANSVERSE RANGES - San Bernardino						
Dollar Lake	$20.1 \pm 0.5$		$21.5 \pm 0.4$	24.5	7.0	Owen et al. (2003)
North Fork	$17.2 \pm 2.2$	5	$18.8 \pm 2.1$	11.2	9.3	Owen et al. (2003)
CASCADE RANGE						
Northern Cascade - Icicle Ck - Leavenworth I terminal	$16.8 \pm 2.4$	8	$19.7 \pm 2.9$	14.7	17.3	Porter and Swanson (2008
( <sup>36</sup> Cl) Northern Cascade - Icicle Ck - Leavenworth I lateral ( <sup>36</sup> C	1) 188 + 28	5	22.7 ± 3.3	14.5	20.7	Porter and Swanson (2008
Northern Cascade - Icicie Ck - Leavenworth i lateral (* C Southern Cascade - Sevenmile ( <sup>3</sup> He)	1) 18.8 $\pm$ 2.8 mean not reported		$22.7 \pm 3.3$ $16.8 \pm 2.1$	12.5	20.7	Speth et al. (2018)
` ,	*		•			
BASIN AND RANGE	100 . 12		20.0 1.2	0.1	F.C.	Lasha et al. (2012)
Ruby Mountains - Seitz 1	$19.8 \pm 1.2$		$20.9 \pm 1.2$	9.1	5.6	Laabs et al. (2013)
Ruby Mountains - Seitz 2	$18.2 \pm 1.3$		$19.2 \pm 1.3$	9.9	5.5	Laabs et al. (2013)
Ruby Mountains - Seitz 3	$20.6 \pm 1.4$		$21.5 \pm 1.3$	6.0	4.4	Laabs et al. (2013)
Ruby Mountains - Hennen	$19.9 \pm 2.7$		$22.0 \pm 2.7$	12.3	10.6	Wesnousky et al. (2016)
East Humboldt Range - Angel Lake 1	$20.4 \pm 0.9$		$18.8 \pm 0.6$	3.2	-7.8	Munroe et al. (2015)
South Snake Range - Snake Creek	$18.1 \pm 1.6$		$17.3 \pm 1.6$	13.3	-4.4	Laabs and Munroe (2016)
Deep Creek Range - Granite Creek	$19.9 \pm 0.4$	3	$19.1 \pm 0.3$	35.6	-4.0	Laabs and Munroe (2016)
COLUMBIA PLATEAU - Wallowa Mtns Wallowa old mode	21.2 ± 0.8	9	22.8 ± 0.8	16.2	7.5	Licciardi et al. (2004)
_	27.2 ± 0.0		22.0 ± 0.0	10.2	7.10	Electarar et all (2001)
COLORADO PLATEAU ( <sup>3</sup> He)	20.4 . 2.2	_	105 . 10	0.7	4.4	Manchatti et al. (2011)
Fish Lake Plateau - Pelican Canyon	$20.4 \pm 2.3$		19.5 ± 1.9	9.7	-4.4	Marchetti et al. (2011)
Fish Lake Plateau - Jorgensen Creek inner	$21.1 \pm 0.1$		$20.0 \pm 0.1$	0.5	-5.2	Marchetti et al. (2011)
Fish Lake Plateau - Sevenmile	$21.4 \pm 0.6$		$20.4 \pm 0.6$	2.9	-4.7	Marchetti et al. (2011)
Boulder Mtn Hickman Pasture (Fish Creek laterals)	$21.6 \pm 1.8$		$20.3 \pm 1.4$	6.9	-5.6	Marchetti et al. (2005)
Boulder Mtn Miller Creek	$20.5 \pm 0.4$		$19.1 \pm 0.4$	2.1	-6.8	Marchetti et al. (2007)
Boulder Mtn Blind Lake outer	$20.0 \pm 1.4$		$18.6 \pm 1.1$	5.9	-7.0	Marchetti et al. (2005)
Boulder Mtn Blind Lake inner	$23.1 \pm 1.3$	4	$20.2 \pm 1.7$	8.4	-12.6	Marchetti et al. (2005)
MIDDLE ROCKY MOUNTAINS - WIND RIVER (WR) & BIGH	ORN (BH)					
WR Pinedale 2 (old mode; <sup>36</sup> Cl)	$23.0 \pm 4.0$	3	$22.4 \pm 2.8$	33.5	-2.6	Phillips et al. (1997)
WR North Fork Popo Agie	$22.9 \pm 0.6$		$21.7 \pm 0.5$	2.3	-5.2	Dahms et al. (2018)
BH North Clear Creek Canyon (old mode)	$22.9 \pm 0.6$		$22.9 \pm 0.6$	2.6	0.0	this study
MIDDLE ROCKY MOUNTAINS - WASATCH & UINTA						
Wasatch - Bells Canyon 1	$22.4 \pm 2.3$	3	$21.9 \pm 2.0$	9.1	-2.3	Laabs and Munroe (2016)
Wasatch - Little Cottonwood Canyon right lateral	$15.8 \pm 0.7$		$17.3 \pm 0.7$	4.0	9.5	Laabs et al. (2011)
Wasatch - Little Cottonwood Canyon left lateral	16.4 ± 5.1	4	$17.3 \pm 0.7$ $20.8 \pm 4.5$	21.6	9.5 N/A	Laabs et al. (2011)  Laabs et al. (2011)
Wasatch - American Fork Canyon	15.8 ± 1.4	9	$16.8 \pm 1.4$	9.5	6.3	Laabs et al. (2011)
· ·						
Wasatch - Big Cottonwood Canyon	$20.2 \pm 0.5$	4	$20.2 \pm 0.5$	2.5	0.0	Quirk et al. (2018)
Uinta - S. Fork Ashley	$21.3 \pm 1.8$	7	$21.4 \pm 1.6$	67.3	0.5	Laabs et al. (2009) Laabs et al. (2009)
Uinta - Burnt Fork	17.9 ± 1.7		$18.6 \pm 1.4$	11.5	3.9	` '
Uinta - Smiths Fork	$18.9 \pm 2.4$		$19.4 \pm 2.2$	62.8	2.6	Laabs et al. (2009)
Uinta - Lake Fork 1	$18.3 \pm 1.1$		$19.0 \pm 1.1$	16.3	3.8	Munroe et al. (2006)
Uinta - Yellowstone	$17.4 \pm 1.4$		$18.2 \pm 1.4$	14.3	4.6	Munroe et al. (2006)
Uinta - North Fork Provo terminal	$17.4 \pm 0.7$		18.3 ± 1.5	8.2	5.2	Refsnider et al. (2008)
Uinta - North Fork Provo lateral	17.5 ± 1.5	4	$18.0 \pm 0.7$	13.9	2.9	Refsnider et al. (2008)
Uinta - Bear River Main Uinta - Bear River East	$17.5 \pm 1.0$ $18.9 \pm 1.3$		$18.2 \pm 0.9$ $19.5 \pm 1.9$	4.9 11.1	4.0 3.2	Laabs et al. (2009) Laabs et al. (2009)
	10.0 1 1.0	,	10.0 ± 1.0		= - <del></del>	
ROCKY MOUNTAINS - GREATER YELLOWSTONE REGION	105 10		170 10	10.0	0.5	richado in monto consti
Eightmile ( <sup>10</sup> Be)	$16.5 \pm 1.2$		3 17.9 ± 1.2	10.6	8.5	Licciardi and Pierce (2008)
mr v				C 7	17	Liceiardi et al. (2001)
	$16.5 \pm 1.4$		$2.16.3 \pm 1.1$	6.7	-1.2	Licciardi et al. (2001)
Eightmile ( <sup>3</sup> He) Pine Creek South Fork Deep Creek	16.5 ± 1.4 17.5 ± 1.4 17.5 ± 1.1	6	18.2 ± 1.3 17.5 ± 1.1	102.2 6.3	4.0 0.0	Licciardi et al. (2001) Licciardi and Pierce (2008) this study

Table 2 (continued)

Sample name/locality	Originally reported mean age $\pm$ 1s (ka)	n Recalc. mean age $\pm 1s (ka)^{b}$		% diff. from original report	Source
Cascade Canyon	$16.9 \pm 0.2$	2 16.9 ± 0.2	1.2	0.0	this study
Clarks Fork	$18.8 \pm 0.9$	9 $19.8 \pm 0.9$	19.2	5.3	Licciardi and Pierce (2008)
Gallatin	$17.3 \pm 0.4$	1 $17.7 \pm 0.4$	N/A	2.3	Licciardi and Pierce (2008)
Jenny Lake outer	$14.6 \pm 0.7$	$11\ 15.2 \pm 0.7$	4.6	4.1	Licciardi and Pierce (2008)
SOUTHERN ROCKY MOUNTAINS - COLORADO					
San Juan - Continental Reservoir ( <sup>36</sup> Cl)	$20.3 \pm 0.7$	$3  20.1 \pm 0.3$	1.5	-1.0	Benson et al. (2004)
San Juan - Hogback Mtn ( <sup>36</sup> Cl)	$18.5 \pm 1.6$	$11\ 19.1 \pm 1.4$	38.2	3.2	Benson et al. (2004)
San Juan - Animas (outwash, 10Be depth profile)	$19.5 \pm 1.4$	1 $21.5 \pm 1.5$	N/A	10.3	Guido et al. (2007)
Park - Roaring Fork ( <sup>36</sup> Cl)	$18.1 \pm 1.3$	$5 18.6 \pm 1.2$	16.1	2.8	Benson et al. (2004)
Park - Roaring Fork (10Be)	$20.6 \pm 2.4$	$3  22.2 \pm 2.3$	10.4	7.8	Benson et al. (2004)
Front - North Boulder	$20.3 \pm 2.3$	5 $20.4 \pm 2.1$	10.3	0.5	Dühnforth and Anderson
					(2011)
Front - Middle Boulder ( <sup>10</sup> Be)	$19.7 \pm 2.1$	$2  20.1 \pm 2.0$	10.0	2.0	Ward et al. (2009)
Front - Middle Boulder ( <sup>36</sup> Cl)	$18.9 \pm 1.8$	$3 19.1 \pm 0.3$	1.6	1.1	Benson et al. (2004)
Mosquito - Fourmile	$21.7 \pm 1.6$	$2  21.7 \pm 1.6$	7.4	0.0	Brugger et al. (2019a)
Mosquito - Iowa Gulch	$20.6 \pm 1.1$	$4  20.6 \pm 1.1$	5.3	0.0	Brugger et al. (2019a)
Central Sawatch - Pine Creek (old mode)	$22.4 \pm 1.4$	5 $22.3 \pm 1.3$	5.8	-0.4	Young et al. (2011)
Central Sawatch - Clear Creek	$18.4 \pm 1.9$	$3 19.5 \pm 0.2$	11.3	6.0	Young et al. (2011)
Central Sawatch - Lake Creek	$19.7 \pm 0.5$	$3 19.9 \pm 0.2$	1.0	1.0	Young et al. (2011)
Central Sawatch - Lake Creek Pinedale terminal	$20.6 \pm 0.6$	$22\ 20.6 \pm 0.6$	2.9	0.0	Schweinsberg et al. (2020)
Northern Sawatch - Rock Creek	$21.5 \pm 2.3$	$6  20.9 \pm 2.3$	11.3	-2.9	Brugger et al. (2019b)
Southern Sawatch - Taylor ( <sup>10</sup> Be)	$18.7 \pm 1.8$	$5  ext{19.5} \pm 2.0$	10.3	4.3	Brugger (2007)
Southern Sawatch - Taylor ( <sup>36</sup> Cl)	$20.8 \pm 2.3$	$3  20.8 \pm 1.9$	9.1	0.0	Brugger (2007)
Sangre de Cristo - Willow Creek terminal	$18.2 \pm 0.3$	$3 17.7 \pm 0.3$	1.7	-2.7	Leonard et al. (2017a)
Sangre de Cristo - South Crestone	$19.5 \pm 1.9$	$3 18.7 \pm 1.7$	10.2	-4.1	Leonard et al. (2017a)
Sangre de Cristo - South Colony	$19.1 \pm 2.1$	$3 18.4 \pm 1.9$	10.3	-3.7	Leonard et al. (2017a)

- <sup>a</sup> Based on the designations described in Rood et al. (2011). Exposure ages of Wesnousky et al. (2016) are considered here as high confidence.
- <sup>b</sup> Excludes outliers identified in original report.
- c Calculated for all TCN exposure ages of moraine/outwash reported in the source. See Tables SR1, SR2, and SR3 for all individual and mean exposure ages.

(n = 6), computed with the same boulder-surface erosion rate of 1 mm/kyr assumed in the original report.

# 4.2.3. The Basin and Range and Columbia Plateau (Utah, Nevada, Oregon)

Numerous mountain ranges in the Basin and Range and Columbia Plateau (Fig. 1) were occupied by glaciers during the Pleistocene and display prominent glacial features suitable for <sup>10</sup>Be exposure dating. Chronologies are available in several ranges in the northern part of the Great Basin sector of the Basin and Range (Nevada and western Utah; Laabs et al., 2013 and Laabs and Munroe, 2016) and in the Wallowa Mountains of the eastern Columbia Plateau in Oregon (Licciardi et al., 2004, Fig. 1). Generally, mountain glaciers in these two settings were small compared to those in the Rocky Mountains to the east and the Sierra Nevada and the Cascade Range to the west.

In the northern Wallowa Mountains, Licciardi et al. (2004) report  $^{10}\text{Be}$  exposure ages of a multi-crested terminal moraine complex. They noted a strong bimodal distribution of exposure ages among moraine crests and report an "old mode" and "young mode" of ages, interpreting these to indicate two distinct episodes of moraine occupation during the last glaciation. The recalculated mean  $^{10}\text{Be}$  exposure ages are  $22.8 \pm 0.8$  ka (n = 9) for the old mode and  $18.5 \pm 0.8$  ka (n = 10) for the young mode (Tables 2 and 3).

In the Basin and Range region, studies by Laabs et al. (2013) and Wesnousky et al. (2016) include  $^{10}$ Be exposure age limits of terminal moraines in the western Ruby Mountains in northeastern Nevada (Fig. 3). Both studies targeted multi-crested moraine complexes at the western front of the mountains, in neighboring Seitz and Hennen Canyons. Laabs et al. (2013) reported exposure ages of seven moraine crests in Seitz Canyon, which they interpret as limiting the duration of the last glaciation. The recalculated exposure ages of the three outer crests are statistically identical, and from distal to proximal have means of  $20.9 \pm 1.2$  ka (n = 4),

 $19.2 \pm 1.3$  ka (n = 6), and  $21.5 \pm 1.3$  ka (n = 5; Table 2). Upvalley from these moraines, four recessional moraine ridges (from farthest downvalley to farthest upvalley) have mean recalculated exposure ages of  $16.9 \pm 1.5$  ka (n = 3),  $17.2 \pm 1.0$  ka (n = 2),  $16.5 \pm 1.2$  (n = 2), and  $16.2 \pm 1.4$  ka (n = 4; Table 3). Recalculated  $^{10}$ Be exposure ages of the three oldest moraine crests in Seitz Canyon are consistent with those from the terminal moraine in Hennen Canyon (Wesnousky et al., 2016), which have a mean of  $22.0 \pm 2.7$  ka (n = 10; Table 2).

North of the Ruby Mountains are the East Humboldt Mountains (Fig. 3), featuring the type locality of the last Pleistocene glaciation in the Great Basin, termed the Angel Lake Glaciation by Sharp (1938). This episode is named after the high-relief lateral moraines and lower-relief end moraines downvalley of Angel Lake in the northeastern sector of the East Humboldt Mountains. Here, the recalculated mean  $^{10}\text{Be}$  exposure age of a terminal moraine dated by Munroe et al. (2015) is  $18.8 \pm 0.6$  ka (n = 3), and a recessional moraine has a recalculated mean exposure age of  $18.2 \pm 1.0$  ka (n = 7).

Finally, in a summary of the chronology of glacial features within the Lake Bonneville basin, Laabs and Munroe (2016) report  $^{10}$ Be ages of terminal moraines from the Deep Creek and South Snake Ranges, both west of Lake Bonneville near the Utah-Nevada border (Fig. 1). The terminal moraine in Granite Creek valley in the Deep Creek Range has a recalculated mean exposure age of  $19.1 \pm 0.3$  ka ( $10.1 \pm 0.3$ ), and the terminal moraine in the Snake Creek valley in the South Snake Range has a mean exposure age of  $10.1 \pm 0.3$  ka ( $10.1 \pm 0.3$ ).

Overall, exposure ages of terminal moraines in the Basin and Range/Columbia Plateau region are variable, ranging from ca. 22-17 ka. This range of exposure ages overlaps with exposure ages of terminal moraines in the Sierra Nevada and the Cascade Range. Downvalley recessional moraines and younger modes of terminal moraines range from ca. 18.5  $\pm$  0.8 ka in the Wallowa Mountains to

 Table 3

 Cosmogenic exposure ages of downvalley recessional moraines of the last glaciation.

Sample name/locality	Originally reported mean age $\pm$ 1s (ka)	n	Recalc. mean age ± 1s (ka) <sup>a</sup>	C.V. (%) <sup>b</sup>	% diff. from original report	Source
SIERRA NEVADA						
Nishiizuumi Tioga terminal (end Tioga 4)	$15.3 \pm 0.6$	7	$15.3 \pm 0.6$	3.9	0.0	Phillips (2017)
Bishop Creek Confluence (Tioga 4, <sup>36</sup> Cl)	16.1 ± 0.3	4	$16.1 \pm 0.3$	1.9	0.0	Phillips (2017)
Humphrey's Basin (end Tioga 4, <sup>36</sup> Cl)	$15.1 \pm 0.7$	5	$15.1 \pm 0.7$	4.6	0.0	Phillips (2017)
TRANSVERSE RANGES - San Bernardino						
North Fork II	$15.8 \pm 0.3$	3	$17.1 \pm 0.3$	19.5	8.2	Owen et al. (2003)
Dollar Lake II	$14.2 \pm 0.9$	4	$15.7 \pm 1.0$	6.4	10.6	Owen et al. (2003)
Dry Lake II lateral	$15.9 \pm 0.9$	5	$17.3 \pm 1.0$	6.4	8.8	Owen et al. (2003)
Dry Lake II frontal	$15.7 \pm 0.4$	5	$17.2 \pm 0.5$	2.9	9.6	Owen et al. (2003)
NORTHERN CASCADE RANGE ( <sup>36</sup> Cl)						
Icicle Creek - Leavenworth II	$15.2 \pm 0.7$	3	$18.3 \pm 1.1$	23.5	20.4	Porter and Swanson (2008)
GREAT BASIN						
Ruby Mountains - Seitz 4	$15.8 \pm 1.6$	3	$16.9 \pm 1.5$	8.9	7.0	Laabs et al. (2013)
Ruby Mountains - Seitz 5	$16.1 \pm 1.0$	2	$17.2 \pm 1.0$	5.8	6.8	Laabs et al. (2013)
Ruby Mountains - Seitz 6	$15.7 \pm 1.6$	2	$16.5 \pm 1.2$	7.3	5.1	Laabs et al. (2013)
Ruby Mountains - Seitz 7	$15.2 \pm 1.4$	4	$16.2 \pm 1.4$	8.6	6.6	Laabs et al. (2013)
East Humboldt Range - Angel Lake 2	$20.1 \pm 1.2$	7	$18.2\pm1.0$	5.5	-9.5	Munroe et al. (2015)
COLUMBIA PLATEAU - Wallowa Mtns						
Wallowa young mode	$17.0 \pm 0.8$	10	$18.5\pm0.8$	4.3	8.8	Licciardi et al. (2004)
ROCKY MOUNTAINS - WASATCH						
Bells Canyon 2	$16.7 \pm 0.7$	2	$16.8 \pm 0.7$	4.2	0.6	Laabs and Munroe (2016)
Lake Fork 2	$16.8 \pm 0.6$	7	$17.7 \pm 0.5$	2.8	5.4	Munroe et al. (2006)
ROCKY MOUNTAINS - GREATER YELLOWSTONE	REGION					
Chico - northern lobe	$15.8 \pm 1.6$	9	$17.1 \pm 1.7$	9.9	8.2	Licciardi and Pierce (2008)
Jenny Lake inner	13.5 ± 1.1	8	$14.4 \pm 0.8$	5.6	4.4	Licciardi and Pierce (2008)
Pinedale 2 - southern lobe	$15.5 \pm 0.5$	5	$15.5 \pm 0.5$	23.2	0.0	Licciardi and Pierce (2018)
ROCKY MOUNTAINS - WIND RIVER & BIGHORN	I					
WR Pinedale PN3 ( <sup>36</sup> Cl)	$18.8 \pm 2.0$	3	$18.9 \pm 1.2$	21.2	0.5	Phillips et al. (1997)
WR Sinks Canyon 1	$21.6 \pm 1.1$	3	$20.4 \pm 1.0$	4.9	-5.9	Dahms et al. (2018)
WR Sinks Canyon 2	$19.4 \pm 1.0$	2	$18.4 \pm 0.9$	4.9	-5.2	Dahms et al. (2018)
BH North Clear young mode	$18.0 \pm 1.1$	3	$18.0 \pm 1.1$	6.1	0.0	this study
BH Tensleep Canyon	$17.9 \pm 0.8$	3	$17.9 \pm 0.8$	4.5	0.0	this study
ROCKY MOUNTAINS - COLORADO						
Mosquito - Sacramento Creek	$17.4 \pm 1.3$	1	$17.4 \pm 1.3$	7.5	0.0	Brugger et al. (2019a)
Mosquito - Union Creek	$17.1 \pm 0.4$	3	$17.1 \pm 0.4$	8.8	0.0	Brugger et al. (2019a)
Central Sawatch - Pine Creek young mode	$15.8 \pm 0.3$	6	$16.3 \pm 0.4$	5.5	3.2	Young et al. (2011)
Central Sawatch - Lake Creek recessional 3	$15.6 \pm 0.7$	5	$15.6 \pm 0.7$	4.5	0.0	Schweinsberg et al. (2020)
Northern Sawatch - Lake Fork proximal	$17.7 \pm 0.8$	3	$17.2 \pm 0.8$	4.7	-2.8	Brugger et al. (2019b)
Northern Sawatch - Half Moon proximal	$16.5 \pm 0.8$	3	$16.0 \pm 0.7$	4.2	-3.0	Brugger et al. (2019b)
Southern Sawatch - Texas Creek	$14.4 \pm 0.8$	2	$15.5 \pm 0.7$	4.5	7.6	Brugger (2007)
Sangre de Cristo - Willow Creek	$16.2 \pm 0.7$	8	$15.7 \pm 0.5$	4.5	-3.1	Leonard et al. (2017a)
Sangre de Cristo - South Colony	$18.7 \pm 0.5$	4	$18.1 \pm 0.5$	2.8	-3.2	Leonard et al. (2017a)

<sup>&</sup>lt;sup>a</sup> Excludes outliers identified in original report.

### $16.2 \pm 1.4$ ka in the Ruby Mountains.

### 4.2.4. The Colorado Plateau (Utah)

Although small mountain-glacier systems were numerous in mountains of the Colorado Plateau during the late Pleistocene, the only two locations where exposure ages of moraines have been reported are glacial valleys around the Fish Lake Plateau Hightop and at Boulder Mountain (Fig. 4), both in central Utah. Marchetti et al. (2005, 2007; 2011) applied <sup>3</sup>He exposure dating to pyroxenes from trachyandesite boulders atop terminal moraines in

multiple glacial valleys in the Fish Lake Plateau area. Terminal moraines at Pelican Canyon, Jorgensen Creek, and Sevenmile have recalculated exposure ages of 19.5  $\pm$  1.9 ka (n = 5), 20.0  $\pm$  0.1 ka (n = 2), and 20.4  $\pm$  0.6 ka (n = 4) (Table 2). At Boulder Mountain, two latero-frontal moraine and one lateral moraine in the Fish Creek drainage at Hickman Pasture have a mean recalculated  $^3{\rm He}$  exposure age of 20.3  $\pm$  1.4 ka (n = 9). The terminal moraine deposited by an outlet glacier in Miller Creek valley has a recalculated mean exposure age of 19.1  $\pm$  0.4 ka (n = 2). A variably spaced (100–500 m apart) set of latero-terminal moraines around Blind

b Calculated by the 1s uncertainty of all recalculated TCN exposure ages of moraine/outwash divided by the mean (see Tables S1, S2, and S3 for individual exposure ages).

Lake has recalculated mean exposure ages of 18.6  $\pm$  1.1 ka (n = 4) (Blind Lake outer), and 20.2  $\pm$  1.7 ka (n = 4) (Blind Lake inner). Although the inner moraine at Blind Lake has a mean exposure age older than the outer moraine, the observed overlap of the mean ages at  $1\sigma$  is consistent with their close spacing.

### 4.2.5. The Middle Rocky Mountains (Northern Utah and Wyoming)

The Middle Rocky Mountains region includes the Wind River Range (Fig. 1), where moraines representing the type locality for the Pinedale Glaciation at Fremont Lake were among the first targeted by <sup>10</sup>Be exposure dating with (Gosse et al., 1995a, b) and where moraine chronologies from southeastern glacial valleys were recently reported by Dahms et al. (2018). This region also includes the Bighorn Range in Wyoming where <sup>10</sup>Be exposure ages are reported here for the first time and the Wasatch and Uinta Mountains in Utah (Fig. 1; the Greater Yellowstone region is discussed separately in section 4.2.6.).

The large set of <sup>10</sup>Be exposure ages from the Wind River Range reported by Gosse et al. (1995a, b), while important, are not recalculated here because the <sup>10</sup>Be chronology of glacial deposits in these mountains is developing with newer data (e.g., Dahms et al., 2018). Instead, we recalculate a large number of <sup>36</sup>Cl and <sup>10</sup>Be exposure ages from the eastern Wind River Range. In the glacial valley occupied by Bull Lake, Phillips et al. (1997) report <sup>36</sup>Cl exposure ages of three moraine crests mapped as Pinedaleequivalent in a terminal moraine complex. The recalculated ages are variably older or vounger than the originally reported ages (depending on native Cl concentration: Table 3), reflecting the new <sup>36</sup>Cl production model implemented in CRONUScale (Marrero et al., 2016b). Mean exposure ages of the three moraines (excluding outliers) are 16.2  $\pm$  2.2 ka (n = 3, outer moraine), 22.4  $\pm$  2.8 ka (n = 3, middle moraine; Table 2), and 18.9  $\pm$  1.2 ka (n = 3, inner moraine; Table 3). The recalculated exposure age of the outer moraine is not given further consideration here because it is younger than the two inner moraines. In the southeastern Wind River Range, Dahms et al. (2018) report <sup>10</sup>Be exposure ages from terminal and recessional moraines in two neighboring glacial valleys of the Popo Agie Basin. The terminal moraine in the North Popo Agie valley (from Dahms et al., 2018) yields a recalculated mean  $^{10}$ Be exposure age of 21.7  $\pm$  0.5 ka (n = 2). Recessional moraines in the neighboring Sinks Canyon (a southern fork of the Popo Agie valley), within a few kilometers of an undated terminal moraine, have recalculated mean  $^{10}$ Be exposure ages of  $20.4 \pm 1.0$  ka (n = 3) (outer recessional) and  $18.4 \pm 0.9$  ka (n = 2) (inner recessional). These recalculated ages are similar to those originally reported by Dahms et al. (2018).

The western Wasatch Mountains and the Uinta Mountains featured the largest valley glacier systems in Utah during the last glaciation (Figs. 8 and 9). Here, <sup>10</sup>Be chronologies of glacial features are largely based on terminal moraines and to a lesser degree on recessional moraines representing near-maximum glacier lengths. In the western Wasatch Mountains, exposure ages of terminal moraines in four neighboring glacial valleys - Big Cottonwood, Little Cottonwood, Bells, and American Fork Canyons - were reported by Laabs et al. (2011), Laabs and Munroe (2016), and Quirk et al. (2018). Laabs and Munroe (2016) report exposure ages of a terminal and recessional moraine at Bells Canyon, which have recalculated mean ages of 21.9  $\pm$  2.0 ka (n = 3) and 16.8  $\pm$  0.7 ka (n = 2), respectively (Fig. 8; Tables 2 and 3). The latter age is similar to the recalculated <sup>10</sup>Be exposure ages of the right lateral moraine in Little Cottonwood Canyon and the terminal moraine in American Fork Canyons, which are 17.3  $\pm$  0.7 ka (n = 9) and 16.8  $\pm$  1.4 ka (n = 7), respectively (Fig. 8, Table 2). The left-lateral segment of the terminal moraine at Little Cottonwood Canyon has highly variable exposure ages (Table S1). Quirk et al. (2018) suggest that three exposure ages from this site are likely young outliers based on  $^{10}$ Be exposure ages of upvalley recessional moraines and glacially scoured bedrock in neighboring Big Cottonwood Canyon. The mean  $^{10}$ Be exposure age of the remaining boulders atop the left-lateral moraine is  $20.8 \pm 4.5$  ka (n = 4). The ages of this moraine and the terminal moraine in Bells Canyon are consistent with the mean exposure age of a terminal moraine segment in Big Cottonwood Canyon of  $20.2 \pm 0.5$  ka (n = 4) (Ouirk et al., 2018).

In the Uinta Mountains, <sup>10</sup>Be exposure ages of terminal moraines in numerous valleys spanning from the western end of the range (nearest the Wasatch Mountains) to the easternmost glacial valley were summarized by Laabs et al. (2009). They identified two groups of exposure ages; an older group represented by terminal moraines in northern and eastern glacial valleys, and a younger group represented by terminal moraines in the southern and western valleys. Recalculated ages representing the older group from the South Fork Ashley, Burnt Fork, and Smiths Fork terminal moraines are  $21.4 \pm 1.6$  ka (n = 7),  $18.6 \pm 1.4$  ka (n = 5), and  $19.4 \pm 2.2$  ka (n = 4), respectively (Fig. 9). Recalculated <sup>10</sup>Be exposure ages representing the southern and western glacial valleys from the Lake Fork, Yellowstone, and North Fork Provo (lateral and terminal segments of the moraine) are  $19.0 \pm 1.1$  ka (n = 7),  $18.2 \pm 1.4$  ka (n = 5),  $18.3 \pm 1.5$ ka (n = 4, and  $18.0 \pm 0.7$  ka (n = 5), respectively. Two moraines in the Bear River valley, also in the western sector of the Uinta Mountains, are 19.5  $\pm$  1.9 ka (East Fork, n = 7) and 18.2  $\pm$  0.9 ka (Main Valley, n = 5). A recessional moraine nested within the terminal moraine in the Lake Fork valley has a recalculated mean <sup>10</sup>Be exposure age of 17.7 + 0.5 ka (n = 7). These exposure ages in the Uinta Mountains are generally 0.5 kyr-1.5 kyr (as much as 8.3%) older than originally reported. The greatest offsets between the recalculated and originally reported ages are for samples from the Lake Fork, Yellowstone, and North Fork Provo moraines (Tables 2 and 3) which were analyzed using an earlier AMS standard (from National Institute of Standards and Technology, Standard Reference Material 4325; cf. Middleton et al., 1993).

A previously unpublished set of <sup>10</sup>Be exposure ages is reported here for the Bighorn Mountains in Wyoming (Fig. 1), one of the easternmost glaciated ranges in the Rocky Mountains. The Bighorn range crest trends northwest-southeast with glacial valleys draining toward the southwest and northeast (Darton, 1906). Two glacial valleys have <sup>10</sup>Be chronologies of terminal moraines, one in Tensleep Canyon in the western sector of the range and another in the North Fork Clear Creek valley in the eastern sector of the range (Fig. 10). In both valleys, the distribution of <sup>10</sup>Be exposure ages includes some older than MIS 2, suggesting the moraines are compound features occupied during multiple glaciations. Exposure ages that fall within MIS 2 display modes at ca. 14-15 ka and 16-19 ka for both moraines, and an older mode of ca. 21-23 ka is displayed for the North Fork Clear Creek moraine (Fig. 10, Table S1). These age modes are consistent with exposure chronologies in the nearby Greater Yellowstone region (Licciardi and Pierce, 2018; Pierce et al., 2018) and in the Uinta and Wasatch Mountains (Laabs et al., 2009; Quirk et al., 2018), but the youngest mode is based on only two individual exposure ages atop each moraine. The two older modes, 16-19 ka and 21-23 ka, are represented by a larger number of individual exposure ages from the two moraines (Table S1). The mean of the oldest grouping of exposure ages from the terminal moraine and intermediate grouping at North Fork Clear Creek are  $22.9 \pm 0.6$  ka (n = 3) and  $18.0 \pm 1.1$  ka (n = 3), respectively. The mean of the older grouping of exposure ages of the terminal moraine in Tensleep Canyon is  $17.9 \pm 1.8$  (n = 3) (Tables 2 and 3).

To summarize the large number of exposure ages from this region, terminal moraines and older modes thereof generally have mean exposure ages from 22 to 18 ka, with the exception of two younger terminal moraines in the western Wasatch Range with

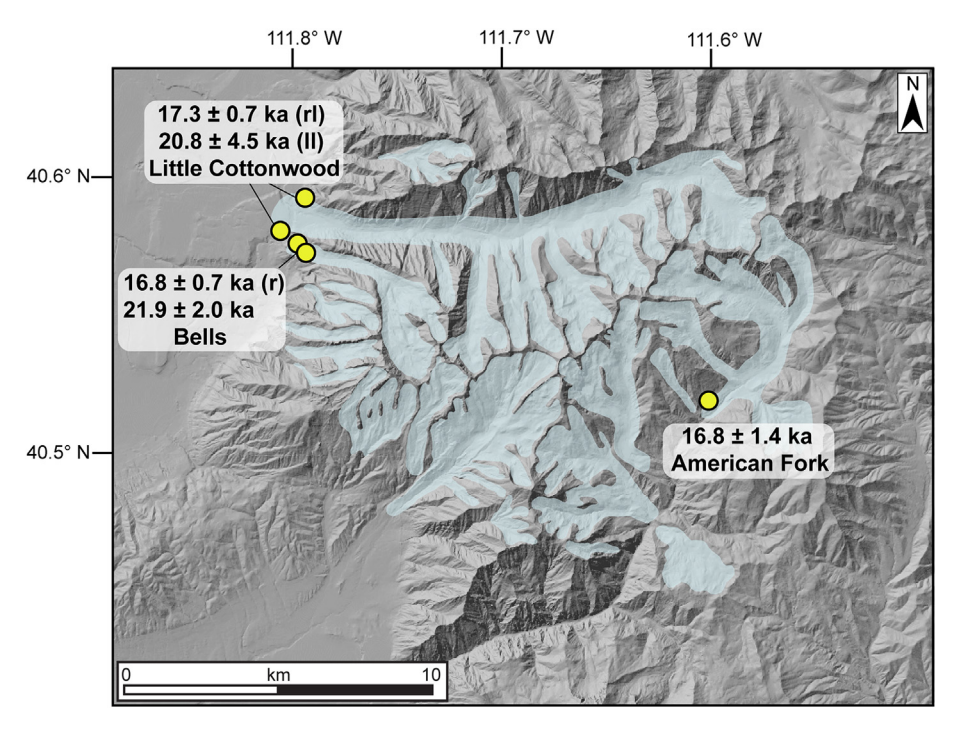


**Fig. 8.** Shaded relief map and reconstructed ice extents of the last glaciation in Little Cottonwood Canyon, American Fork Canyon, and Bells Canyon in the western Wasatch Mountains. Mean  $^{10}$ Be exposure ages ( $\pm 1\sigma$ ) of terminal, right lateral (rl), left lateral (ll), and recessional (r) moraines (yellow circles) are recalculated from Laabs et al. (2011) and Laabs and Munroe (2016). See Table S1 for individual exposure ages. Not shown are  $^{10}$ Be exposure ages of moraines and other glacial features in Big Cottonwood Canyon; see Quirk et al. (2018).

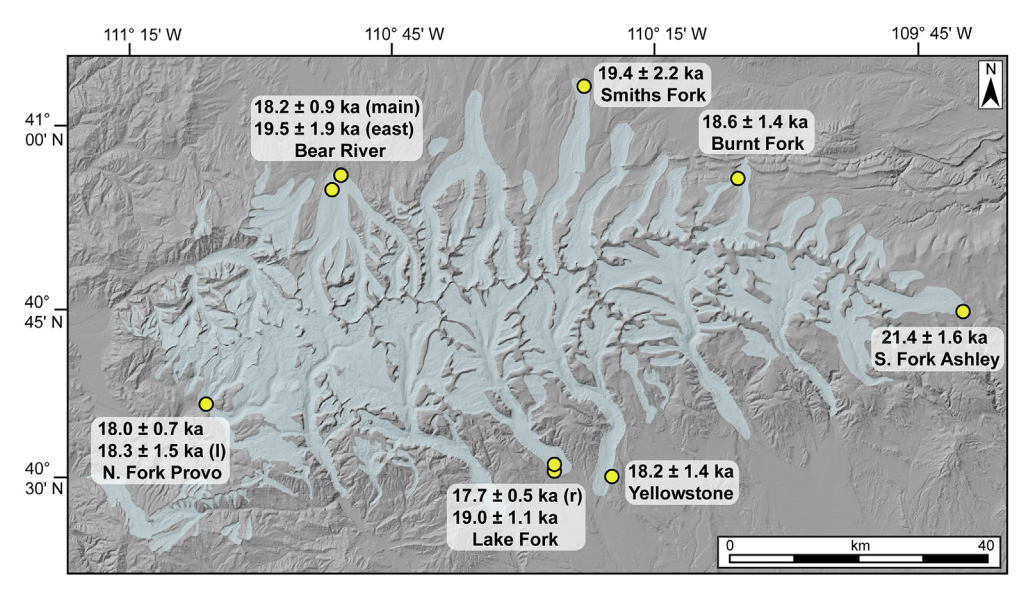


Fig. 9. Shaded relief map and reconstructed ice extents of the last glaciation in the Uinta Mountains. Glaciated areas are shaded blue. Mean  $^{10}$ Be exposure ages  $(\pm 1\sigma)$  of terminal, lateral (I), and recessional (r) moraines (yellow circles) are recalculated from Munroe et al. (2006), Refsnider et al. (2008), and Laabs et al. (2009) are shown. See Table S1 for mean and individual exposure ages.

mean exposure ages of ca. 17 ka. Downvalley recessional moraines have mean exposure ages ranging from ca. 19 ka in the Wind River Range to 18-17 ka in the Uinta and Wasatch Ranges.

# 4.2.6. The Greater Yellowstone region (Wyoming, Montana, and Idaho)

Cosmogenic glacial chronologies in the Rocky Mountains include numerous dated moraines in the Greater Yellowstone region, including the Yellowstone Plateau and neighboring

mountains in southwestern Montana and northwestern Wyoming (Licciardi et al., 2001; Licciardi and Pierce, 2008, 2018). Licciardi and Pierce (2018) recalculated all available exposure ages (>130) from this region using the same production and scaling models used in this review. Their recalculated exposure ages from the Yellowstone region are summarized here (see Licciardi and Pierce (2018) for a complete description), along with a small number of previously unpublished exposure ages from the Absaroka Range in the northern sector of the region.

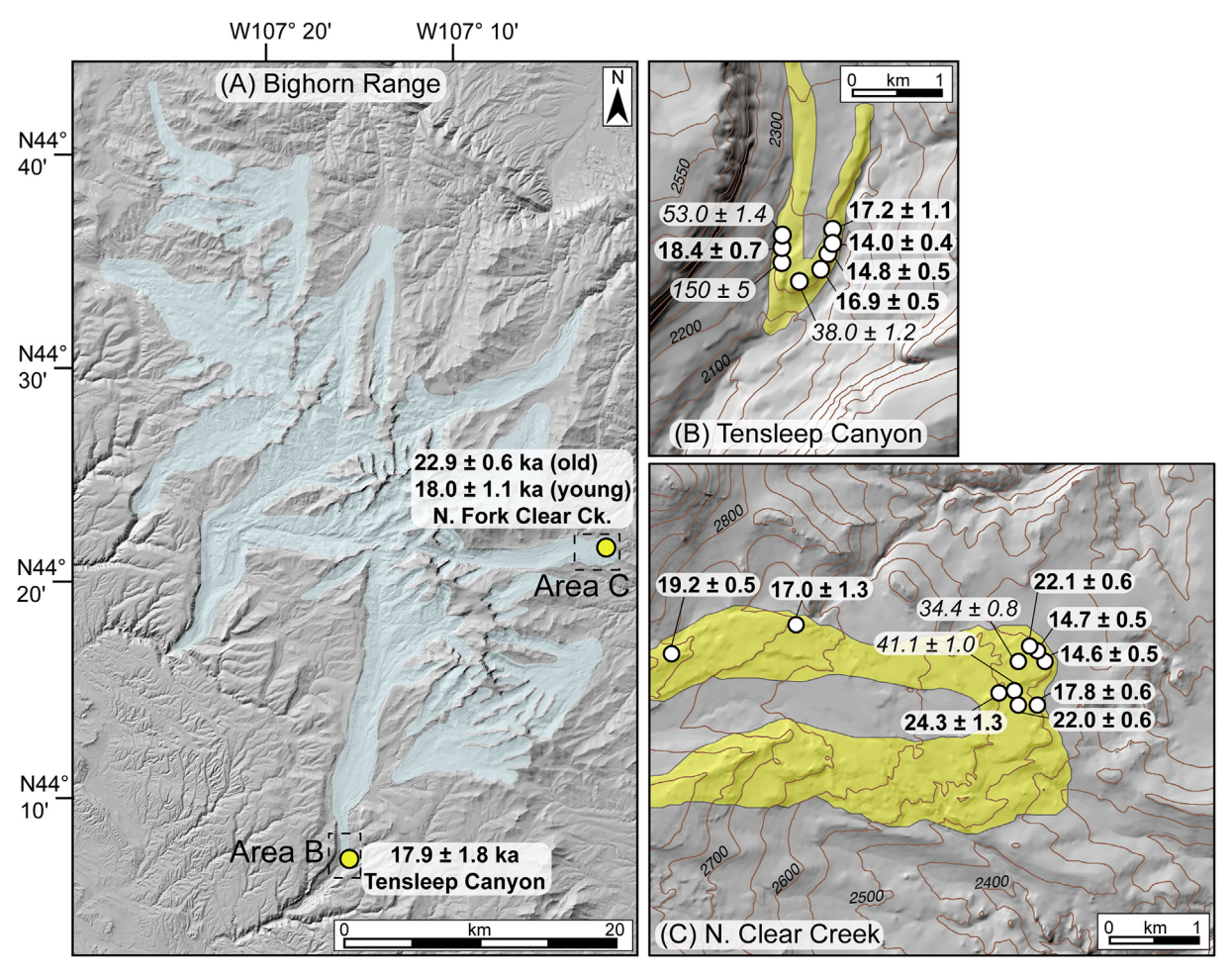


Fig. 10. Shaded relief map of the glaciated portion of the Bighorn Range, Wyoming. (A) Glaciated area and locations of inset maps of exposure-dated moraines; (B) Terminal moraines in Tensleep Canyon; (C) Terminal moraines in North Fork Clear Creek valley (C). Ice extents of the last glaciation (shaded blue) in panel A are based on the mapping of Darton (1906) and the authors' interpretations of topographic maps and aerial imagery. Mean <sup>10</sup>Be exposure ages  $(\pm 1\sigma)$  of each moraine (excluding outliers) are given in panel A. Mapping of terminal moraines (shaded yellow) in panels B and C are from field mapping of moraines by J. Munroe and B. Laabs. Topographic contours are in meters above sea level. White circles indicate the locations of erratic boulders sampled for <sup>10</sup>Be exposure dating with individual exposure ages  $(ka) \pm 1\sigma$  internal uncertainty. Ages given in italics are considered outliers.

At the northern outlet of the Yellowstone glacial system (Fig. 5), the exposure age of the Eightmile terminal moraine is limited by both cosmogenic <sup>10</sup>Be and <sup>3</sup>He (Licciardi et al., 2001). The recalculated <sup>10</sup>Be ages have a mean of 17.9  $\pm$  1.2 ka (n = 13) (Table 2). The recalculated <sup>3</sup>He ages have a mean of 16.3  $\pm$  1.1 ka (n = 12), similar to the reported age of 16.5  $\pm$  1.4 ka by Licciardi et al. (2001). A recessional moraine in the same valley, termed the Chico moraine, has a recalculated mean  $^{10}$ Be age of 17.1  $\pm$  1.7 ka (n = 9) (Table 3). In the Absaroka Range, terminal moraines of smaller valley glaciers that flowed toward the valley occupied by the northern Yellowstone outlet glacier have <sup>10</sup>Be exposure ages similar to that of the Eightmile moraine. These include the lateral portion of the moraine at Pine Creek, which has a recalculated mean exposure age of  $18.2 \pm 1.3$  ka (n = 6). This age limit overlaps with previously unreported mean  $^{10}$ Be exposure ages of 17.5  $\pm$  1.1 ka (n = 3) and  $16.9 \pm 0.2$  ka (n = 2) for terminal moraines in the neighboring South Fork Deep Creek and Cascade Creek valleys, respectively (A. Spears, unpublished) (Table 2).

A large outlet glacier occupying the Clarks Fork drainage in the northeastern sector of the Yellowstone glacial system deposited a terminal moraine along the eastern edge of the Beartooth Uplift (Fig. 5; Licciardi and Pierce, 2008). The recalculated  $^{10}$ Be exposure age of this moraine is  $19.8 \pm 0.9$  ka (n = 9). Terminal moraines

deposited by western outlets of the Yellowstone glacier system were reported by Licciardi and Pierce (2008) to feature very few boulders suitable for exposure dating; there, a single boulder atop a terminal moraine in the Gallatin River valley (Fig. 5) yields an exposure age of 17.7  $\pm$  0.4 ka (Table 2).

Exposure-dated terminal moraines from the last (Pinedale) glaciation in the southern part of the greater Yellowstone glacial system are several kyr younger than those in the north, indicating asynchronous glacial culminations around the periphery of the glacier complex (Licciardi and Pierce, 2008, 2018). Valley glaciers in the southern part of the Teton Range (Fig. 5) were distinct from the southern lobes of the Yellowstone glacial system. Licciardi and Pierce (2008) report exposure <sup>10</sup>Be ages of two moraine positions along the broad terminal complex impounding Jenny Lake on the east side of the range. The recalculated mean <sup>10</sup>Be exposure age of the outer moraine is  $15.2 \pm 0.7$  ka (n = 11) and the inner crest dates to 14.4 + 0.8 ka (n = 8) (Pierce et al., 2018, Tables 2 and 3), Just north of the Jenny Lake moraines, recently developed <sup>10</sup>Be ages of moraine boulders along the southern terminus of the Snake River lobe, which was sourced from the Yellowstone ice cap to the north, yield a mean of 15.5  $\pm$  0.5 ka (n = 5) (Licciardi and Pierce, 2018). Overall, the recalculated <sup>10</sup>Be exposure ages of moraines in the Greater Yellowstone region are 4-8% older than originally reported

(Licciardi and Pierce, 2018), with the greatest difference associated with the earliest reported ages (Licciardi et al., 2001).

### 4.2.7. The Southern Rocky Mountains (Colorado)

All published exposure ages of terminal and recessional moraines in the Southern Rocky Mountains are from Colorado. Here, more than  $200^{-10}$ Be exposure ages in twenty-two valleys in six ranges, and a smaller number of <sup>36</sup>Cl exposure ages from the San Juan, Sawatch, Elk, and Park Ranges, are available for moraines of the last glaciation (Fig. 6). Cosmogenic chronologies of glacial features in Colorado were reported and reviewed by Leonard et al. (2017a, 2017b) using the same calibrated production rate from Promontory Point, but with the time-dependent scaling of Lal (1991) and Stone (2000), the "Lm" model in the Version 3 online calculator. Differences among recalculated <sup>10</sup>Be exposure ages reported here and in Leonard et al. (2017a, 2017b) are minimal. Other recently published <sup>10</sup>Be exposure ages of moraines in the Mosquito Range (Brugger et al., 2019a) and the Sawatch Range (Brugger et al., 2019b; Schweinsberg et al., 2020) are calculated using the same production rate and scaling scheme as in this review.

In three of the Colorado ranges—the San Juan Mountains, the Park Range, and the Front Range in the western and northern portions of the state (Fig. 6, sites 1–6)—available exposure ages from outer moraine complexes of the last glaciation display an older mode, all greater than ca. 18–19 ka. In the two other ranges—the Sawatch Range and the Sangre de Cristo Mountains (Fig. 11, sites 7–22) further south and east—the available exposure ages suggest that although parts of the moraine complexes there are as old as elsewhere in the state, final recession from these moraines took place considerably later at ca. 17-16 ka (Leonard et al., 2017b).

In the Animas River valley of the western San Juan Mountains (Fig. 6, site 1), a recalculated  $^{10}$ Be profile age from an outwash terrace of the last glaciation and recalculated  $^{10}$ Be ages from glacially polished bedrock upvalley (Guido et al., 2007) suggest that outwash deposition ceased at  $21.5 \pm 1.5$  ka and that ice had retreated more than 20 km upvalley by  $18.8 \pm 0.5$  ka. In the eastern San Juan Mountains, Benson et al. (2004) report  $^{36}$ Cl exposure ages of terminal moraines at Continental Reservoir and at Hogback Mountain (Fig. 6, sites 2–3). Recalculated mean exposure ages of the moraines are  $20.1 \pm 0.3$  ka (n = 3) and  $19.1 \pm 1.4$  ka (n = 11),

respectively (Table 2). In north-central Colorado, recalculated  $^{10}$ Be exposure ages of a terminal moraine in the Roaring Fork/Red Canyon valley of the Park Range in north-central Colorado (Fig. 11, site 4) (Benson et al., 2005) have a mean of  $22.2 \pm 2.3$  ka (n = 3). Six  $^{36}$ Cl ages from the same terminal moraine (Benson et al., 2004, 2005) yield a recalculated age of  $18.6 \pm 1.2$  (n = 5).

In the Colorado Front Range, TCN chronologies are available for North ( $^{10}\text{Be}$ ) and Middle ( $^{10}\text{Be}$  and  $^{36}\text{Cl}$ ) Boulder Creek valleys (Fig. 6, sites 5–6) (Schildgen et al., 2002; Ward et al., 2009; Dühnforth and Anderson, 2011), and a single moraine boulder has been dated in the North St. Vrain Creek valley (Fig. 6, site 6) (Benson et al., 2004). Terminal moraine complexes at North and Middle Boulder Creek yield recalculated  $^{10}\text{Be}$  exposure ages of 20.4  $\pm$  2.1 (n = 5) and 20.1  $\pm$  2.0 ka (n = 2), respectively. The terminal moraine in Middle Boulder Creek has a mean  $^{36}\text{Cl}$  exposure age of 19.1  $\pm$  0.3 ka (n = 3). The single boulder atop the North St. Vrain terminal moraine has a recalculated  $^{10}\text{Be}$  exposure age of 21.7  $\pm$  1.1 ka and a  $^{36}\text{Cl}$  exposure age of 19.1  $\pm$  0.3 ka (Tables S1 and S2).

In the Mosquito Range (Fig. 6, sites 7–10), Brugger et al. (2019a) report  $^{10}$ Be chronologies of terminal and recessional moraines in four valleys. There, terminal moraines in the Iowa Gulch and Fourmile valleys have exposure ages of 21.7  $\pm$  1.6 ka (n = 2) and 20.6  $\pm$  1.1 ka (n = 4; Table 2), respectively, and recessional moraines in the Sacramento Creek and Union Creek valleys have exposure ages of 17.4  $\pm$  1.3 ka (n = 1) and 17.1  $\pm$  0.4 ka (n = 3; Table 3).

In the nearby Sawatch Range of central Colorado (Fig. 6, sites 11–19). <sup>10</sup>Be exposure ages are available on boulders from last glaciation moraine complexes in nine valleys (Schildgen et al., 2002: Brugger, 2007: Briner, 2009: Young et al., 2011: Brugger et al., 2019b; Schweinsberg et al., 2020). Three adjacent valleys on the east side of the central portion of the range (Fig. 6, sites 11–13) have been the subject of intensive study. Young et al. (2011) concluded that deposition of moraine complexes in the three valleys spanned a significant time interval and that the timing of individual culminations may have differed valley-to-valley. In Pine Creek valley, two clusters of recalculated <sup>10</sup>Be exposure ages from the main lateral moraine led Briner (2009) to suggest that the moraine was occupied during two advances with retreat of ice from the moraine, recalculated to 22.3  $\pm$  1.3 ka (n = 5) and 16.3  $\pm$  0.4 ka (n = 6), respectively (Tables 2 and 3). Glacially scoured bedrock with recalculated  $^{10}$ Be exposure ages of 16.0  $\pm$  0.3 and 15.8  $\pm$  0.4

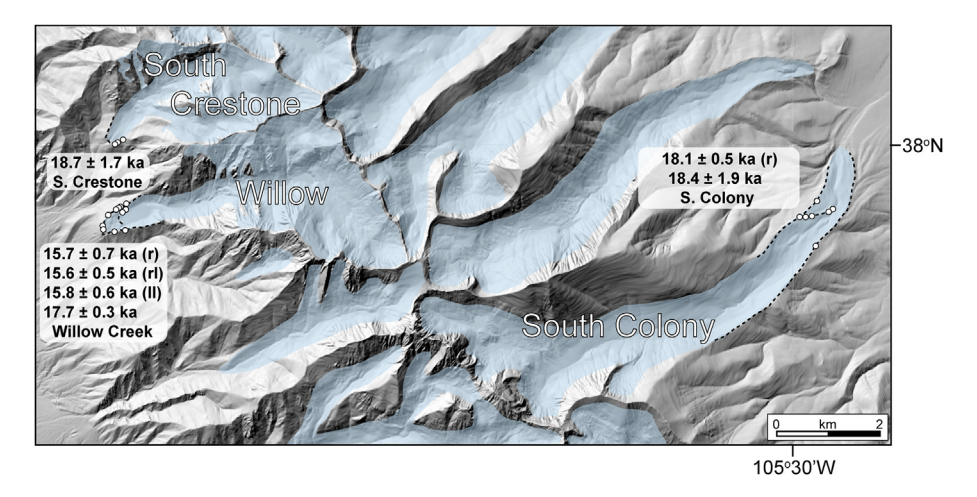


Fig. 11. Shaded relief map showing reconstructed ice extents of the last glaciation in the Crestone Peaks area of the Sangre de Cristo Mountains, Colorado. Glaciated areas are shaded blue, moraine crests shown with dashed lines, and white circles indicate boulders sampled for  $^{10}$ Be exposure dating. Reconstructed ice extents from the last glaciation in the South Crestone and Willow Creek valleys are based on glacier modeling of Leonard et al. (2017a). In other valleys, ice extent is approximated based on the authors' interpretation of aerial imagery and maps and the field mapping of McCalpin (2011). Mean  $^{10}$ Be exposure ages ( $\pm 1\sigma$ ) of terminal, right lateral (rl), left lateral (ll), and recessional (r) moraines are recalculated from Leonard et al. (2017a). See Table S1 for individual exposure ages.

(Young et al., 2011) indicate ice recession of about 4 km (or ~25% of total glacier length) within a few hundred years after the final abandonment of the terminal moraine (Table S1). In Clear Creek valley, Young et al. (2011) report <sup>10</sup>Be exposure ages of a lateral moraine, with a recalculated mean of 19.5  $\pm$  0.2 ka (n = 3, excluding two outliers identified by Young et al., 2011). In adjacent Lake Creek valley, Schweinsberg et al. (2020) developed a detailed <sup>10</sup>Be moraine chronology of terminal and recessional moraines from the last glaciation. Numerous large boulders distributed among two terminal moraines and two recessional ridges directly inboard of the terminal positions yield remarkably consistent <sup>10</sup>Be exposure ages averaging  $20.6 \pm 0.6$  ka (n = 22), suggesting that all four of these closely spaced moraines were constructed within a short time interval (Table 2). Boulders resting on a prominent recessional moraine ~5 km upvalley from the terminal moraines in Lake Creek valley have a mean  $^{10}$ Be exposure age of 15.6  $\pm$  0.7 ka (n = 5) (Table 3). To the north of the Lake Creek valley, also on the east side of the range, Brugger et al. (2019b) report <sup>10</sup>Be exposure ages from terminal moraine complexes in four additional adjacent areas (Fig. 6, sites 14–17). Boulder samples from the terminal complex in the Rock Creek valley yield a recalculated mean exposure age of  $20.9 \pm 2.3$  ka (n = 6) and a single boulder sampled from the outermost moraine in Lake Fork Creek valley yields a recalculated exposure age of 19.7  $\pm$  0.4 ka. Two boulders from the outermost moraine of the Tennessee Ice complex at Longs Gulch yield exposure ages of 20.7  $\pm$  0.4 ka and 27.9  $\pm$  0.5 ka (Table 2). Brugger et al. (2019b) interpret the latter age to reflect inheritance. In Lake Fork Creek and Halfmoon Creek valleys, boulders sampled from moraines a short distance upvalley from the outermost moraines yielded <sup>10</sup>Be ages of 17.2  $\pm$  0.8 ka (n = 3) and 16.0  $\pm$  0.7 ka (n = 3) respectively (Table 3). In the Taylor River valley on the west side of the southern Sawatch Range (Fig. 6, sites 18–19), recalculated <sup>10</sup>Be exposure ages on multiple ridges of the moraine complex built during the last glaciation (Brugger, 2007) indicate ice retreat at  $19.5 \pm 2.0$  ka (n = 5). Here, recalculated  $^{36}$ Cl exposure ages on three of the same boulders have a mean exposure age of 20.8  $\pm$  1.9 ka (Table 2). Recalculated <sup>10</sup>Be exposure ages are  $16.0 \pm 0.7$  ka and  $15.0 \pm 0.7$  ka (with a mean of  $15.5 \pm 0.7$  ka) from two boulders on the inner portion of the moraine complex in the Texas Creek valley

The Sangre de Cristo Mountains are the southeasternmost range of the Rocky Mountains. <sup>10</sup>Be exposure ages are available from three valleys in the Crestone Peaks section of the range in southern Colorado (Fig. 6, sites 20–22) using the same production model as used here but with time-dependent scaling of Lal (1991) and Stone (2000), designated "Lm" in the original CRONUS Earth calculator (Leonard et al. (2017a)). Exposure ages recalculated here (with LSDn scaling) are slightly younger but statistically identical to the ages reported by Leonard et al. (2017a) at 1 $\sigma$ , with mean ages slightly younger. Ages on the outermost moraines of the last glaciation range from 18.7  $\pm$  1.7 ka (n = 3) and 18.4  $\pm$  1.9 ka (n = 2) in South Crestone and South Colony Creek valleys to 17.7  $\pm$  0.3 ka (n = 3) in Willow Creek valley (Fig. 11; Table 2). A younger moraine crest at South Colony yields a mean  $^{10}$ Be exposure age of 18.1  $\pm$  0.5 ka (n = 4), while the more proximal and inner portions of the moraine complex at Willow Creek yield a mean <sup>10</sup>Be exposure age of  $15.7 \pm 0.5$  ka (n = 8) (Fig. 11, Table 3).

To summarize, <sup>10</sup>Be exposure ages of terminal moraines in the Colorado portion of the Southern Rocky Mountains span a broad time interval, from ca. 22.5–18.0 ka. In the San Juan and Front ranges (Fig. 11), terminal moraines may have been abandoned early in this time interval and extensive deglaciation appears to have occurred by about 18–19 ka. In contrast, in the Sawatch and Sangre de Cristo ranges, terminal and recessional moraine ages suggest that glaciers remained at (or close to) their maximum extents until

16.5-15.5 ka.

4.2.8. Discussion of recalculated exposure ages of last-glaciation moraines

Most recalculated <sup>10</sup>Be exposure ages summarized here are 5–11% older than originally reported, although differences are greater than this for some earlier studies and less for more recent studies. Recalculated <sup>36</sup>Cl exposure ages also differ significantly from previously reported ages, but the magnitude of the difference is more variable. For <sup>10</sup>Be exposure ages, the differences are largely due to the use of a lower SLHL production rate and time-dependent scaling schemes in our exposure-age calculations compared to those used in previous studies.

While additional considerations of selecting a globally averaged or regionally calibrated production rate and scaling scheme (St, Lm, or LSDn) are important (see section 2.1 above), the difference among individual exposure ages recalculated using different combinations of newer production rates and scaling models (Table S1) is generally small (<1-4%) compared to the 5-11% difference between the recalculated and originally reported ages (Tables 2 and 3). On average, <sup>10</sup>Be exposure ages computed using a globally averaged SLHL production rate are 3% older than exposure ages computed using the regional calibration from Promontory Point and the same scaling model. This is consistent with the difference in SLHL production rates from the globally averaged calibration set described by Borchers et al. (2016) and from the Promontory Point calibration (Lifton et al., 2015),  $\sim$ 3.9 and 4.0 atoms  $g^{-1}$   $yr^{-1}$ , respectively. The small differences among <sup>10</sup>Be exposure ages computed with globally averaged and regionally calibrated production rates and time-dependent scaling models Lm and LSDn are, in general, less than the  $1\sigma$  uncertainty of the mean exposure age for most moraines, which is typically ~5% of the exposure age (Tables 2 and 3). This observation suggests that the variability of individual exposure ages of boulders atop moraines is, in most cases, an equal or larger source of uncertainty than the production rate and is therefore an important consideration in comparisons of moraine ages with other records of Late Pleistocene climate.

The greatest difference among <sup>10</sup>Be exposure ages shown in Table S1 is between the ages computed using the same production models but with differing implementations in online exposure-age calculators. Both the Version 3 Calculator and CRONUScalc compute <sup>10</sup>Be exposure ages using globally averaged SLHL production rates and implementations of the scaling model of Lifton et al. (2014), denoted "LSDn" in the Version 3 Calculator and "SA" in CRONUScalc. For this same combination of production and scaling model, exposure ages computed by CRONUScalc are 3–5% older than those computed using the Version 3 Calculator. The reasons for this difference are unclear and merit further consideration, but it is worth reiterating that the recalculated <sup>10</sup>Be exposure ages based on the Promontory Point calibration set with LSDn scaling are the youngest among all the <sup>10</sup>Be exposure ages shown in Table S1.

Recalculated <sup>36</sup>Cl exposure ages differ to a variable degree and are generally younger than originally reported, with the exception of exposure ages from the northern Cascade Range (Porter and Swanson, 2008) that are 15–20% older than originally reported as described above (Table 2). This exception is due to the difference between production models for moraine boulders in the northern Cascade Range. The anomalously high production rate of Swanson and Caffee (2001) used by Porter and Swanson (2008) differs greatly from most calibrations of <sup>36</sup>Cl (Licciardi et al., 2008; Marrero et al., 2016b) and has not been used in other studies of moraine chronologies in the western U.S. (e.g., Phillips et al., 2009, 2016a, b). Differences between the originally reported exposure ages of Tioga moraines in the Sierra Nevada and recalculated ages are described

in Phillips et al. (2016a, b). Recalculated <sup>3</sup>He exposure ages are younger than originally reported by only 1.2% in the Greater Yellowstone region and by 4–8% in the Colorado Plateau (Table 2), reflecting the fact that <sup>3</sup>He production rate estimates have remained virtually unchanged from those used in previous reports. The small differences from original reports are due to the newer scaling models used here.

# 5. Moraine chronologies and inferences of past climate change

The recalculated exposure ages summarized in the preceding sections provide an updated framework for inferring Pleistocene climate change. Here, the timing of the last two major Pleistocene glaciations is compared across the conterminous western U.S., with consideration of the choice of production model for *in situ* <sup>10</sup>Be and in the context of global and regional-scale records of climate change from MIS 6 to MIS 2. The recalculated moraine chronologies reported here are interpreted to represent the last time of terminal or downvalley recessional moraine occupation for comparison with other climate proxy records such as global ice volume, summer insolation, marine sediments and ice cores.

# 5.1. Synchrony and asynchrony of exposure ages of terminal moraines

Consideration of numerous recalculated exposure ages affords the opportunity to identify region-wide temporal and spatial patterns in the chronology of the last two Pleistocene glaciations: these are described in the following sections. For the penultimate glaciation, we rely on oldest (or oldest mode of) exposure ages to define patterns of glaciation, whereas for the last glaciation we favor the mean or peak probability of ages (as shown in relative probability plots) for reasons described above (Figs. 12 and 13). For the penultimate glaciation, cosmogenic chronologies generally focus on single moraine ridges rather than multiple moraine crests within a single valley. In cases where several penultimateglaciation moraine crests are dated, such as the <sup>36</sup>Cl chronologies of Bull Lake moraines in the Wind River Range (Phillips et al., 1997) and the moraine sequence in Icicle Creek of the northern Cascade Range (Porter and Swanson, 2008), distinguishing the timing of multiple ice culminations during the penultimate glaciation is complicated by the high variability of exposure ages. The following discussion therefore focuses on identifying first-order trends in the timing of the penultimate glaciation. In contrast, for the more extensive and higher-resolution chronologies of the last glaciation, some studies report exposure ages of terminal and recessional moraine sequences with known relative ages in single glacial valleys that represent multiple times when glaciers reached maximum or near-maximum lengths. In the discussion below. exposure ages of successive moraine crests within glacial valleys are distinguished and are used to identify settings where multiple glacial culminations occurred during MIS 2.

### 5.1.1. The penultimate glaciation

In the conterminous western U.S., the oldest exposure ages of moraines and outwash spanning ~150-125 ka have a mean of  $138 \pm 13$  ka and overlap with the latter part of MIS 6 (Figs. 7 and 14). Given previous studies suggesting that the oldest exposure age(s) from moraines of the penultimate glaciation are likely closest to the true age of the moraine (Putkonen and Swanson, 2003; Hein et al., 2009; Applegate et al., 2012; Wesnousky et al., 2016), we conclude that most moraines of the penultimate glaciation were deposited during MIS 6. This conclusion agrees with that of Quirk et al. (2018) for the Wasatch Range, Rood et al. (2011) for the Sierra Nevada,

Licciardi and Pierce (2008, 2018) for the Greater Yellowstone region, and Marchetti et al. (2011) for the Colorado Plateau.

Although the reasons for using the oldest exposure age as the best estimate of the true age of moraines and outwash of the penultimate glaciation are substantiated in previous studies and applying this approach results in well-aligned moraine chronologies in the western U.S., doing so without consideration of TCN age distributions assumes that none of the sampled boulders on these moraines are affected by inherited isotopes. Applegate et al. (2012) caution that positively skewed (skew > 0) distributions of exposure ages can indicate that some moraine boulders have TCN inventories inherited from intervals of exposure prior to moraine deposition. As noted above, however, inheritance is less probable for moraine boulder surfaces in comparison with bedrock outcrops and is especially unlikely for boulders transported to terminal moraines by glaciers with lengths >10 km. Furthermore, a positive skew of exposure ages can also result from moraine crest denudation during one or more cool and wet intervals of the last 105 yr. Additionally, only two of the original reports of exposure ages of penultimate glaciation moraines compiled here identified signals of isotope inheritance; Porter and Swanson (2008) exclude some older <sup>36</sup>Cl exposure ages from calculations of the mean of penultimate glaciation moraines in the northern Cascade Range, and Schweinsberg et al. (2020) attribute two old outlying <sup>10</sup>Be ages  $(187 \pm 2 \text{ ka})$  and  $172 \pm 2 \text{ ka}$  among the eight Bull Lake moraine boulders they dated in the Sawatch Range to inheritance. While we do not identify any other signals of inherited TCNs within our compilation of ages from penultimate glaciation moraines, the possible influence of inherited nuclides among exposure ages of moraines cannot be ruled out.

Aside from the observed variability of exposure ages of pre-LGM moraines, two other potential uncertainties must be considered in the interpretation of penultimate glaciation moraine ages. First, the degree of boulder-surface erosion is difficult to infer from field observations and, in most studies, has been assumed to be zero to 1 mm/kyr. Boulder erosion rates can be limited by two-isotope measurement of surfaces, but nearly all studies of penultimate glaciation moraines compiled here have involved only a single isotope. Phillips et al. (1997) and Brugger (2007) did measure <sup>10</sup>Be and <sup>36</sup>Cl inventories for a small number of boulder surfaces, finding that boulder-surface erosion rates atop penultimate glaciation moraines are negligible. While most subsequent studies of penultimate glaciation moraines in the conterminous western U.S. have also assumed small or negligible erosion rates, it is worth noting that assuming even a modest boulder-surface erosion rate of 1 mm/ kyr generally increases exposure ages of MIS 6 moraines by 10<sup>4</sup> yr compared to exposure ages computed with zero erosion (Table 1). For penultimate glaciation moraines, this amount of time exceeds the exposure-age uncertainty related to cosmogenic nuclide production rate estimates and therefore remains a significant potential source of error in cases where boulder surface erosion rates are unknown. Regardless, exposure ages of penultimate-glaciation moraines should be considered minimum limits, especially in cases where boulder-surface erosion rates are unknown.

A second source of uncertainty is related to production rate scaling through time, owing to the lack of time-integrated production rate calibrations from independently dated surfaces as old as the penultimate glaciation. Most production rate calibration sites measure TCN inventories of surfaces with known ages of  $10^3-10^4$  yr (Borchers et al., 2016). As a result, production rates used in any scaling model must be extrapolated over  $10^5$  yr to compute exposure ages of penultimate glaciation moraines. The effect of this extrapolation is generally unknown, although Fenton et al. (2019) reported evidence of minimal change in the production of  $^3$ He from 72 to 20 ka in a production calibration study at a high-altitude

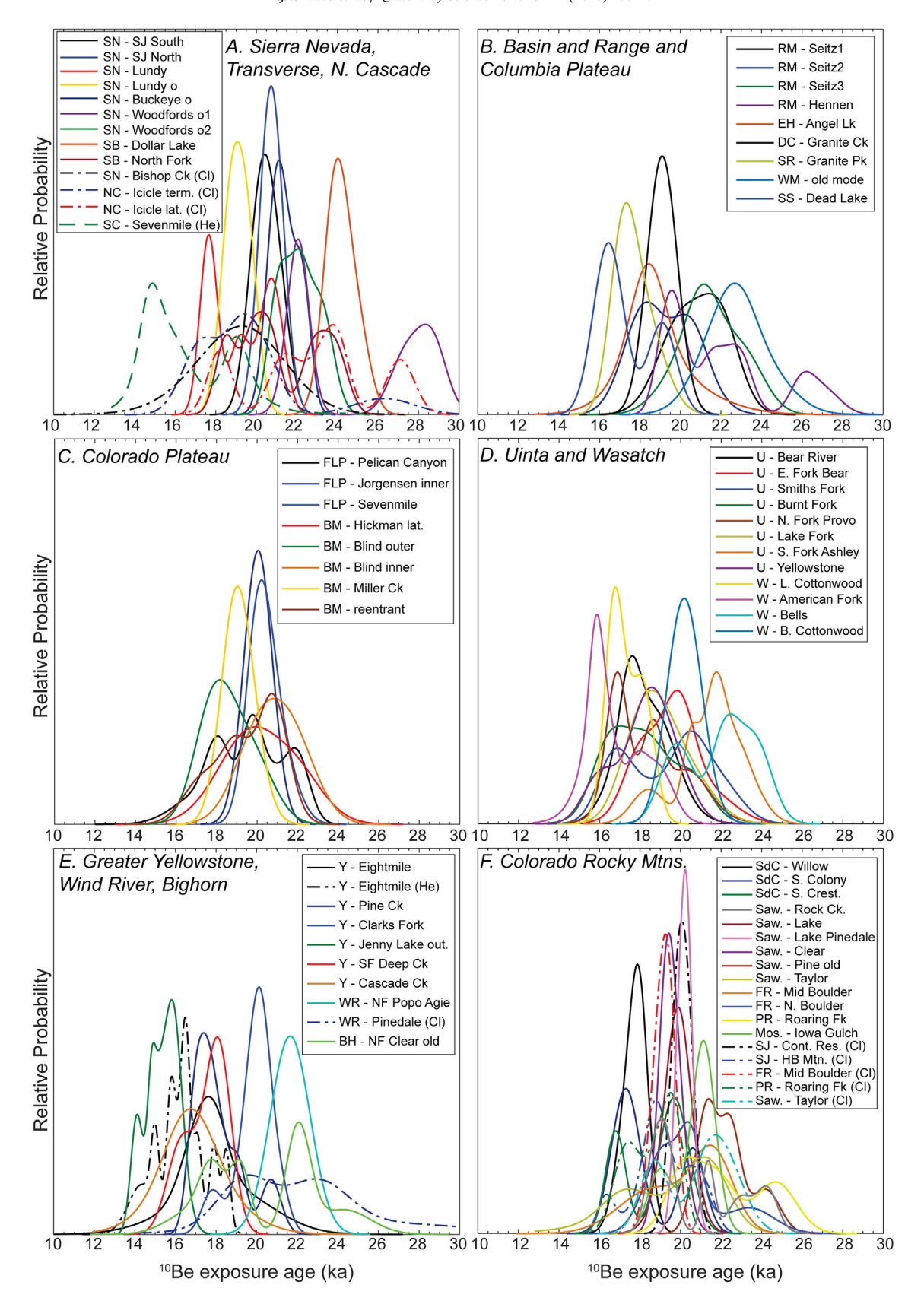


Fig. 12. Normal kernel density estimates of exposure ages of terminal moraines of the last glaciation in the conterminous western U.S. (A) the Sierra Nevada (SN), Transverse (SB, San Bernardino) Range, northern Cascade Range (NC) and southern Cascade Range (SC); (B) Basin and Range and Columbia Plateau, including the Ruby Mountains (RM), East Humboldt Mountains (EH), Deep Creek Range (DC), Santa Rosa Range (SR), Wallowa Mountains (WM), and South Snake Range (SS); (C) the Colorado Plateau, including Fish Lake Plateau (FLP) and Boulder Mountain (BM); (D) the Uinta Mountains (U) and Wasatch Mountains (W); the Greater Yellowstone region (Y), Wind River Range (WR) and Bighorn Range (BH); and (F) the Colorado Rocky Mountains, including the Sangre de Cristo Mountains (SdC), Sawatch Range (Saw.), Front Range (FR), Park Range (PR), Mosquito Range (Mos.), and San Juan Mountains (SJ). The top of each panel has a relative probability value of 1.

site in northern Arizona. In our compilation of exposure ages, the extrapolation is illustrated by the differences in exposure ages computed using time-constant and time-varying production models, which for most penultimate glaciation moraine surfaces is > 20 kyr (Tables S1 and S3). For <sup>10</sup>Be exposure ages, the "Lm" and "LSDn" time-dependent scaling models yield younger exposure ages of moraines than the time-constant "St" model. The external uncertainties of exposure ages (as computed by the Version 3 Calculator; Table S1) include the uncertainty of the production rate through time, significantly exceeding the internal (measurement) uncertainty. The external uncertainty computed by the Version 3 Calculator or the total uncertainty as computed by the CRONUScalc is therefore used in comparisons of moraine exposure ages with other paleoclimate proxy records.

#### 5.1.2. Terminal moraines of the last glaciation

Compared to exposure ages of moraines of the penultimate glaciation, the coefficient of variation of exposure ages for individual terminal moraines of the last glaciation is less (Table 2), averaging only 13%. This degree of variability is less than reported in previous assessments of exposure ages (e.g., Putkonen and Swanson, 2003; Applegate et al., 2012) and does not appear to vary from earlier to later applications of TCN exposure dating or with the number of exposure ages determined for individual moraines. The smaller coefficient of variation of exposure ages from moraines of the last glaciation indicates a more consistent exposure history among sampled boulders. This most likely reflects a lesser degree of moraine denudation since the last glaciation compared to the penultimate glaciation, which is consistent with results of moraine degradation modeling studies of Putkonen and Swanson (2003) and Applegate et al. (2012).

Given the low coefficient of variation of exposure ages of most terminal moraines of the last glaciation, the mean exposure age is considered to provide a reliable estimate of the time when the moraine was last occupied by an ice margin (as is inferred in most original reports of the data compiled here). In a few cases, bimodal age distributions from single moraine crests have been interpreted to represent multiple episodes of moraine occupation during the last glaciation (see descriptions in section 4.2). In most cases, exposure ages of terminal moraines are normally distributed or have skew values closer to zero compared to moraines of the penultimate glaciation (Fig. 12), further justifying the use of mean exposure age as the best limit on the time when the moraine was last occupied by an ice margin that subsequently began to retreat.

Exposure ages of all terminal moraines from the last glaciation reviewed here fall within MIS 2, displaying both intra-range and inter-range variability among exposure ages within this time interval (Fig. 12). Intra-range variability has been linked in some previous studies to differences in climate between glacial valleys (e.g., Refsnider et al., 2008; Laabs et al., 2009). Other studies have attributed intra-range variability in terminal moraine ages to contrasting valley glacier response times related to ice dynamics and/ or differences in glacier shape and hypsometry (e.g., Young et al., 2011), to influences of shifting orographic precipitation patterns (Licciardi and Pierce, 2018), or to differences in boulder exposure history related to moraine crest erosion through time (Applegate et al., 2010, 2012). Such differences remain evident among recalculated exposure ages. In contrast, inter-range variability of exposure ages of moraines has been identified in some previous studies as evidence of differences in the timing of glacial maxima across regional transects of the western U.S. (e.g., Licciardi et al., 2004; Thackray et al., 2004; Thackray, 2008; Licciardi and Pierce, 2008; Laabs et al., 2009). These studies reported post-LGM exposure ages or radiocarbon limits on terminal moraines in mountains at higher latitudes in Idaho (Thackray et al., 2004), Oregon (Licciardi et al., 2004) and Montana (Licciardi et al., 2001), closer to the southern margin of North American Ice Sheets. These younger ages were interpreted as a sign of glacial culmination after the LGM in response to increased delivery of westerly derived moisture to reach the northern continental interior of the western U.S. after the Laurentide Ice Sheet started to retreat. Similarly, Munroe et al. (2006) and Laabs et al. (2009) suggested that younger exposure ages of terminal moraines in the western Uinta Mountains. compared to mountain ranges farther east and north, reflected the influence of pluvial Lake Bonneville (location shown in Fig. 1) on glacier mass balance, with glaciers reaching their maximum lengths during the Bonneville highstand. Although these ideas and explanations for inter-range variability in exposure ages have remained under consideration in more recent studies of late Pleistocene glaciation and paleoclimate, the proliferation of exposure dating of moraines in the western U.S. and attendant improvements in sample collection, preparation, analysis, along with consideration of production rates as shown in this review has revealed a greater degree of inter-range consistency among glacial chronologies. The overall range of mean recalculated exposure ages of terminal moraines is still wide, from as old as 24-25 ka for some moraines and outwash in the Sierra Nevada to as young as 15-17 ka for some terminal moraines in the Rocky Mountains, but a clear central tendency exists with a mean of 19.5  $\pm$  2.3 ka. The paleoclimatic significance of this central tendency and the variability among recalculated exposure ages are discussed in section 5.2. below.

### 5.1.3. Downvalley recessional moraines of the last glaciation

Exposure ages of downvalley recessional moraines delimiting ice margin positions >75% of the maximum glacier lengths are less abundant compared to those of terminal moraines, but are sufficient in number to afford a preliminary assessment of the timing of glacier culminations during initial recession and prior to largerscale ice retreat during the last deglaciation of western U.S. mountain ranges. As expected, recessional moraines display exposure ages that either overlap with or are younger than exposure ages of terminal moraines from the same glacial valley and exhibit a lesser coefficient of variation (averaging 7.1% for moraines included in this review; Table 3). Recessional moraines tend to have lower relief than terminal moraines, which may result from being constructed over a shorter amount of time or deposition along a more gently sloping ice margin. If so, this in turn would result in less denudation through time (Putkonen and Swanson, 2003) and more consistent boulder exposure history.

The differences between originally reported and recalculated exposure ages of recessional moraines are similar to those for terminal moraines. Recalculated <sup>10</sup>Be exposure ages of recessional moraines are generally older than those originally reported in earlier (pre-2009) <sup>10</sup>Be exposure dating studies. An extreme case is the inner moraine crest of the Leavenworth moraines in the northern Cascade Range, which have recalculated <sup>36</sup>Cl exposure ages 25% older than originally reported, reflecting differences between older and newer production models.

Intra-range and inter-range variability among exposure ages of recessional moraines is less than that of terminal moraines (Table 3; Fig. 13). The oldest exposure-dated recessional moraines (19–21 ka) that fall within  $\geq$ 75% of the full-glacial length are located in the Wind River Range (Phillips et al., 1997; Dahms et al., 2018), whereas downvallley recessional moraines with younger exposure ages (ranging from 17 to 14 ka) are widespread across other mountain ranges (Table 3). The region-wide mean exposure age of downvalley recessional moraines is  $17.0 \pm 1.8$  ka, overlapping with the mean exposure age of terminal moraines of  $19.5 \pm 2.3$  ka but signifying a later culmination or persistence of near-maximum

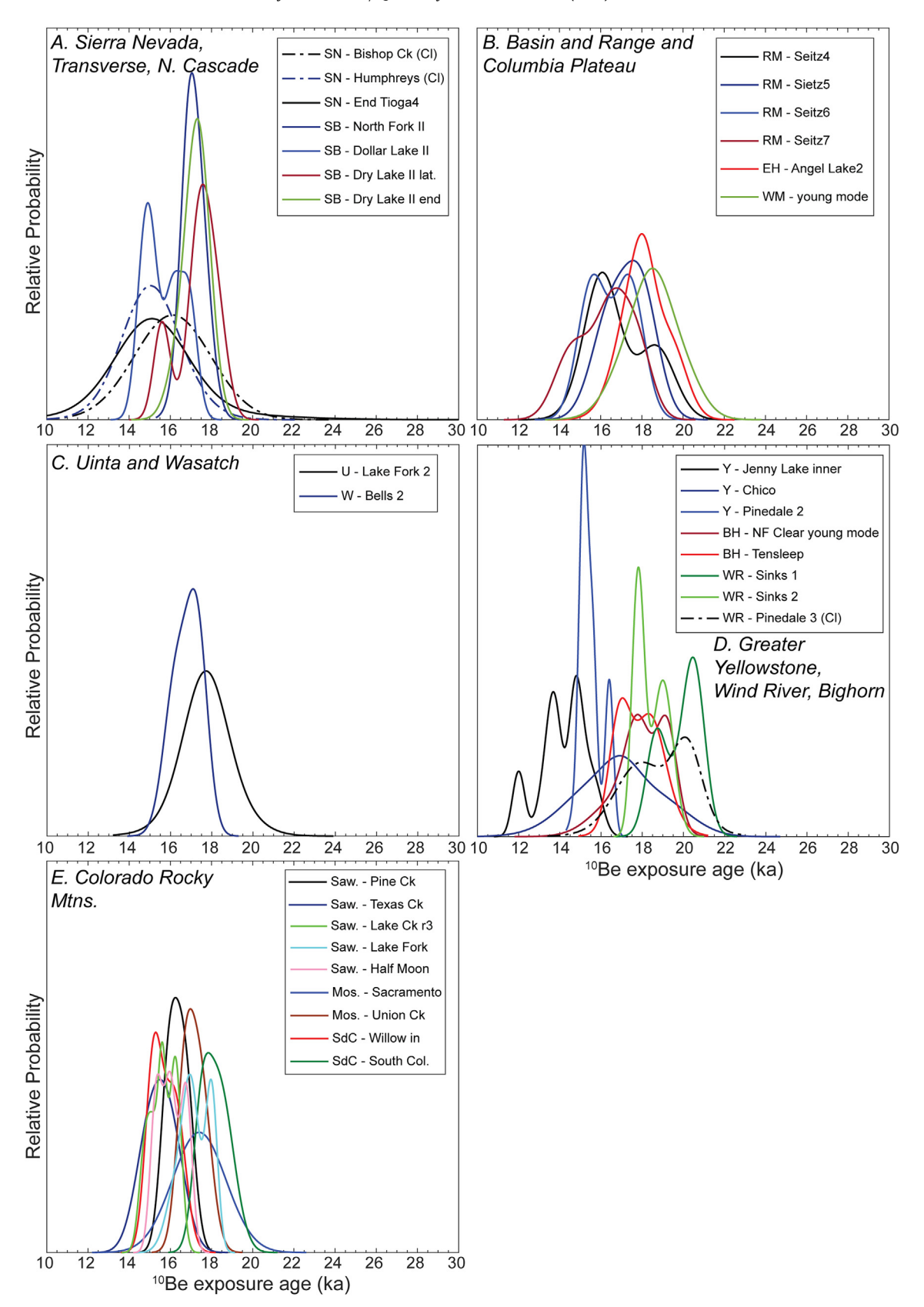
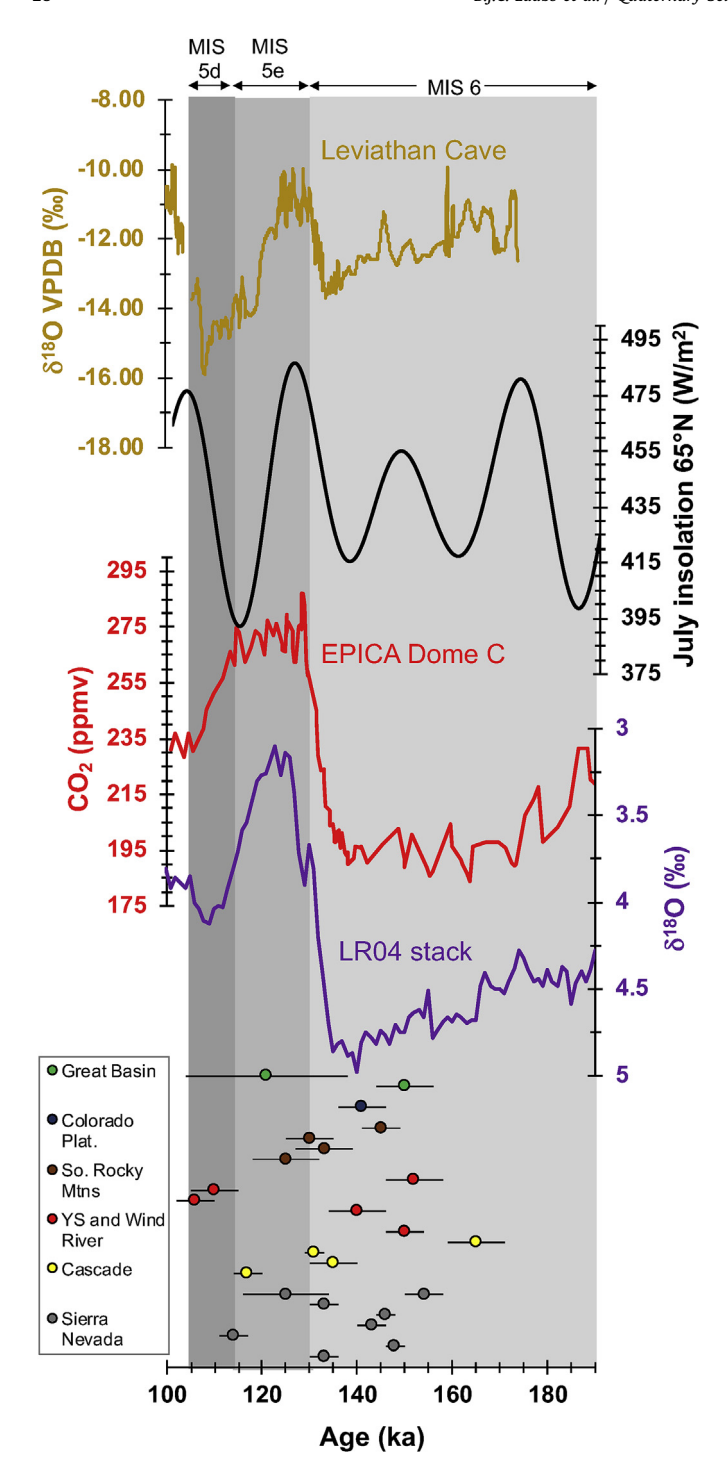


Fig. 13. Normal kernel density estimates of exposure ages of downvalley recessional moraines of the last glaciation in (A) the Sierra Nevada (SN), Transverse (SB, San Bernardino) Range; (B) Basin and Range and Columbia Plateau, including the Ruby Mountains (RM), East Humbolt Mountains (EH), and Wallowa Mountains (WM); (C) the Uinta (U) and Wasatch (W) Mountains; (D) Greater Yellowstone region (Y), Bighorn Range (BH), and Wind River Range (WR); and (E) the Colorado Rocky Mountains, including the Sawatch Range (Saw.), Mosquito Range (Mos.) and Sangre de Cristo Mountains (SdC). The top of each panel has a relative probability value of 1.



**Fig. 14.** Comparison of climate proxy records with penultimate glaciation moraine ages in the conterminous western U.S. Climate proxy records for MIS 6 (light gray), MIS 5e (medium gray), and 5d (darker gray) intervals include the LR04 series of marine  $\delta^{18}$ O in benthic foraminifers (Lisiecki and Raymo, 2005); atmospheric CO<sub>2</sub> as recorded in the EPICA Dome C ice core (Lüthi et al., 2008), July insolation at latitude 65° N (Laskar et al., 2004), and speleothem calcite  $\delta^{18}$ O from Leviathan Cave in Nevada (Lachniet et al., 2014), and the oldest individual or oldest groupings of exposure ages of the penultimate glaciation moraines (YS = Greater Yellowstone). Error bars are  $\pm$  external uncertainty of individual exposure ages or  $\pm 1\sigma$  for averaged groupings of oldest exposure ages. Exposure ages are given in Table 2.

glacier lengths  $\sim 1-5$  kyr after terminal moraines were last occupied.

### 5.2. Glacial chronologies and inferences of climate change

The majority of studies involving TCN glacial chronologies have interpreted exposure ages of moraines to represent the time when deposition of erratic boulders ceased and ice retreat began. The following discussion uses this same logic in comparing exposuredated glacial chronologies to other proxies of past climate from within and beyond western North America. The discussion focuses on the last two Pleistocene glaciations, subdividing the last glaciation into an older interval of terminal moraine deposition and a younger interval of downvalley recessional moraine deposition. Recalculated exposure ages discussed below are as reported in Tables 1–3 (with individual and mean exposure ages in Tables S1, S2, and S3). For the penultimate glaciation, the oldest individual or oldest grouping of exposure ages are used for comparing moraine ages with other paleoclimate proxies for reasons discussed above (see section 4.1.6.). For the last glaciation, the arithmetic mean exposure age of terminal and recessional moraines are compared to other paleoclimate records.

### 5.2.1. The penultimate glaciation

The correspondence of most of the oldest exposure ages of moraines of the penultimate glaciation with the latter part of MIS 6 suggests that glaciers attained their maximum length during the penultimate global glacial maximum, ca. 165-135 ka as defined by the compiled  $\delta^{18}$ O record of marine benthic foraminifera (Lisiecki and Raymo, 2005, Fig. 14). This finding is consistent with original reports of exposure ages reviewed here from the Greater Yellowstone region (Licciardi and Pierce, 2008), the Sierra Nevada (Phillips et al., 2009; Rood et al., 2011; Wesnousky et al., 2016), the Wind River Range (Phillips et al., 1997), Colorado Rocky Mountain ranges (Brugger et al., 2019a; Schweinsberg et al., 2020) and the Colorado Plateau (Marchetti et al., 2011). New <sup>10</sup>Be exposure ages from the Great Basin also indicate that moraines of the penultimate glaciation were last occupied late in MIS 6, as do limiting <sup>10</sup>Be exposure ages of glacially scoured bedrock in the Wasatch Range reported by Quirk et al. (2018). Additionally, oldest recalculated <sup>36</sup>Cl exposure ages of two penultimate glacial maximum moraines in the northern Cascade Range and the oldest <sup>3</sup>He exposure age of a penultimate glaciation moraine in the southern Cascade Range suggest a local penultimate glacial maximum during MIS 6. The region-wide mean of the oldest exposure ages from penultimate glaciation moraines in the conterminous western U.S.,  $138 \pm 13$  ka, aligns with minima observed in records of atmospheric CO<sub>2</sub> (Lüthi et al., 2008), northern high latitude summer insolation (Laskar et al., 2004), and speleothem calcite  $\delta^{18}O$  compiled in the Leviathan Cave record (Lachniet et al., 2014) in Nevada (Fig. 14). This mean exposure age also predates by ~5–10 kyr the timing of Termination II as observed in the marine  $\delta^{18}$ O record (Lisiecki and Raymo, 2005) and in the Devils Hole calcite  $\delta^{18}$ O record in Nevada (Moseley et al., 2016).

Overall, terrestrial paleoclimate records of the penultimate glaciation are rare in the conterminous western U.S., but records from the Great Basin sector of the Basin and Range (Utah and Nevada) provide an opportunity to compare the moraine record with other sedimentary records from caves and Pleistocene lakes. Stable isotopes of speleothem calcite in the Great Basin include the Leviathan Cave record, which spans much of the past 180 kyr (Lachniet et al., 2014), and the Devils Hole record that spans multiple Quaternary glaciations (Winograd et al., 1992; Moseley et al., 2016). Additionally, Wendt et al. (2018, 2020) interpret U—Th dated subaqueous carbonate deposits and uranium-isotope records from Devils Hole calcite to represent groundwater

fluctuations over multiple Pleistocene glacial-interglacial intervals. Stable isotope records in the Great Basin reveal pacing between summer insolation variations at latitude 65°N and calcite  $\delta^{18}O$  (as a proxy for changes in temperature or precipitation amount, source, and/or seasonality), with insolation and temperature changes likely great enough to force changes in mountain glacier length. The uranium-isotope record at Devils Hole further suggests increased effective precipitation in the southern Great Basin during glacial intervals (Wendt et al., 2020). The correspondence of mountain glacial maxima at 138  $\pm$  13 ka with calcite  $\delta^{18}$ O minima suggests that cooling accompanied ice advance late in MIS 6, which is consistent with the global ice volume record (Lisiecki and Raymo, 2005) and evidence for expansion of pluvial lakes in the Great Basin during MIS 6 (Scott et al., 1983). Interestingly, the Leviathan Cave record displays a  $\delta^{18}$ O minimum at ca. 108 ka (MIS 5d) of about 2.5% lower than the minimum during MIS 6, which Lachniet et al. (2014) interpret to suggest a greater degree of cooling in the Great Basin during MIS 5d (109-123 ka; Lisiecki and Raymo, 2005) compared to MIS 6. The summary of glacial chronologies presented here does not support greater ice extents during MIS 5d compared to MIS 6, although exposure ages of a recessional moraine in the Wind River Range (the Bull Lake VI stage of Chadwick et al., 1997), a terminal moraine at Sonora Junction (Rood et al., 2011), and a moraine in the southern Cascade Range (Speth et al., 2018) may suggest expanded glaciers during MIS 5d or later. Alternatively, if our interpretive framework for exposure ages of the penultimate glaciation is incorrect, and mean exposure ages of moraines better represent the time when penultimate glaciation moraines were last occupied, then ice maxima during MIS 5d would be represented in multiple glacial valleys in the Sierra Nevada, the innermost moraine of the penultimate glaciation in the northern Cascade Range, the Wind River Range, and the Colorado Plateau. In either case, the majority of recalculated exposure ages fall within MIS 6 whether the mean or the oldest exposure age is considered the best limit on glacial culminations. Additional exposure dating of penultimateglaciation moraine sequences or of corresponding outwash terraces could help to resolve signals of ice advance during MIS 6 and/ or MIS 5d.

Mountain glacier moraines corresponding to MIS 6 are found in numerous settings outside the western U.S. In the western hemisphere, moraines corresponding to MIS 6 are found in the northwest Yukon Territory in Canada and in mountains of Alaska (Briner et al., 2005; Ward et al., 2008; Dortch et al., 2010; Stroeven et al., 2014). In South America, moraines and outwash with exposure ages corresponding to MIS 6 are found in the northern and central Andes (e.g., Smith et al., 2005a; Zech et al., 2009) and Patagonia (Kaplan et al., 2005; Douglass et al., 2006; Hein et al., 2009). Mountain glaciers in the eastern hemisphere also attained maxima during MIS 6 based on exposure ages from New Zealand (Shulmeister et al., 2010; Putnam et al., 2013) and from the Himalaya and Tibetan Plateau (e.g., Chevalier et al., 2011; Owen and Dortch, 2014; Heyman et al., 2011). In each of these regions, and in most settings of the western U.S. (outside of the northern and eastern parts of the Greater Yellowstone region and portions of the Wind River Range), mountain glacier lengths were greater during MIS 6 compared to MIS 2, suggesting either greater cooling during the latter part of MIS 6 or possibly significant erosion in mountain glacial valleys from MIS 6 to MIS 2 (e.g., Anderson et al., 2012). On the other hand, global records suggest that the next-to-last mountain glaciation does not correspond to MIS 6 on all continents. TCN glacial chronologies for many mountains in Alaska indicate that the local penultimate glaciation corresponds to MIS 4 (e.g., Briner and Kaufman, 2008; Dortch et al., 2010; Tulenko et al., 2018). Exposure ages of moraines corresponding to MIS 4 are also found in the southwestern Yukon Territory (Stroeven et al., 2014), New Zealand (Schaefer et al., 2015), and the Himalaya and Tibetan Plateau (e.g., Chevalier et al., 2011; Owen et al., 2012). Additionally, within the conterminous western U.S., Thackray (2001) report greater mountain glacier lengths during or before MIS 3 (57-29 ka; Lisiecki and Raymo, 2005) compared to MIS 2 based on radiocarbon age limits on glacial sediment on the Olympic Peninsula. This is attributed to greater maritime precipitation in coastal mountains of the Pacific Northwest during late MIS 4/early MIS 3 compared to MIS 2 (Thackray, 2008). The influence of such augmented precipitation appears to be spatially limited to maritime settings in the western U.S., although some proglacial deposits near Jackson (Pierce et al., 2011) and the Wind River Range (Hancock et al., 1999) have been attributed to glacial climates and processes during MIS 3.

The absence of MIS 4 moraines in mountains of the western U.S. is perhaps unusual when viewed globally, although evidence of glacial activity during MIS 4 includes aggradation of outwash downstream of the heavily glaciated Wind River Mountains (e.g., Hancock et al., 1999; Sharp et al., 2003) and varying degrees of soil development in multi-crested moraines in the Wind River Range and northern Uinta Mountains (Hall and Shroba, 1995; Douglass and Mickelson, 2007). This suggests that mountain glaciers advanced during MIS 4, but any moraines constructed during this time were presumably obliterated by subsequent ice advance during MIS 2. Shorter glacier lengths during MIS 4 compared to MIS 2 are consistent with relative global ice volumes between the two glaciations (Lisiecki and Raymo, 2005) and records showing that mountain glaciers in the western U.S. generally advanced and retreated in step with the Laurentide Ice Sheet, which was also smaller during MIS 4 compared to MIS 2 (Kleman et al., 2013). Smaller glaciers during MIS 4 also imply contrasting magnitudes of climate change between northern high latitudes and middle latitudes in North America. Tulenko et al. (2018, 2020) suggest that mountain glacier advance to greater-than-LGM lengths in Alaska during MIS 4 was caused by enhanced cooling and augmented precipitation, the latter being possible when North American ice sheets were restricted in size and the neighboring Pacific Ocean was warmer than during MIS 2. Even though westerly airflow and attendant moisture delivery to mountains of the western U.S. may have been stronger in the presence of smaller ice sheets during MIS 4, this was apparently insufficient to cause mountain glacier expansion to lengths beyond those of MIS 6 and 2. This observation further implies that the magnitude of cooling at middle latitudes of the western U.S. was less than cooling at high latitudes in North America during MIS 4 or that moisture reduction associated with MIS 2 glaciation was more pronounced at high latitudes compared to middle latitudes.

### 5.2.2. The last glaciation

The correspondence of terminal moraines of the last glaciation to MIS 2 is consistent with original reports of the TCN data compiled here, with the important update that recalculated <sup>10</sup>Be exposure ages based on newer production rate models are generally older than originally reported. Along with the recalculated <sup>3</sup>He, <sup>26</sup>Al, and <sup>36</sup>Cl exposure ages presented here, the updated <sup>10</sup>Be chronologies affect inferences of paleoclimate based on the mountain glacial record. Furthermore, the great number of exposure ages combined with other paleoclimate proxies affords an opportunity to examine details in the structure of the last glaciation and reconsider some existing models of Late Pleistocene climate. Here, we examine the overall timing of the last glaciation based on terminal and downvalley recessional moraines in comparison to climate proxy records and model results from within and beyond western North America.

The alignment of the region-wide  $19.5 \pm 2.3$  ka mean exposure age of terminal moraines with the latter part of the LGM time

interval (spanning 26.5 to 19.0 ka; Clark et al., 2009) (Fig. 15A) is consistent with the notion that mountain glaciation in the western U.S. was in phase with global ice volume changes (e.g., Young et al., 2011; Shakun et al., 2015). However, the variability among exposure ages of individual terminal moraines spans a range of ~7 kyr, with some moraines dating to early in the LGM (e.g., ~22 ka in the Sierra Nevada, northern Cascade Range, Ruby Mountains, and in some glacial valleys in the Rocky Mountains) and others that post-date the LGM (e.g., ~18-15 ka in some other glacial valleys in the Rocky Mountains) (Table 2). Nearly all mountain settings considered here have exposure ages of terminal moraines in at least one glacial valley that fall within the latter part of the LGM. This includes features in northern Utah (Wasatch and Uinta Mountains), the Greater Yellowstone region, and the northern Cascade Range, that were previously determined to have experienced local glacial maxima after the end of the LGM (Laabs et al., 2009; Licciardi and Pierce, 2008, 2018; Porter and Swanson, 2008; respectively). Even with recalculated exposure ages, the northern Utah mountains and Greater Yellowstone region still feature terminal moraines in one or more valleys (as do the southern Rocky Mountains) with exposure ages that post-date the end of the LGM, but also feature one or more terminal moraines with exposure ages that fall within the LGM time interval. Correspondence of terminal moraines to the global LGM as indicated by marine benthic  $\delta^{18}O$  (Lisiecki and Raymo, 2005) and by sea level reconstructions (Clark et al., 2009), low atmospheric CO<sub>2</sub> (Lüthi et al., 2008), and a summer insolation minimum at middle latitudes (Laskar et al., 2004) supports previous assertions that mountain glaciers attained their maxima in response to cooling (Fig. 16). General circulation model simulations of the LGM (e.g., PMIP3; Braconnot et al., 2007) suggest temperature depressions of 5-10 °C at the latitudes of most terminal moraines in the western U.S. Numerical glacier modeling of maximum mountain glacier extents suggests the same, with lesser or equal temperatures depressions in the southern Rocky Mountains (Dühnforth and Anderson, 2011; Schweinsberg et al., 2016; Leonard et al., 2017a; Brugger et al., 2019a) and the Sierra Nevada (Plummer and Phillips, 2003) compared to mountains in northern Utah and Wyoming (Laabs et al., 2006; Refsnider et al., 2008; Birkel et al., 2012; Quirk et al., 2018). Most glaciated mountains of the western U.S. fall between the ends of the north-tosouth LGM precipitation dipole identified by Oster et al. (2015a), a region that GCM experiments suggest experienced near-modern precipitation during glacial times (Braconnot et al., 2007). The southernmost glaciated mountains may have featured relatively wet climates during the LGM, as evidenced by the expansion of most southern Great Basin pluvial lakes during this time (Broecker and Putnam, 2012; Lyle et al., 2012; Munroe and Laabs, 2013) and the climate data-model compilation of Oster et al. (2015a). In contrast, some glaciated mountains of the Pacific Northwest featured glacier lengths during the LGM that were less than that of late MIS 4/early MIS 3 (Thackray, 2001), which along with other proxy records from the same region suggests relatively dry LGM conditions (Oster et al., 2015a).

The correspondence of terminal-moraine exposure ages in the western U.S. with the latter part of the LGM is broadly consistent with cosmogenic moraine chronologies at middle latitudes in the Swiss Alps (Kelly et al., 2004; Ivy-Ochs et al., 2006), eastern Europe (Akçar et al., 2007; Sarıkaya et al., 2009), Argentina (Kaplan et al., 2004; Davies et al., 2020), and New Zealand (Shulmeister et al., 2010; Putnam et al., 2013), and generally with chronologies of moraines at tropical latitudes in Peru (e.g., Smith et al., 2005b; Farber et al., 2005; Bromley et al., 2011; Mark et al., 2017) (see http://alpine.ice-d.org for recalculated exposure ages from these areas). This observation is consistent with the previous assertions that mountain glaciation at middle and low latitudes was in phase with global ice volume changes (e.g., Schaefer et al., 2006), even though forcings and reconstructed magnitudes of climate change varied with latitude (Shakun et al., 2015).

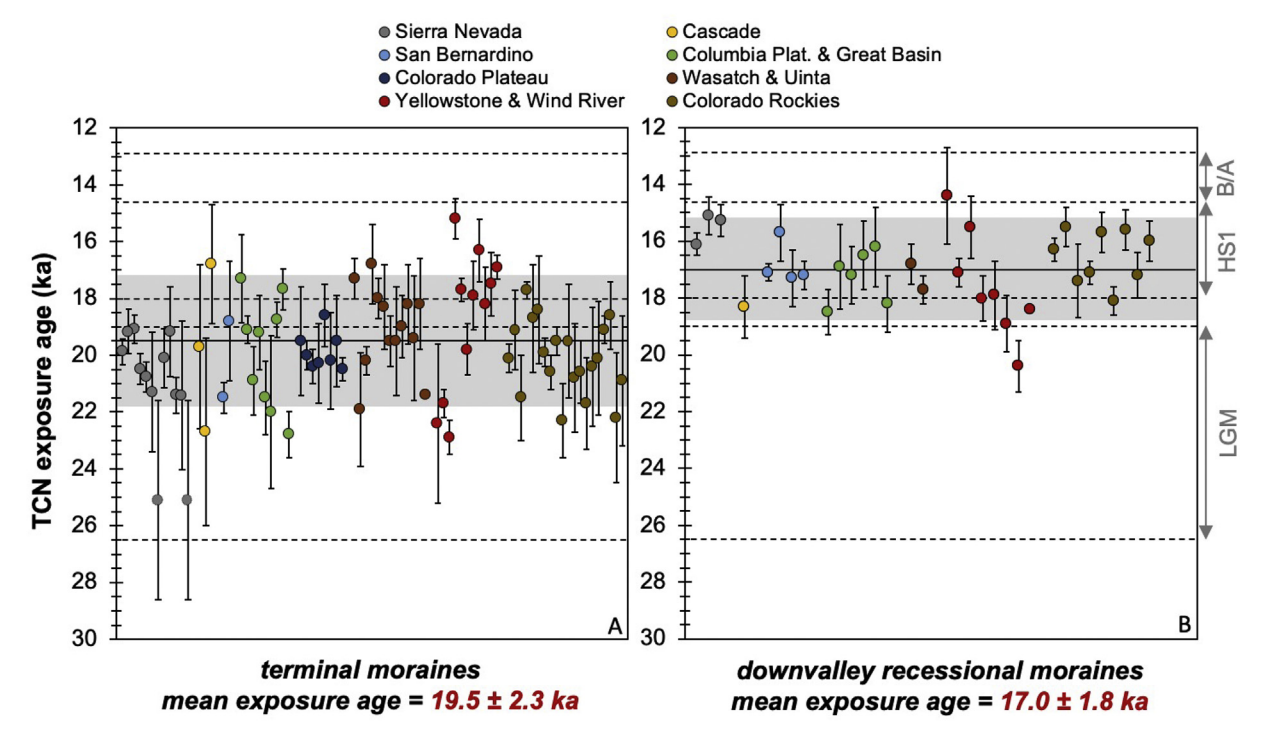
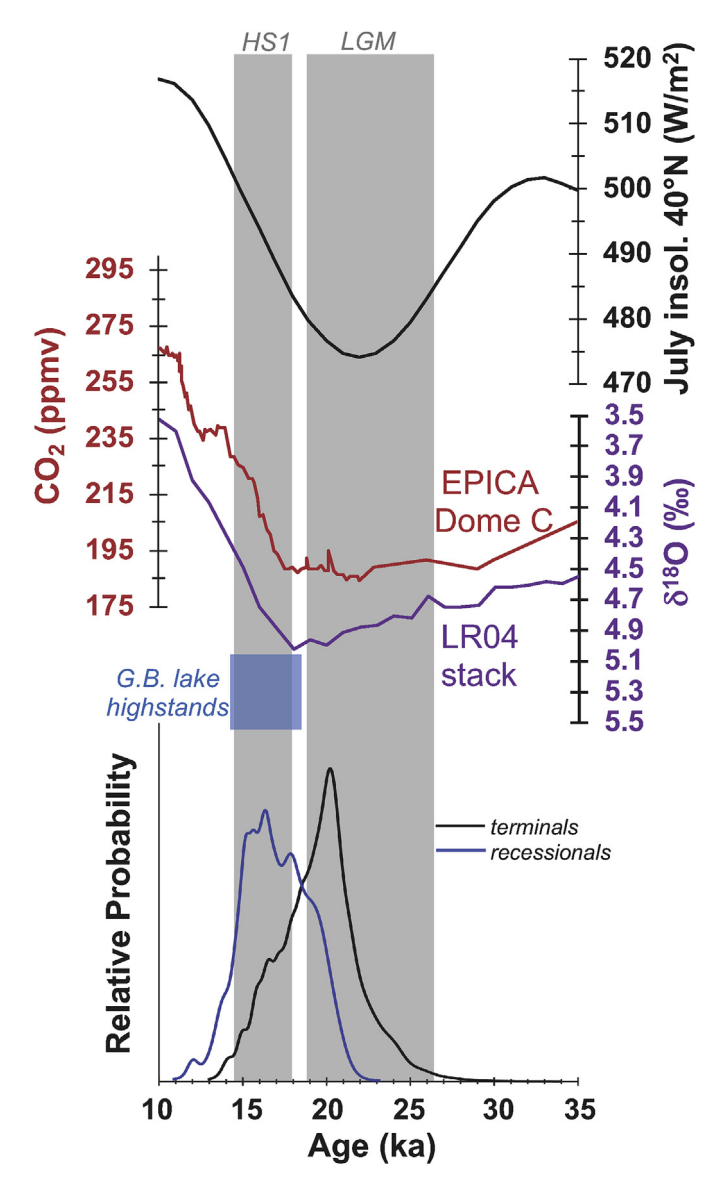


Fig. 15. Mean exposure ages  $(\pm 1\sigma)$  of terminal moraines (A) and downvalley recessional moraines (B) in the western U.S. compared to the time interval of the Last Glacial Maximum (LGM, 26.5-19.0 ka; Clark et al., 2009) Heinrich Stadial 1 (HS1, 18.0-14.6 ka; Hemming, 2004), and Bølling/Allerød interstadial (B/A, 14.6-12.9 ka; Rasmussen et al., 2006). Solid horizontal line and gray band in each plot represent the mean exposure ages  $(\pm 1\sigma)$  atop terminal moraines and recessional moraines.



**Fig. 16.** Climate proxy records for the last glaciation and deglaciation including the LRO4 series of marine  $\delta^{18}$ O of benthic foraminifers (Lisiecki and Raymo, 2005); atmospheric CO<sub>2</sub> as recorded in the EPICA Dome C ice core (Lüthi et al., 2008), July insolation at latitude  $40^{\circ}$ N (Laskar et al., 2004), and normal kernel density estimates based on all recalculated exposure ages of terminal (black) and downvalley recessional (blue) moraines compiled here. The approximate duration of Pleistocene lake highstands in the northern Great Basin is represented as 18.5-14.5 ka (blue bar) based on chronologies from Munroe and Laabs (2013), Ibarra et al. (2014), Barth et al. (2016), and Hudson et al. (2019). Durations of the LGM and HS1 (vertical gray bars) are as shown in Fig. 15.

Recessional moraines representing near-maximum glacier lengths are found in many glaciated valleys in the conterminous western U.S., but only a modest number have TCN chronologies. Mean exposure ages among downvalley recessional moraines are less variable than those of terminal moraines and are younger than 19 ka, with one exception; downvalley recessional moraines have mean exposure ages of 20–21 ka in the southeastern Wind River Range (Dahms et al., 2018). The younger downvalley recessional moraines and the small number of younger (<19 ka) terminal moraines signify persistence or later culmination of many mountain glaciers after the global LGM, and are a better indicator than terminal moraines of the time when regional deglaciation began in earnest in the conterminous western U.S.

Downvalley recessional moraines in most glaciated mountains were last occupied at ca. 18.5-16.0 ka (Fig. 15B) with an overall mean exposure age of 17.0  $\pm$  1.8 ka, corresponding to the time when the largest Great Basin pluvial lakes, Lahontan and Bonneville (e.g., Benson et al., 2011; Oviatt, 2015), attained their hydrologic maxima along with many smaller pluvial lakes of the northern Great Basin (Munroe and Laabs, 2013: Ibarra et al., 2014: Barth et al., 2016: Hudson et al., 2019; Munroe et al., 2020, Fig. 16), likely in response to enhanced regional precipitation. Many of these lakes were below their highstand elevations at  $19.5 \pm 2.3$  when most mountain glaciers in the western U.S. were at their maximum lengths, suggesting that LGM climate at the latitude of these lakes was too dry for the expansion of lakes to their maximum size. The coincidence of near-maximum glacier lengths with Great Basin pluvial-lake highstands suggests a shift in climate at 18.5-16.0 ka to conditions favoring both expanded glaciers and lakes. Such climate conditions likely featured cold temperatures and augmented winter precipitation, which is supported by recent studies of Great Basin pluvial lakes. Ibarra et al. (2014) and Barth et al. (2016) note that an increase in precipitation above modern levels was required to sustain two northern Great Basin lakes at their highstands (Lakes Surprise and Jakes Lake, respectively), and Hudson et al. (2019) note that precipitation throughout the southwestern U.S. during the interval 18.5-16.0 ka was likely derived from westerly sources. The highstand of Lake Surprise (at ca. 15.5 ka) was apparently accompanied by precipitation 80% above modern, and the coincident (or slightly earlier) highstand of lakes Lake was accompanied by precipitation 90% above modern (Ibarra et al., 2014; Barth et al., 2016). Ouirk et al. (2018) compared numerical simulations of glaciers in the Wasatch Mountains, including recessional extents, with output of hydrologic models of Great Basin paleolakes and found a similar result, suggesting that augmented precipitation and cold temperatures were required to sustain both glaciers and lakes. Licciardi and Pierce (2018) note that augmented precipitation likely impacted the Yellowstone Plateau ice cap during the late LGM through ~15 ka. They suggest that the main body of the ice cap thickened due to persistent cooling and orographically augmented precipitation during the interval 18.5-16.0 ka while the western and southern outlets advanced to their maximum lengths. While the degree to which regional temperature rose in the western U.S. during the interval 18.5-16.0 ka appears to be minimal (He, 2011; Quirk et al., 2018), the increase in winter precipitation is evident from multiple paleoclimate records and may have helped to sustain near-maximum glacier lengths in several mountains. Although the TCN chronologies of recessional moraines farther upvalley (indicating glacier lengths <75% of the Late Pleistocene maximum) in mountains of the western U.S. are not considered in this review, such moraines have been dated in the northern Cascade Range, San Bernardino Range, and Colorado Plateau yielding exposure ages of 18.5-16.0 ka (Porter and Swanson, 2008; Owen et al., 2003; Marchetti et al., 2011) or younger, including cirque-floor moraines that have been dated by Marcott et al. (2019). In combination with the chronology of recessional moraines reported here, these moraines suggest that pauses in ice retreat or readvances of glacier termini at 18.5-16.0 ka occurred in numerous mountain ranges in the western U.S.

The TCN chronology of downvalley recessional moraines and young (post-LGM) terminal moraines indicates that many of these features were built during Heinrich Stadial 1 (HS1, 18.0–14.6 ka; Figs. 15 and 16), an interval of cooling in the northern hemisphere likely initiated by high-volume discharges of ice to the North Atlantic (Hemming, 2004). Diverse evidence of cooling in the southwestern U.S. during this interval is found beyond the limit of mountain glaciers and paleolakes. Examples include lacustrine stable isotope records in southern California (Kirby et al., 2013,

2018) and speleothem calcite  $\delta^{18}$ O records in Leviathan Cave (northern Great Basin; Lachniet et al., 2014) and from caves in southern Arizona, New Mexico, and California (Asmerom et al., 2010; Wagner et al., 2010; Oster et al., 2015b). The latter three studies note that the teleconnection between the North Atlantic and western North America was likely through the North Pacific Ocean, where a strengthened Aleutian Low combined with a southward shift in westerly storm tracks resulted in greater precipitation in the southwestern U.S. Hudson et al. (2019) describe further evidence of elevated precipitation in and around the Great Basin during HS1 and attribute this to conditions in the North Pacific Ocean. The important role of atmospheric rivers delivering moisture to the western U.S. during this time is consistent with the data-model comparisons of Oster et al. (2015a) for the LGM and with the more recent modeling studies of Lora et al. (2017).

Generally, the exposure ages of downvalley recessional moraines indicate that mountain glacier retreat began in most glacial valleys during the interval 18.0-16.5 ka and prior to northern hemisphere-scale warming associated with the onset of the Bølling/Allerød interval. Only a small number of downvalley recessional moraines have exposure ages approaching the start of the Bølling interval at 14.6 ka; these are found in the Greater Yellowstone region (Teton Range and southern margin of the Yellowstone glacial system), Sierra Nevada (Bishop Creek only), and two valleys in the southern Rocky Mountains (Sawatch and Sangre de Cristo Ranges; Table 3). The earlier onset of overall deglaciation in most ranges is consistent with the commencement of warming at middle latitudes throughout the northern hemisphere based on terrestrial and marine temperature proxies (Shakun et al., 2012) and the deglaciation chronologies compiled by Shakun et al. (2015). This correspondence suggests that increasing summer insolation at middle and high latitudes in the northern hemisphere (Laskar et al., 2004) starting at 21 ka and followed by rising atmospheric CO<sub>2</sub> starting at 17 ka (Lüthi et al., 2008, Fig. 16) initiated warming and drove mountain glacier retreat at middle latitudes as inferred by Schaefer et al. (2006) and Shakun et al. (2015). The persistence of many Great Basin pluvial lakes at their highstands until ca. 15.5 ka or later, after most mountain glaciers began retreating, suggests that precipitation remained above modern levels throughout HS1 (Munroe and Laabs, 2013; Ibarra et al., 2014; Hudson et al., 2019; Munroe et al., 2020) but was not sufficient to sustain glaciers in most mountains at near-maximum lengths. Net warming at 16.0 ka is not represented in the Trace 21ka simulations (He, 2011) or speleothem calcite  $\delta^{18}$ O from the Great Basin (Lachniet et al., 2014; which may represent winter temperatures to a greater degree than summer temperatures), but summer warming forced by rising insolation and a strengthening greenhouse effect could have driven negative mass balance even with sustained winter precipitation.

In summary, the structure of the last glaciation in the western U.S. revealed by the recalculated TCN chronologies reviewed here as well as other paleoclimate records from the western U.S. includes multiple glacial culminations at near-maximum lengths. The first culmination corresponds to the latter part of the global LGM when the Laurentide Ice Sheet and much of the Cordilleran Ice Sheet were near their maximum size, and was likely driven chiefly by cooling associated with minima in insolation and atmospheric CO<sub>2</sub> (Fig. 16), along with feedbacks associated with the presence of North American ice sheets. Licciardi and Pierce (2018) note that the presence of a cold and dry anticyclone over the Laurentide Ice Sheet does not appear to have inhibited mountain glacier growth during the global LGM in northern mountains as suggested in some previous studies (Licciardi et al., 2004; Thackray, 2008). This inference is supported by the exposure ages of terminal moraines compiled here. The second culmination coincides with HS1 (Fig. 16) and was accompanied by persistent or renewed cooling (albeit less extreme than during the LGM) and augmented winter precipitation. This structure has been inferred from previous reports on glacial chronologies (e.g., Licciardi et al., 2004; Thackray et al., 2004; Thackray, 2008) and is supported by the larger set of chronological data reviewed here. The TCN chronologies by themselves do not permit distinction of multiple glacial culminations during the HS1 interval, which may have featured fluctuating climates (Oster et al., 2015a: Hudson et al., 2019). Glacial valleys with exposure ages of multiple recessional moraines suggest that glaciers may have persisted at near-maximum lengths throughout the interval 18.5-16.0 ka, although such detailed TCN chronologies are currently available for only the glacial valleys and subregions shown in Table 3. Additionally, resolving sub-millennial scale climate signals from TCN chronologies of moraines may be complicated by terminus fluctuations driven by short-term climate changes (Anderson et al., 2014) and non-climatic factors that can result in valley-to-valley differences in moraine chronologies (Young et al., 2011).

### 6. Conclusions

Recalculated exposure ages of moraines of the last two glaciations in the western U.S. support more consistent intercomparisons among glaciated mountains and more accurate comparisons with other climate proxies. Although this review compiles the existing TCN data from terminal and downvalley recessional moraines in the conterminous western U.S., additional mountain glacial chronologies are still being developed from this region to address the ongoing need for a denser and more detailed network of chronologies as proxies for Pleistocene climate change. The majority of the TCN data compiled here are also available in the ICE-D Alpine online database (http://alpine.ice-d.org), which is regularly updated and covers the western U.S. and other mountain glacier settings worldwide (Balco, 2020).

For the penultimate glaciation, oldest exposure ages of moraines throughout the conterminous western U.S. are better aligned with one another than are mean exposure ages and correspond to the latter part of MIS 6, indicating that, much like during the last glaciation, mountain glaciers were broadly in phase with global ice volume during the penultimate glaciation. While a few age limits on recessional penultimate-glaciation moraines and outwash sediments provide some evidence of glacier growth during MIS 5d, 4, and 3, such evidence is generally restricted to coastal/maritime mountains of the Pacific Northwest and is sparse or absent elsewhere in the conterminous western U.S. Future development of additional glacial chronologies may reveal signals of glacier change during MIS 5d or 4 in other mountains of the western U.S., but the available data suggest that the penultimate mountain glacial maximum in this region corresponds to MIS 6.

The TCN chronology of the last glaciation includes a greater number of moraines, the majority of which were dated with <sup>10</sup>Be. The recalculated exposure ages based on <sup>3</sup>He <sup>10</sup>Be, <sup>26</sup>Al, and <sup>36</sup>Cl nuclides are more coherent for the last glaciation compared to those from the penultimate glaciation, but still display some variability within MIS 2. Exposure ages of most terminal moraines correspond to the latter part of the LGM time interval, although a small number of moraines post-date the end of the LGM at 19 ka. These younger terminal moraines have exposure ages similar to those of downvalley recessional moraines delimiting nearmaximum glacier lengths in numerous valleys in the western U.S. The TCN chronologies of terminal and recessional moraines reveal a regional temporal structure of the last glaciation, with culminations of maximum or near-maximum glacier lengths occurring both during and after the global LGM. The earlier culmination, represented by a region-wide mean exposure age of 19.5  $\pm$  2.3 ka for terminal moraines, signifies correspondence with the cold and relatively dry LGM. The later culmination, represented by a region-wide mean exposure of 17.0  $\pm$  1.8 ka for downvalley recessional moraines, corresponds to the early part of HS1 and was likely accompanied by persistent cooling and a relatively wetter climate. The second culmination appears to be a regional event that was not limited to northern mountain ranges or mountains nearest Great Basin pluvial lakes in the western U.S. as some previous studies suggested.

Although this review encompasses exposure ages of numerous moraines and provides some insight on climate accompanying the last two Pleistocene glaciations, the mountain glacial record remains an underutilized proxy for past climate change in the western U.S. The record of ice retreat during the last glacialinterglacial transition is a valuable proxy for past climate that can be further developed through building of additional TCN chronologies and applying paleoglaciological methods to determine the pace and magnitude of climate change accompanying ice retreat. TCN chronologies of upvalley/cirque floor recessional moraines have been extensively developed in the western U.S. (e.g., Marcott et al., 2019) but chronologies covering the full glacial record from terminal moraines to cirque headwalls remain rare (Guido et al., 2007). Studies that have developed TCN chronologies of moraine sequences and glacially scoured bedrock have helped to resolve the pace and timing of ice retreat and have identified local and regional-scale climatic drivers of glacier change (e.g., Guido et al., 2007; Porter and Swanson, 2008; Marchetti et al., 2011; Dahms et al., 2018), and studies combining TCN chronologies with paleoglaciological reconstructions through time provide important limits on the magnitudes of temperature and precipitation change during deglaciation (Leonard et al., 2017a; Quirk et al., 2018; Brugger et al., 2019a, 2019b). Similar efforts to expand TCN chronologies of the glacial record throughout the western U.S. are key to developing a more comprehensive understanding of spatiotemporal climatic changes accompanying ice retreat during the last deglaciation.

### Credit author statement

Benjamin J.C. Laabs: Conceptualization, Methodology, Investigation, Data Curation, Writing — Original Draft, Review & Editing. Joseph M. Licciardi: Conceptualization, Methodology, Data Curation, Writing — Original Draft, Review & Editing. Eric M. Leonard: Writing — Original Draft, Review & Editing. Jeffrey S. Munroe: Methodology, Investigation, Writing — Original Draft, Review & Editing. David W. Marchetti: Data Curation, Writing — Original Draft, Review & Editing.

### **Declaration of competing interest**

The authors report no conflicts of interest associated with this manuscript.

### Acknowledgments

The authors thank the international community of scientists who have worked to develop and apply cosmogenic nuclide surface exposure dating to glacial deposits, especially those who have developed the mountain glacial record in the western United States. New <sup>10</sup>Be data reported here were generated with support from the U.S. National Science Foundation grant 0902472 to B. Laabs. The authors also thank G. Bromley and an anonymous reviewer for comments that helped to improve this paper along with Timothy Horscroft and the editorship at Quaternary Science Reviews for the opportunity to contribute this invited paper.

### Appendix A. Supplementary data

Supplementary data to this article can be found online at https://doi.org/10.1016/j.quascirev.2020.106427.

### References

- Akçar, N., Yavuz, V., Ivy-Ochs, S., Kubik, P.W., Vardar, M., Schlüchter, C., 2007. Paleoglacial records from Kavron Valley, NE Turkey: field and cosmogenic exposure dating evidence. Quat. Int. 164, 170–183.
- Amos, C.B., Kelson, K.I., Rood, D.H., Simpson, D.T., Rose, R.S., 2010. Late Quaternary slip rate on the Kern Canyon fault at Soda Spring, Tulare County, California. Lithosphere 2 (6), 411–417.
- Anderson, R.S., Dühnforth, M., Colgan, W., Anderson, L., 2012. Far-flung moraines: exploring the feedback of glacial erosion on the evolution of glacier length. Geomorphology 179, 269–285.
- Anderson, L.S., Roe, G.H., Anderson, R.S., 2014. The effects of interannual climate variability on the moraine record. Geology 42 (1), 55–58.
- Antevs, E., 1955. Geologic-climatic dating in the West. Am. Antiq. 20 (4Part1), 317–335.
- Applegate, P.J., Urban, N.M., Keller, K., Lowell, T.V., Laabs, B.J., Kelly, M.A., Alley, R.B., 2012. Improved moraine age interpretations through explicit matching of geomorphic process models to cosmogenic nuclide measurements from single landforms. Quat. Res. 77 (2), 293–304.
- Applegate, P.J., Urban, N.M., Laabs, B.J.C., Keller, K., Alley, R.B., 2010. Modeling the statistical distributions of cosmogenic exposure dates from moraines. Geoscientific Model Development 3 (1), 293.
- Asmerom, Y., Polyak, V.J., Burns, S.J., 2010. Variable winter moisture in the southwestern United States linked to rapid glacial climate shifts. Nat. Geosci. 3 (2), 114
- Balco, G., 2011. Contributions and unrealized potential contributions of cosmogenicnuclide exposure dating to glacier chronology, 1990—2010. Quat. Sci. Rev. 30 (1-2). 3—27.
- Balco, G., 2017. Production rate calculations for cosmic-ray-muon-produced <sup>10</sup>Be and <sup>26</sup>Al benchmarked against geological calibration data. Quat. Geochronol. 39, 150–173.
- Balco, G., 2020. Glacier change and paleoclimate applications of cosmogenicnuclide exposure dating, Annu. Rev. Earth Planet Sci. 48.
- Balco, G., Stone, J.O., Lifton, N.A., Dunai, T.J., 2008. A complete and easily accessible means of calculating surface exposure ages or erosion rates from 10Be and 26Al measurements. Quat. Geochronol. 3 (3), 174–195.
- Barth, C., Boyle, D.P., Hatchett, B.J., Bassett, S.D., Garner, C.B., Adams, K.D., 2016. Late Pleistocene climate inferences from a water balance model of Jakes Valley, Nevada (USA). J. Paleolimnol. 56 (2-3), 109–122.
- Bartlein, P.J., Anderson, K.H., Anderson, P.M., Edwards, M.E., Mock, C.J., Thompson, R.S., Webb, R.S., Webb, Whitlock, C., 1998. Paleoclimate simulations for North America over the past 21,000 years: features of the simulated climate and comparisons with paleoenvironmental data. Quaternary Science Reviews 17 (6–7), 549–585.
- Benedict, J.B., 1993. Influence of snow upon rates of granodiorite weathering, Colorado Front Range, USA. Boreas 22 (2), 87–92.
- Benn, D.I., Owen, L.A., Finkel, R.C., Clemmens, S., 2006. Pleistocene lake outburst floods and fan formation along the eastern Sierra Nevada, California: implications for the interpretation of intermontane lacustrine records. Quat. Sci. Rev. 25 (21-22), 2729–2748.
- Benson, L., Madole, R., Phillips, W., Landis, G., Thomas, T., Kubik, P., 2004. The probable importance of snow and sediment shielding on cosmogenic ages of north-central Colorado Pinedale and pre-Pinedale moraines. Quat. Sci. Rev. 23 (1-2), 193–206.
- Benson, L., Madole, R., Landis, G., Gosse, J., 2005. New data for Late Pleistocene Pinedale alpine glaciation from southwestern Colorado. Quat. Sci. Rev. 24 (1–2), 49–65.
- Benson, L.V., Lund, S.P., Smoot, J.P., Rhode, D.E., Spencer, R.J., Verosub, K.L., Louderback, L.A., Johnson, C.A., Rye, R.O., Negrini, R.M., 2011. The rise and fall of Lake Bonneville between 45 and 10.5 ka. Quat. Int. 235 (1-2), 57–69.
- Birkel, S.D., Putnam, A.E., Denton, G.H., Koons, P.O., Fastook, J.L., Putnam, D.E., Maasch, K.A., 2012. Climate inferences from a glaciological reconstruction of the Late Pleistocene Wind River ice cap, Wind River Range, Wyoming. Arctic Antarct. Alpine Res. 44 (3), 265–276.
- Blackwelder, E., 1915. Post-Cretaceous history of the mountains of central western Wyoming. J. Geol. 23 (4), 307–340.
- Blackwelder, E., 1931. Pleistocene glaciation in the Sierra Nevada and basin ranges. Bull. Geol. Soc. Am. 42 (4), 865–922.
- Borchers, B., Marrero, S., Balco, G., Caffee, M., Goehring, B., Lifton, N., Nishiizumi, K., Phillips, F., Schaefer, J., Stone, J., 2016. Geological calibration of spallation production rates in the CRONUS-Earth project. Quat. Geochronol. 31, 188–198.
- Braconnot, P., Otto-Bliesner, B., Harrison, S., Joussaume, S., Peterchmitt, J.Y., Abe-Ouchi, A., Crucifix, M., Driesschaert, E., Fichefet, T., Hewitt, C.D., Kageyama, M., 2007. Results of PMIP2 coupled simulations of the Mid-Holocene and Last Glacial Maximum—Part 1: experiments and large-scale features. Clim. Past 3 (2), 261–277.
- Braconnot, P., Harrison, S.P., Kageyama, M., Bartlein, P.J., Masson-Delmotte, V., Abe-Ouchi, A., Otto-Bliesner, B., Zhao, Y., 2012. Evaluation of climate models using

- palaeoclimatic data. Nat. Clim. Change 2 (6), 417-424.
- Briner, J.P., 2009. Moraine pebbles and boulders yield indistinguishable <sup>10</sup>Be ages: a case study from Colorado, USA. Quat. Geochronol. 4 (4), 299–305.
- Briner, J.P., Kaufman, D.S., 2008. Late Pleistocene mountain glaciation in Alaska: key chronologies. J. Quat. Sci.: Publ. Quat. Res. Assoc. 23 (6-7), 659–670.
- Briner, J.P., Kaufman, D.S., Manley, W.F., Finkel, R.C., Caffee, M.W., 2005. Cosmogenic exposure dating of late Pleistocene moraine stabilization in Alaska. Geol. Soc. Am. Bull. 117 (7-8), 1108–1120.
- Broecker, W., Putnam, A.E., 2012. How did the hydrologic cycle respond to the twophase mystery interval? Ouat, Sci. Rev. 57, 17–25.
- Bromley, G.R., Hall, B.L., Schaefer, J.M., Winckler, G., Todd, C.E., Rademaker, K.M., 2011. Glacier fluctuations in the southern Peruvian Andes during the late-glacial period, constrained with cosmogenic 3He. J. Quat. Sci. 26 (1), 37–43.
- Brown, E.T., Edmond, J.M., Raisbeck, G.M., Yiou, F., Kurz, M.D., Brook, E.J., 1991. Examination of surface exposure ages of Antarctic moraines using *in situ* produced 10Be and 26Al. Geochem. Cosmochim. Acta 55 (8), 2269–2283.
- Brugger, K.A., 2007. Cosmogenic <sup>10</sup>Be and <sup>36</sup>Cl ages from Late Pleistocene terminal moraine complexes in the Taylor River drainage basin, central Colorado, USA.

  Ouat Sci Rey 26 (3-4) 494–499
- Brugger, K.A., Laabs, B., Reimers, A., Bensen, N., 2019a. Late pleistocene glaciation in the Mosquito range, Colorado, USA: chronology and climate. J. Quat. Sci.
- Brugger, K.A., Ruleman, C.A., Caffee, M.W., Mason, C.C., 2019b. Climate during the Last Glacial Maximum in the Northern Sawatch Range, Colorado, USA. Quaternary 2 (4), 36.
- Cerling, T.E., Craig, H., 1994. Cosmogenic <sup>3</sup>He production rates from 39 N to 46 N latitude, western USA and France. Geochem. Cosmochim. Acta 58 (1), 249–255.
- Chadwick, O.A., Hall, R.D., Phillips, F.M., 1997. Chronology of Pleistocene glacial advances in the central Rocky Mountains. Geol. Soc. Am. Bull. 109 (11), 1443–1452
- Chevalier, M.L., Hilley, G., Tapponnier, P., Van Der Woerd, J., Liu-Zeng, J., Finkel, R.C., Ryerson, F.J., Li, H., Liu, X., 2011. Constraints on the late Quaternary glaciations in Tibet from cosmogenic exposure ages of moraine surfaces. Quat. Sci. Rev. 30 (5-6), 528–554.
- Chmeleff, J., von Blanckenburg, F., Kossert, K., Jakob, D., 2010. Determination of the <sup>10</sup>Be half-life by multicollector ICP-MS and liquid scintillation counting. Nucl. Instrum. Methods Phys. Res. Sect. B Beam Interact. Mater. Atoms 268 (2), 192–199
- Clark, D.H., Bierman, P.R., Larsen, P., 1995. Improving *in situ* cosmogenic chronometers. Quat. Res. 44 (3), 367–377.
- Clark, P.U., Dyke, A.S., Shakun, J.D., Carlson, A.E., Clark, J., Wohlfarth, B., Mitrovica, J.X., Hostetler, S.W., McCabe, A.M., 2009. The last glacial maximum. Science 325 (5941), 710–714.
- COHMAP Members, 1988. Climatic changes of the last 18,000 years: observations and model simulations. Science 1043–1052.
- Dahms, D., Egli, M., Fabel, D., Harbor, J., Brandová, D., de Castro Portes, R., Christl, M., 2018. Revised Quaternary glacial succession and post-LGM recession, southern Wind River Range, Wyoming, USA. Quat. Sci. Rev. 192, 167–184.
- Darton, N.H., 1906. Geology of the Bighorn Mountains. U.S. Geological Survey Professional Paper 51 (129). US Government Printing Office, pp. 1–46.
- Davies, B.J., Darvill, C.M., Lovell, H., Bendle, J.M., Dowdeswell, J.A., Fabel, D., García, J.L., Geiger, A., Glasser, N.F., Gheorghiu, D.M., Harrison, S., 2020. The evolution of the Patagonian Ice Sheet from 35 ka to the present day (PATICE). Earth Sci. Rev. 103152.
- Desilets, D., Zreda, M., Prabu, T., 2006. Extended scaling factors for in situ cosmogenic nuclides: new measurements at low latitude. Earth and Planetary Science Letters 246 (3–4), 265–276.
- Dortch, J.M., Owen, L.A., Caffee, M.W., Brease, P., 2010. Late Quaternary glaciation and equilibrium line altitude variations of the McKinley River region, central Alaska Range. Boreas 39 (2), 233–246.
- Douglass, D.C., Mickelson, D.M., 2007. Soil development and glacial history, west fork of Beaver Creek, Uinta Mountains, Utah. Arctic Antarct. Alpine Res. 39 (4), 592–602.
- Douglass, D.C., Singer, B.S., Kaplan, M.R., Mickelson, D.M., Caffee, M.W., 2006. Cosmogenic nuclide surface exposure dating of boulders on last-glacial and late-glacial moraines, Lago Buenos Aires, Argentina: interpretive strategies and paleoclimate implications. Quat. Geochronol. 1 (1), 43–58.
- Dühnforth, M., Anderson, R.S., 2011. Reconstructing the glacial history of Green Lakes Valley, North Boulder Creek, Colorado Rront Range. Arctic Antarct. Alpine Res. 43 (4), 527–542.
- Dunai, T.J., 2001. Influence of secular variation of the geomagnetic field on production rates of in situ produced cosmogenic nuclides. Earth and Planetary Science Letters 193 (1–2), 197–212.
- Farber, D.L., Hancock, G.S., Finkel, R.C., Rodbell, D.T., 2005. The age and extent of tropical alpine glaciation in the Cordillera Blanca, Peru. J. Quat. Sci. 20, 759–776. https://doi.org/10.1002/jqs.994.
- Fenton, C.R., Niedermann, S., Dunai, T., Binnie, S.A., 2019. The SPICE project: production rates of cosmogenic <sup>21</sup>Ne, <sup>10</sup>Be, and <sup>14</sup>C in quartz from the 72 ka SP basalt flow, Arizona, USA. Quat. Geochronol. 54, 101019.
- Gillespie, A.R., Clark, D.H., 2011. Glaciations of the Sierra Nevada, California, USA. In: *Developments in Quaternary Sciences*, (Vol. 15, Elsevier, pp. 447–462.
- Goehring, B.M., Kurz, M.D., Balco, G., Schaefer, J.M., Licciardi, J., Lifton, N., 2010. A reevaluation of *in situ* cosmogenic <sup>3</sup>He production rates. Quat. Geochronol. 5 (4), 410–418.
- Gosse, J.C., Phillips, F.M., 2001. Terrestrial *in situ* cosmogenic nuclides: theory and application. Quat. Sci. Rev. 20 (14), 1475–1560.

- Gosse, J.C., Klein, J., Lawn, B., Middleton, R., Evenson, E.B., 1995a. Beryllium-10 dating of the duration and retreat of the last Pinedale glacial sequence. Science 268 (5215), 1329–1333.
- Gosse, J.C., Evenson, E.B., Klein, J., Lawn, B., Middleton, R., 1995b. Precise cosmogenic 10Be measurements in western North America: support for a global Younger Dryas cooling event. Geology 23 (10), 877–880.
- Guido, Z.S., Ward, D.J., Anderson, R.S., 2007. Pacing the post—last glacial maximum demise of the Animas Valley glacier and the San Juan Mountain ice cap, Colorado. Geology 35 (8), 739–742.
- Hall, R.D., Shroba, R.R., 1995. Soil evidence for a glaciation intermediate between the Bull Lake and Pinedale glaciations at Fremont Lake, Wind River Range, Wyoming, USA. Arct. Alp. Res. 27 (1), 89–98.
- Hancock, G.S., Anderson, R.S., Chadwick, O.A., Finkel, R.C., 1999. Dating fluvial terraces with <sup>10</sup>Be and <sup>26</sup>Al profiles: application to the Wind River, Wyoming. Geomorphology 27 (1-2), 41–60.
- He, F., 2011. Simulating transient climate evolution of the last deglaciation with CCSM 3. Ph.D. Dissertation, University of Wisconsin-Madison, p. 171.
   Hein, A.S., Hulton, N.R., Dunai, T.J., Schnabel, C., Kaplan, M.R., Naylor, M., Xu, S.,
- Hein, A.S., Hulton, N.R., Dunai, T.J., Schnabel, C., Kaplan, M.R., Naylor, M., Xu, S., 2009. Middle Pleistocene glaciation in Patagonia dated by cosmogenic-nuclide measurements on outwash gravels. Earth Planet Sci. Lett. 286 (1-2), 184–197.
- Hemming, S.R., 2004. Heinrich events: massive late Pleistocene detritus layers of the North Atlantic and their global climate imprint. Rev. Geophys. 42 (1).
- Heyman, J., Applegate, P.J., Blomdin, R., Gribenski, N., Harbor, J.M., Stroeven, A.P., 2016. Boulder height—exposure age relationships from a global glacial <sup>10</sup>Be compilation. Quat. Geochronol. 34, 1–11.
- Heyman, J., Stroeven, A.P., Caffee, M.W., Hättestrand, C., Harbor, J.M., Li, Y., Alexanderson, H., Zhou, L., Hubbard, A., 2011. Palaeoglaciology of Bayan Har Shan, NE Tibetan Plateau: exposure ages reveal a missing LGM expansion. Quaternary Science Reviews 30 (15–16), 1988–2001.
- Hostetler, S.W., Clark, P.U., 1997. Climatic controls of western US glaciers at the last glacial maximum. Quat. Sci. Rev. 16 (6), 505–511.
- Hudson, A.M., Hatchett, B.J., Quade, J., Boyle, D.P., Bassett, S.D., Ali, G., Marie, G., 2019. North-south dipole in winter hydroclimate in the western United States during the last deglaciation. Sci. Rep. 9 (1), 4826.
- Ibarra, D.E., Egger, A.E., Weaver, K.L., Harris, C.R., Maher, K., 2014. Rise and fall of late Pleistocene pluvial lakes in response to reduced evaporation and precipitation: evidence from Lake Surprise, California. Geol. Soc. Am. Bull. 126 (11-12), 1387–1415.
- Ivy-Ochs, S., Kerschner, H., Reuther, A., Maisch, M., Sailer, R., Schaefer, J., Kubik, P.W., Synal, H., Schluchter, C., 2006. The timing of glacier advances in the northern European Alps based on surface exposure dating with cosmogenic <sup>10</sup>Be, <sup>26</sup>Al, <sup>36</sup>Cl, and <sup>21</sup>Ne. Geological Society of America Special Paper 415, 43–60.
- James, L.A., Harbor, J., Fabel, D., Dahms, D., Elmore, D., 2002. Late Pleistocene glaciations in the northwestern Sierra Nevada, California. Quat. Res. 57 (3), 409–419.
- Kaplan, M.R., Ackert, R.P., Singer, B.S., Douglass, D.C., Kurz, M.D., 2004. Cosmogenic nuclide chronology of millennial-scale glacial advances during O-isotope stage 2 in Patagonia. GSA Bull. 116 (3-4), 308–321.
- Kaplan, M.R., Douglass, D.C., Singer, B.S., Ackert, R.P., Caffee, M.W., 2005. Cosmogenic nuclide chronology of pre-last glacial maximum moraines at Lago Buenos Aires, 46°S, Argentina. Quart. Res. 63, 301–315.
- Kelly, M.A., Kubik, P.W., Von Blanckenburg, F., SchlÜchter, C., 2004. Surface exposure dating of the Great Aletsch Glacier Egesen moraine system, western Swiss Alps, using the cosmogenic nuclide <sup>10</sup>Be. J. Quat. Sci. 19, 431–441. https://doi.org/ 10.1002/jqs.854.
- Kirby, M.E., Feakins, S.J., Bonuso, N., Fantozzi, J.M., Hiner, C.A., 2013. Latest Pleistocene to Holocene hydroclimates from Lake Elsinore, California. Quat. Sci. Rev. 76. 1–15.
- Kirby, M.E., Heusser, L., Scholz, C., Ramezan, R., Anderson, M.A., Markle, B., Rhodes, E., Glover, K.C., Fantozzi, J., Hiner, C., Price, B., 2018. A late Wisconsin (32–10k cal a BP) history of pluvials, droughts and vegetation in the Pacific south-west United States (Lake Elsinore, CA). J. Quat. Sci. 33 (2), 238–254.
- Kleman, J., Fastook, J., Ebert, K., Nilsson, J., Caballero, R., 2013. Pre-LGM Northern Hemisphere ice sheet topography. Clim. Past 9 (5).
- Laabs, B.J.C., Munroe, J.S., 2016. Late Pleistocene Mountain Glaciation in the Lake Bonneville Basin, in Oviatt, C.G., and Schroeder, J., Lake Bonneville: A Scientific Update. Elsevier, Amsterdam, The Netherlands, pp. 462–503.
- Laabs, B.J., Plummer, M.A., Mickelson, D.M., 2006. Climate during the last glacial maximum in the Wasatch and southern Uinta Mountains inferred from glacier modeling. Geomorphology 75 (3-4), 300–317.
- Laabs, B.J., Refsnider, K.A., Munroe, J.S., Mickelson, D.M., Applegate, P.J., Singer, B.S., Caffee, M.W., 2009. Latest Pleistocene glacial chronology of the Uinta Mountains: support for moisture-driven asynchrony of the last deglaciation. Quat. Sci. Rev. 28 (13-14), 1171–1187.
- Kutzbach, J.E., Wright Jr., H.E., 1985. Simulation of the climate of 18,000 years BP: Results for the North American/North Atlantic/European sector and comparison with the geologic record of North America. Quaternary Science Reviews 4 (3), 147–187.
- Laabs, B.J., Marchetti, D.W., Munroe, J.S., Refsnider, K.A., Gosse, J.C., Lips, E.W., Becker, R.A., Mickelson, D.M., Singer, B.S., 2011. Chronology of latest Pleistocene mountain glaciation in the western Wasatch Mountains, Utah, USA. Quat. Res. 76 (2), 272–284.
- Laabs, B.J., Munroe, J.S., Best, L.C., Caffee, M.W., 2013. Timing of the last glaciation and subsequent deglaciation in the Ruby Mountains, Great Basin, USA. Earth Planet Sci. Lett. 361, 16–25.

- Lachniet, M.S., Denniston, R.F., Asmerom, Y., Polyak, V.J., 2014. Orbital control of western North America atmospheric circulation and climate over two glacial cycles. Nat. Commun. 5, 3805.
- Lal, D., 1991. Cosmic ray labeling of erosion surfaces: in situ nuclide production rates and erosion models. Earth Planet Sci. Lett. 104 (2-4), 424-439.
- Lal, D., Peters, B., 1967. Cosmic ray produced radioactivity on the Earth. In: Kosmische Strahlung II/Cosmic Rays II. Springer, Berlin, Heidelberg, pp. 551–612.
- Laskar, J., Robutel, P., Joutel, F., Gastineau, M., Correia, A.C.M., Levrard, B., 2004. A long-term numerical solution for the insolation quantities of the Earth Astron. Astrophys. 428 (1), 261–285.
- Leonard, E.M., 1989, Climatic change in the Colorado Rocky Mountains: estimates based on modern climate at late Pleistocene equilibrium lines. Arct. Alp. Res. 21 (3), 245-255.
- Leonard, E.M., Laabs, B.J., Plummer, M.A., Kroner, R.K., Brugger, K.A., Spiess, V.M., Refsnider, K.A., Xia, Y., Caffee, M.W., 2017a. Late Pleistocene glaciation and deglaciation in the Crestone Peaks area, Colorado Sangre de Cristo Mountains, USA-chronology and paleoclimate. Quat. Sci. Rev. 158, 127–144. Leonard, E.M., Laabs, B.J., Schweinsberg, A.D., Russell, C.M., Briner, J.P., Young, N.E.,
- 2017b. Glaciation in the Colorado Rocky Mountains, USA, following the last glacial maximum. Cuadernos de Investigación Geográfica 43 (2), 497-526.
- Leydet, D.J., Carlson, A.E., Teller, J.T., Breckenridge, A., Barth, A.M., Ullman, D.J., Sinclair, G., Milne, G.A., Cuzzone, J.K., Caffee, M.W., 2018. Opening of glacial Lake Agassiz's eastern outlets by the start of the Younger Dryas cold period. Geology 46 (2), 155-158.
- Licciardi, J.M., Pierce, K.L., 2008. Cosmogenic exposure-age chronologies of Pinedale and Bull Lake glaciations in greater Yellowstone and the Teton Range, USA. Quat. Sci. Rev. 27 (7-8), 814-831.
- Licciardi, I.M., Pierce, K.L., 2018, History and dynamics of the Greater Yellowstone Glacial System during the last two glaciations. Quat. Sci. Rev. 200, 1–33.
- Licciardi, J.M., Clark, P.U., Brook, E.J., Pierce, K.L., Kurz, M.D., Elmore, D., Sharma, P., 2001. Cosmogenic 3He and 10Be chronologies of the late Pinedale northern Yellowstone ice cap, Montana, USA. Geology 29 (12), 1095-1098.
- Licciardi, J.M., Clark, P.U., Brook, E.J., Elmore, D., Sharma, P., 2004. Variable responses
- of western US glaciers during the last deglaciation. Geology 32 (1), 81–84. Licciardi, J.M., Denoncourt, C.L., Finkel, R.C., 2008. Cosmogenic <sup>36</sup>Cl production rates from Ca spallation in Iceland. Earth Planet Sci. Lett. 267, 365-377.
- Lifton, N., Sato, T., Dunai, T.J., 2014. Scaling in situ cosmogenic nuclide production rates using analytical approximations to atmospheric cosmic-ray fluxes. Earth Planet Sci. Lett. 386, 149-160.
- Lifton, N.A., Bieber, J.W., Clem, J.M., Duldig, M.L., Evenson, P., Humble, J.E., Pyle, R., 2005. Addressing solar modulation and long-term uncertainties in scaling secondary cosmic rays for in situ cosmogenic nuclide applications. Earth and Planetary Science Letters 239 (1-2), 140-161.
- Lifton, N., Caffee, M., Finkel, R., Marrero, S., Nishiizumi, K., Phillips, F.M., Goehring, B., Gosse, J., Stone, J., Schaefer, J., Theriault, B., 2015. In situ cosmogenic nuclide production rate calibration for the CRONUS-Earth project from Lake Bonneville, Utah, shoreline features. Quat. Geochronol. 26, 56-69.
- Lisiecki, L.E., Raymo, M.E., 2005. A Pliocene-Pleistocene stack of 57 globally distributed benthic δ180 records. Paleoceanography 20 (1).
- Lora, J.M., Ibarra, D.E., 2019. The North American hydrologic cycle through the last deglaciation. Quat. Sci. Rev. 226, 105991.
- Lora, J.M., Mitchell, J.L., Risi, C., Tripati, A.E., 2017. North Pacific atmospheric rivers and their influence on western North America at the last glacial maximum. Geophys. Res. Lett. 44 (2), 1051-1059.
- Lüthi, D., Le Floch, M., Bereiter, B., Blunier, T., Barnola, J.M., Siegenthaler, U., Raynaud, D., Jouzel, J., Fischer, H., Kawamura, K., Stocker, T.F., 2008. High-resolution carbon dioxide concentration record 650,000-800,000 years before present. Nature 453 (7193), 379.
- Lyle, M., Heusser, L., Ravelo, C., Yamamoto, M., Barron, J., Diffenbaugh, N.S., Herbert, T., Andreasen, D., 2012. Out of the tropics: the Pacific, Great Basin lakes, and Late Pleistocene water cycle in the western United States. Science 337 (6102), 1629-1633.
- Mahan, S.A., Gray, H.J., Pigati, J.S., Wilson, J., Lifton, N.A., Paces, J.B., Blaauw, M., 2014. A geochronologic framework for the Ziegler Reservoir fossil site, Snowmass Village, Colorado. Quat. Res. 82 (3), 490-503.
- Marchetti, D.W., Cerling, T.E., Lips, E.W., 2005. A glacial chronology for the Fish Creek drainage of Boulder Mountain, Utah, USA. Quat. Res. 64 (2), 264–271.
- Marchetti, D.W., Cerling, T.E., Dohrenwend, J.C., Gallin, W., 2007. Ages and significance of glacial and mass movement deposits on the west side of Boulder Mountain, Utah, USA. Palaeogeogr. Palaeoclimatol. Palaeoecol. 252 (3-4),
- Marchetti, D.W., Harris, M.S., Bailey, C.M., Cerling, T.E., Bergman, S., 2011. Timing of glaciation and last glacial maximum paleoclimate estimates from the Fish Lake Plateau, Utah. Quat. Res. 75 (1), 183–195.
- Marcott, S.A., Clark, P.U., Shakun, J.D., Brook, E.J., Davis, P.T., Caffee, M.W., 2019. 10 Be age constraints on latest Pleistocene and Holocene cirque glaciation across the western United States. NPJ Clim. Atmospheric Sci. 2 (1). Article 5.
- Mark, B., Stansell, N., Zeballos, G., 2017. The last deglaciation of Peru and Bolivia. Cuadernos de investigación geográfica 2 (2), 591–628.
- Marrero, S.M., Phillips, F.M., Borchers, B., Lifton, N., Aumer, R., Balco, G., 2016a. Cosmogenic nuclide systematics and the CRONUScalc program. Quat. Geochronol, 31, 160-187.
- Marrero, S.M., Phillips, F.M., Caffee, M.W., Gosse, J.C., 2016b. CRONUS-Earth cosmogenic <sup>36</sup>Cl calibration. Quat. Geochronol. 31, 199–219.
- Martin, L.C.P., Blard, P.H., Balco, G., Lavé, J., Delunel, R., Lifton, N., Laurent, V., 2017.

- The CREp program and the ICE-D production rate calibration database: a fully parameterizable and updated online tool to compute cosmic-ray exposure ages. Quat. Geochronol. 38, 25–49.
- McCalpin, I., 2011. Crestone: Gateway to the Higher Realms, vol. 7. Keystone Science Center, Guidebook, p. 256pp. B&B Printing, Gunnison, Colorado, Middleton, R., Brown, L., Dezfouly-Arjomandy, B., Klein, J., 1993. On <sup>10</sup>Be standards
- and the half life of <sup>10</sup>Be. Nucl. Instrum. Methods Phys. Res. B82, 399–403.
- Mitchell, V.L., 1976. The regionalization of climate in the western United States. Journal of Applied Meteorology 15 (9), 920-927.
- Moseley, G.E., Edwards, R.L., Wendt, K.A., Cheng, H., Dublyansky, Y., Lu, Y., Boch, R., Spötl, C., 2016. Reconciliation of the Devils Hole climate record with orbital forcing, Science 351 (6269), 165–168.
- Munroe, J.S., Laabs, B.J., 2013. Temporal correspondence between pluvial lake highstands in the southwestern US and Heinrich Event 1. J. Quat. Sci. 28 (1), 49-58.
- Munroe, J.S., Laabs, B.J., Shakun, J.D., Singer, B.S., Mickelson, D.M., Refsnider, K.A., Caffee, M.W., 2006, Latest Pleistocene advance of alpine glaciers in the southwestern Uinta Mountains, Utah, USA: evidence for the influence of local moisture sources. Geology 34 (10), 841-844.
- Munroe, I.S., Walcott, C.K., Amidon, W.H., Landis, I.D., 2020. A top-to-bottom luminescence-based chronology for the post-LGM regression of a Great Basin pluvial Lake. Quaternary 3 (2), 11p. https://doi.org/10.3390/quat3020011.
- Nishiizumi, K., Winterer, E.L., Kohl, C.P., Klein, J., Middleton, R., Lal, D., Arnold, J.R., 1989. Cosmic ray production rates of <sup>10</sup>Be and <sup>26</sup>Al in quartz from glacially polished rocks. J. Geophys. Res.: Solid Earth 94 (B12), 17907–17915.
- Nishiizumi, K., Kohl, C.P., Arnold, J.R., Dorn, R., Klein, I., Fink, D., Middleton, R., Lal, D., 1993. Role of *in situ* cosmogenic nuclides <sup>10</sup>Be and <sup>26</sup>Al in the study of diverse geomorphic processes, Earth Surf. Process, Landforms 18 (5), 407-425.
- Nishiizumi, K., Imamura, M., Caffee, M.W., Southon, J.R., Finkel, R.C., McAninch, J., 2007. Absolute calibration of <sup>10</sup>Be AMS standards. Nucl. Instrum. Methods Phys. Res. Sect. B Beam Interact. Mater. Atoms 258 (2), 403–413.
- Oster, J.L., Ibarra, D.E., Winnick, M.J., Maher, K., 2015a. Steering of westerly storms over western North America at the last glacial maximum. Nat. Geosci. 8 (3), 201.
- Oster, J.L., Montanez, I.P., Santare, L.R., Sharp, W.D., Wong, C., Cooper, K.M., 2015b. Stalagmite records of hydroclimate in central California during termination 1. Quat. Sci. Rev. 127, 199-214.
- Oviatt, C.G., 2015. Chronology of Lake Bonneville, 30,000 to 10,000 yr BP. Quat. Sci. Rev. 110, 166-171.
- Owen, L.A., Dortch, J.M., 2014. Nature and timing of Quaternary glaciation in the Himalayan-Tibetan orogen. Quat. Sci. Rev. 88, 14-54.
- Owen, L.A., Finkel, R.C., Minnich, R.A., Perez, A.E., 2003. Extreme southwestern margin of late Quaternary glaciation in North America: timing and controls. Geology 31 (8), 729-732.
- Owen, L.A., Chen, J., Hedrick, K.A., Caffee, M.W., Robinson, A.C., Schoenbohm, L.M., Yuan, Z., Li, W., Imrecke, D.B., Liu, J., 2012. Quaternary glaciation of the Tashkurgan valley, southeast Pamir. Quat. Sci. Rev. 47, 56-72
- Phillips, F.M., Zreda, M.G., Smith, S.S., Elmore, D., Kubik, P.W., Sharma, P., 1990. Cosmogenic chlorine-36 chronology for glacial deposits at Bloody Canyon, eastern Sierra Nevada. Science 248 (4962), 1529-1532.
- Phillips, F.M., Zreda, M.G., Benson, L.V., Plummer, M.A., Elmore, D., Sharma, P., 1996. Chronology for fluctuations in late Pleistocene Sierra Nevada glaciers and lakes. Science 274 (5288), 749-751.
- Phillips, F.M., Zreda, M.G., Gosse, J.C., Klein, J., Evenson, E.B., Hall, R.D., Chadwick, O.A., Sharma, P., 1997. Cosmogenic <sup>36</sup>Cl and <sup>10</sup>Be ages of Quaternary glacial and fluvial deposits of the Wind River Range, Wyoming. Geol. Soc. Am. Bull. 109 (11), 1453-1463.
- Phillips, F.M., Zreda, M., Plummer, M.A., Elmore, D., Clark, D.H., 2009. Glacial geology and chronology of Bishop Creek and vicinity, eastern Sierra Nevada, California. Geol. Soc. Am. Bull. 121 (7-8), 1013-1033.
- Palacios, D., Stokes, C.R., Phillips, F.M., Clague, J.J., Alcalá-Reygosa, J., Andrés, N., Angel, I., Blard, P.H., Briner, J.P., Hall, B.L., Dahms, D., 2020. The deglaciation of the Americas during the Last Glacial Termination. Earth-Science Reviews 203,
- Phillips, F., 2017. Glacial chronology of the Sierra Nevada, California, from the last glacial maximum to the Holocene. Cuadernos de investigación geográfica/ Geographical Research Letters (43),, 527–552.
- Phillips, F.M., Argento, D.C., Balco, G., Caffee, M.W., Clem, J., Dunai, T.J., Finkel, R., Goehring, B., Gosse, J.C., Hudson, A.M., Jull, A.T., 2016a. The CRONUS-Earth project: a synthesis. Quat. Geochronol. 31, 119-154.
- Phillips, F.M., Hinz, M., Marrero, S.M., Nishiizumi, K., 2016b. Cosmogenic nuclide data sets from the Sierra Nevada, California, for assessment of nuclide production models: II. Sample sites and evaluation. Quat. Geochronol. 35, 101–118. Pierce, K.L., 2003. Pleistocene glaciations of the Rocky Mountains. Dev. Quat. Sci. 1,
- Pierce, K.L., Good, J.D., 1992. Field Guide to the Quaternary Geology of Jackson Hole, Wyoming (No. 92-504). US Dept. of the Interior, US Geological Survey.
- Pierce, K.L., Muhs, D.R., Fosberg, M.A., Mahan, S.A., Rosenbaum, J.G., Licciardi, J.M., Pavich, M.J., 2011. A loess-paleosol record of climate and glacial history over the past two glacial—interglacial cycles (~ 150 ka), southern Jackson Hole, Wyoming. Quat. Res. 76 (1), 119–141.
- Pierce, K.L., Licciardi, J.M., Good, J.M., Jaworowski, C., 2018. Pleistocene Glaciation of the Jackson Hole Area, Wyoming (No. 1835). US Geological Survey.
- Plummer, M.A., Phillips, F.M., 2003. A 2-D numerical model of snow/ice energy balance and ice flow for paleoclimatic interpretation of glacial geomorphic features. Quat. Sci. Rev. 22 (14), 1389-1406.

- Porter, S.C., Swanson, T.W., 2008. <sup>36</sup>Cl dating of the classic Pleistocene glacial record in the northeastern Cascade Range, Washington. Am. J. Sci. 308 (2), 130–166.
- Porter, S.C., Pierce, K.L., Hamilton, T.D., 1983. Late Wisconsin mountain glaciation in the western United States. In: Porter, S.C. (Ed.), Late-Quaternary Environments of the United States, vol. 1. University of Minnesota, Minneapolis, pp. 71–111. The Late Pleistocene.
- Putkonen, J., O'Neal, M., 2006. Degradation of unconsolidated Quaternary landforms in the western North America. Geomorphology 75 (3-4), 408–419.
- Putkonen, J., Swanson, T., 2003. Accuracy of cosmogenic ages for moraines. Quat. Res. 59 (2), 255–261.
- Putnam, A.E., Schaefer, J.M., Denton, G.H., Barrell, D.J., Birkel, S.D., Andersen, B.G., Kaplan, M.R., Finkel, R.C., Schwartz, R., Doughty, A.M., 2013. The last glacial maximum at 44°S documented by a <sup>10</sup>Be moraine chronology at Lake Ohau, Southern Alps of New Zealand. Quat. Sci. Rev. 62, 114–141.
- Quirk, B.J., Moore, J.R., Laabs, B.J., Caffee, M.W., Plummer, M.A., 2018. Termination II, Last Glacial Maximum, and Lateglacial chronologies and paleoclimate from Big Cottonwood Canyon, Wasatch Mountains, Utah. Geol. Soc. Am. Bull. 130 (11–12), 1889–1902.
- Rasmussen, S.O., Andersen, K.K., Svensson, A.M., Steffensen, J.P., Vinther, B.M., Clausen, H.B., Siggaard-Andersen, M.L., Johnsen, S.J., Larsen, L.B., Dahl-Jensen, D., Bigler, M., 2006. A new Greenland ice core chronology for the last glacial termination. J. Geophys. Res.: Atmosphere 111 (D6).
- Refsnider, K.A., Laabs, B.J., Plummer, M.A., Mickelson, D.M., Singer, B.S., Caffee, M.W., 2008. Last glacial maximum climate inferences from cosmogenic dating and glacier modeling of the western Uinta ice field, Uinta Mountains, Utah. Quat. Res. 69 (1), 130—144.
- Rood, D.H., Burbank, D.W., Finkel, R.C., 2011. Chronology of glaciations in the Sierra Nevada, California, from <sup>10</sup>Be surface exposure dating. Quat. Sci. Rev. 30 (5-6), 646–661.
- Sarıkaya, M.A., Zreda, M., Çiner, A., 2009. Glaciations and paleoclimate of Mount Erciyes, central Turkey, since the Last Glacial Maximum, inferred from 36Cl cosmogenic dating and glacier modeling. Quat. Sci. Rev. 28 (23-24), 2326–2341.
- Schaefer, J.M., Denton, G.H., Barrell, D.J., Ivy-Ochs, S., Kubik, P.W., Andersen, B.G., Phillips, F.M., Lowell, T.V., Schlüchter, C., 2006. Near-synchronous interhemispheric termination of the last glacial maximum in mid-latitudes. Science 312 (5779), 1510–1513.
- Schaefer, J.M., Denton, G.H., Kaplan, M., Putnam, A., Finkel, R.C., Barrell, D.J., Andersen, B.G., Schwartz, R., Mackintosh, A., Chinn, T., Schlüchter, C., 2009. High-frequency Holocene glacier fluctuations in New Zealand differ from the northern signature. Science 324 (5927), 622–625.
- Schaefer, J.M., Putnam, A.E., Denton, G.H., Kaplan, M.R., Birkel, S., Doughty, A.M., Kelley, S., Barrell, D.J., Finkel, R.C., Winckler, G., Anderson, R.F., 2015. The southern glacial maximum 65,000 years ago and its unfinished termination. Quat. Sci. Rev. 114, 52–60.
- Schildgen, T., Dethier, D.P., Bierman, P., Caffee, M., 2002. <sup>26</sup>Al and <sup>10</sup>Be dating of late Pleistocene and Holocene fill terraces: a record of fluvial deposition and incision, Colorado Front Range. Earth Surf. Process. Landforms: J. Br. Geomorphol. Res. Group 27 (7), 773–787.
- Schweinsberg, A.D., Briner, J.P., Licciardi, J.M., Shroba, R.R., Leonard, E.M., 2020. Cosmogenic <sup>10</sup>Be exposure dating of Bull Lake and Pinedale moraine sequences in the upper Arkansas River valley, Colorado Rocky Mountains, USA. Quat. Res. 1–15
- Schweinsberg, A.D., Briner, J.P., Shroba, R.R., Licciardi, J.M., Leonard, E.M., Brugger, K.A., Russell, C.M., 2016. Pinedale glacial history of the upper Arkansas River valley: New moraine chronologies, modeling results, and geologic mapping. *Unfolding the Geology of the West*. Geological Society of America Field Guide 44, 335–353.
- Scott, W.E., McCoy, W.D., Shroba, R.R., Rubin, M., 1983. Reinterpretation of the exposed record of the last two cycles of Lake Bonneville, western United States. Quat. Res. 20 (3), 261–285.
- Shakun, J.D., Clark, P.U., He, F., Marcott, S.A., Mix, A.C., Liu, Z., Otto-Bliesner, B., Schmittner, A., Bard, E., 2012. Global warming preceded by increasing carbon dioxide concentrations during the last deglaciation. Nature 484 (7392), 49.
- Shakun, J.D., Clark, P.U., He, F., Lifton, N.A., Liu, Z., Otto-Bliesner, B.L., 2015. Regional and global forcing of glacier retreat during the last deglaciation. Nat. Commun. 6, 8059.
- Sharp, R.P., 1938. Pleistocene glaciation in the Ruby-East Humboldt range, northeastern Nevada. J. Geomorphol. 1.
- Sharp, R.P., Allen, C.R., Meier, M.F., 1959. Pleistocene glaciers on southern California mountains. Am. J. Sci. 257 (2), 81–94.
- Sharp, W.D., Ludwig, K.R., Chadwick, O.A., Amundson, R., Glaser, L.L., 2003. Dating fluvial terraces by 230 Th/U on pedogenic carbonate, Wind River Basin, Wyoming. Quat. Res. 59 (2), 139–150.
- Sheppard, P.R., Comrie, A.C., Packin, G.D., Angersbach, K., Hughes, M.K., 2002. The climate of the US Southwest. Clim. Res. 21 (3), 219–238.
- Shulmeister, J., Fink, D., Hyatt, O.M., Thackray, G.D., Rother, H., 2010. Cosmogenic <sup>10</sup>Be and <sup>26</sup>Al exposure ages of moraines in the Rakaia Valley, New Zealand and the nature of the last termination in New Zealand glacial systems. Earth Planet Sci. Lett. 297 (3-4), 558–566.
- Smith, J.A., Finkel, R.C., Farber, D.L., Rodbell, D.T., Seltzer, G.O., 2005a. Moraine preservation and boulder erosion in the tropical Andes: interpreting old surface exposure ages in glaciated valleys. J. Quat. Sci.: Publ. Quat. Res. Assoc. 20 (7-8),

- 735-758.
- Smith, J.A., Seltzer, G.O., Farber, D.L., Rodbell, D.T., Finkel, R.C., 2005b. Early local last glacial maximum in the tropical Andes. Science 308, 678–681. https://doi.org/10.1126/science.1107075.
- Speth, G.T., Amos, C.B., Amidon, W.H., Balco, G., Meigs, A.J., Graf, S., 2018. Glacial chronology and slip rate on the west Klamath Lake fault zone, Oregon. Geol. Soc. Am. Bull. 131 (3-4), 444–460.
- Steenburgh, W.J., Redmond, K.T., Kunkel, K.E., Doesken, N., Gillies, R.R., Horel, J.D., Hoerling, M.P., Painter, T.H., 2013. Present weather and climate: average conditions. In: Garfin, G., Jardine, A., Merideth, R., Black, M., LeRoy, S. (Eds.), Assessment of Climate Change in the Southwest United States: A Report Prepared for the National Climate Assessment. A report by the Southwest Climate Alliance, Washington, DC, pp. 56–73 (Island Press).
- Stone, J.O., 2000. Air pressure and cosmogenic isotope production. J. Geophys. Res.: Solid Earth 105 (B10), 23753–23759.
- Stroeven, A.P., Fabel, D., Margold, M., Clague, J.J., Xu, S., 2014. Investigating absolute chronologies of glacial advances in the NW sector of the Cordilleran Ice Sheet with terrestrial in situ cosmogenic nuclides. Quat. Sci. Rev. 92, 429–443.
- Swanson, T.W., Caffee, M.L., 2001. Determination of <sup>36</sup>Cl production rates derived from the well-dated deglaciation surfaces of Whidbey and Fidalgo Islands, Washington. Quat. Res. 56 (3), 366–382.
- Thackray, G.D., 2001. Extensive early and middle Wisconsin glaciation on the western Olympic Peninsula, Washington, and the variability of Pacific moisture delivery to the northwestern United States. Quat. Res. 55 (3), 257–270.
- Thackray, G.D., 2008. Varied climatic and topographic influences on Late Pleistocene mountain glaciation in the western United States. J. Quat. Sci.: Publ. Quat. Res. Assoc. 23 (6-7), 671–681.
- Thackray, G.D., Staley, A.E., 2017. Systematic variation of Late Pleistocene fault scarp height in the Teton Range, Wyoming, USA: variable fault slip rates or variable landform ages? Geosphere 13 (2), 287–300.
- Thackray, G.D., Lundeen, K.A., Borgert, J.A., 2004. Latest Pleistocene alpine glacier advances in the Sawtooth Mountains, Idaho, USA: reflections of midlatitude moisture transport at the close of the last glaciation. Geology 32 (3), 225–228.
- Thompson, R.S., Whitlock, C., Bartlein, P.J., Harrison, S.P., Spaulding, W.G., Wright, H.E., Kutzbach, J.E., Webb, T.I.I.I., Ruddiman, W.F., 1993. Climatic changes in the western United States since 18,000 yr BP. Global Climates since the Last Glacial Maximum, pp. 468–513.
- Tulenko, J.P., Briner, J.P., Young, N.E., Schaefer, J.M., 2018. Beryllium-10 chronology of early and late Wisconsinan moraines in the Revelation Mountains, Alaska: insights into the forcing of Wisconsinan glaciation in Beringia. Quat. Sci. Rev. 197, 129–141.
- Tulenko, J.P., Lofverstrom, M., Briner, J.P., 2020. Ice sheet influence on atmospheric circulation explains the patterns of Pleistocene alpine glacier records in North America. Earth Planet Sci. Lett. 534 https://doi.org/10.1016/j.epsl.2020.116.115.
- Wagner, J.D., Cole, J.E., Beck, J.W., Patchett, P.J., Henderson, G.M., Barnett, H.R., 2010. Moisture variability in the southwestern United States linked to abrupt glacial climate change. Nat. Geosci. 3 (2), 110.
- Ward, B.C., Bond, J.D., Froese, D., Jensen, B., 2008. Old Crow tephra (140±10 ka) constrains penultimate Reid glaciation in central Yukon Territory. Quat. Sci. Rev. 27 (19-20), 1909–1915.
- Ward, D.J., Anderson, R.S., Guido, Z.S., Briner, J.P., 2009. Numerical modeling of cosmogenic deglaciation records, Front Range and San Juan Mountains, Colorado. J. Geophys. Res.: Earth Surface 114 (F1).
- Wendt, K.A., Dublyansky, Y.V., Moseley, G.E., Edwards, R.L., Cheng, H., Spötl, C., 2018. Moisture availability in the southwest United States over the last three glacial-interglacial cycles. Sci. Adv. 4, 8 eaau1375.
- Wendt, K.A., Pythoud, M., Moseley, G.E., Dublyansky, Y.V., Edwards, R.L., Spötl, C., 2020. Paleohydrology of southwest Nevada (USA) based on groundwater 234U/238U over the past 475 ky. Geol. Soc. Am. Bull. 132 (3-4), 793–802.
- Wesnousky, S.G., Briggs, R.W., Caffee, M.W., Ryerson, F.J., Finkel, R.C., Owen, L.A., 2016. Terrestrial cosmogenic surface exposure dating of glacial and associated landforms in the Ruby Mountains-East Humboldt Range of central Nevada and along the northeastern flank of the Sierra Nevada. Geomorphology 268, 72–81.
- Winograd, I.J., Coplen, T.B., Landwehr, J.M., Riggs, A.C., Ludwig, K.R., Szabo, B.J., Kolesar, P.T., Revesz, K.M., 1992. Continuous 500,000-year climate record from vein calcite in Devils Hole, Nevada. Science 258 (5080), 255–260.
- Yokoyama, Y., Reyss, J.L., Guichard, F., 1977. Production of radionuclides by cosmic rays at mountain altitudes. Earth Planet Sci. Lett. 36 (1), 44–50.
- Young, N.E., Briner, J.P., Leonard, E.M., Licciardi, J.M., Lee, K., 2011. Assessing climatic and nonclimatic forcing of Pinedale glaciation and deglaciation in the western United States. Geology 39 (2), 171–174.
- Zech, R., Smith, J., Kaplan, M.R., 2009. Chronologies of the last glacial maximum and its termination in the Andes (~ 10–55° S) based on surface exposure dating. In: Past Climate Variability in South America and Surrounding Regions. Springer, Dordrecht, pp. 61–87.
- Zielinski, G.A., McCoy, W.D., 1987. Paleoclimatic implications of the relationship between modern snowpack and late Pleistocene equilibrium-line altitudes in the mountains of the Great Basin, western USA. Arct. Alp. Res. 19 (2), 127–134.
- Munroe, J.S., Laabs, B.J.C., Oviatt, C.G. and Jewell, P.W., 2015, June. New investigations of Pleistocene pluvial and glacial records from the northeastern Great Basin. In, Sixth International Limnogeology Congress—Field Trip Guidebook, Reno, Nevada, (pp. 1-60), U.S. Geological Survey Open-File Report 2015-1092.